DE –EE0004391

Final Technical Report: Upgrading of Bio-Oil Produced by Pyrolysis

Battelle Memorial Institute
505 King Avenue
Columbus OH 43201

Project Location(s): Columbus, Ohio and Richland, Washington

Project Period: September 30, 2010 to March 31, 2015

Date of Report: June 30, 2015

Written by: Zia Abdullah, Brad Chadwell, Rachid Taha, Barry Hindin, Kevin Ralston

Program Manager: Brad Chadwell

Principal Investigators: Zia Abdullah

Subcontractors: None

Cost-Sharing Partners: Marathon; Domtar

DOE Field Project Officer: Prasad Gupte; prasad.gupte@ee.doe.gov; 202-586-8943

Battelle
The Business *of* Innovation

Acknowledgment: This material is based upon work supported by the Department of Energy under Award Number DE -EE0004391

Executive Summary

The objectives of this project were to (1) develop a process to upgrade catalytic pyrolysis bio-oil, (2) investigate new upgrading catalysts suited for upgrading catalytic pyrolysis bio-oil, (3) demonstrate upgrading system operation for more than 1,000 hours using a single catalyst charge, and (4) produce a final upgraded product that can be blended to 30 percent by weight with petroleum fuels or that is compatible with existing petroleum refining operations.

This project has, to the best of our knowledge, for the first time enabled a commercially viable bio-oil hydrotreatment process to produce renewable blend stock for transportation fuels.

At the beginning of the project, the state of the art catalyst lifetime before deactivation was 100 to 150 hours. We identified catalyst deactivation due to poisoning and coke formation to be the dominant contributors to the short catalyst life, and developed approaches to overcome these barriers to commercial deployment of bio-oil upgrading systems. Specifically, we developed a novel, low cost bio-oil cleanup process, a non-carbon supported bio-oil stabilization catalyst and successful regeneration process to enable long-term hydrotreater operation. We then performed hydro-processing of the stabilized bio-oil using a commercial sulfided catalyst.

We demonstrated over 1,200 hours of operation of the combined bio-oil stabilization and hydro-processing system on a single catalyst charge, producing a final upgraded product analyzed by our oil and gas industry partner to be capable of being blended with petroleum transportation fuels. A detailed techno-economic analysis and life cycle greenhouse gas (GHG) emission modeling resulted in a minimum fuel selling price of $3.62/gallon and GHG emission reduction estimates of approximately 80% over conventional fuels, well within biofuel definitions under the Renewable Fuel Standard (50% reduction for advanced biofuel and 60% reduction for cellulosic biofuel).

The technology developed under this project can be scaled up and commercialized in the near future. Battelle is developing small scale (approximately 100 tons/day), factory-built bio-refineries using fast pyrolysis bio-oil as a platform intermediate product to produce fuels and chemicals. In contrast to conventional large scale bio-refineries, this commercialization model will require much lower capital and therefore will be accessible to a broader range of financing options.

Distributed deployment of a large number of these systems where biomass is available at low cost will contribute significantly toward meeting goals and objectives of the DOE Biomass Program. A biochemicals company is already being spun off in FY2015. This company will scale up the ‘front end’ (pyrolysis) process. Hydrotreatment catalysts and processes developed under this project can be licensed to the spin-off company for the production of biofuels, using the already proven pyrolysis process.

Table of Contents

Page

List of Tables

Page

List of Figures

Page

1.0 Introduction

Biomass conversion to hydrocarbon fuel through fast pyrolysis followed by bio-oil upgrading (Figure 1) offers potentially tremendous market advantages because of the feedstock flexibility and scalability of the basic fast pyrolysis step. However it has proven to be extremely challenging to deploy the upgrading step within the overall commercial constraints of the market; conventional fast pyrolysis bio-oils corrode equipment and rapidly coke/deteriorate the catalyst. The state of the art of hydrotreatment catalyst life at the time this project was started was approximately 100 hrs. to 200 hrs. Time On Stream (TOS) at a Liquid Hourly Space Velocity (LHSV) of 0.2 before catalyst coking and deactivation required process shutdown. This corresponded to processing of bio oil volume of approximately 20 to 30 times the volume of the catalyst charge in the hydrotreater.

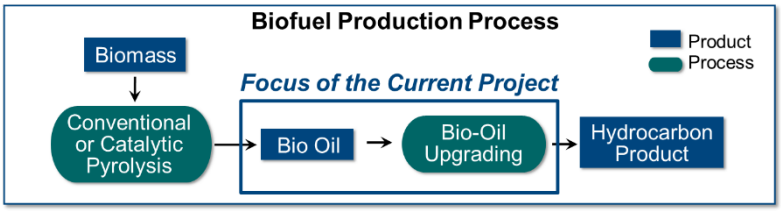

Figure 1. Biomass to hydrocarbon fuel production process.

The intent of the DOE project under Award # DE-EE000439 was to break through this barrier of catalyst coking and deactivation, and demonstrate commercially meaningful improvements in hydrotreatment performance. Specifically, Battelle's objectives for this DOE project were to:

- Develop an integrated hydroprocessing system and catalysts tailored to reliably and consistently de-oxygenate/upgrade by hydroprocessing the Intermediate Bio-Oil produced by Battelle's fast pyrolysis and vapor-phase upgrading system
- Demonstrate extended operation (more than 1,000 hours) of the Intermediate Bio-Oil hydroprocessing system using a single catalyst charge
- Provide extensive data on system performance, catalyst performance, material corrosion, and hydrocarbon product composition
- Conduct and provide results from Techno-Economic Analyses (TEA) and Life-Cycle Analyses (LCA) to demonstrate the commercialization potential of the technology
- Demonstrate that Battelle's novel integrated fast pyrolysis, vapor-phase catalysis, and Intermediate Bio-Oil upgrading system can produce a hydrocarbon product that can be blended to 30 percent by weight with ASTM petroleum fuels or produce an upgraded bio-oil compatible with existing petroleum refining operations.

The project effort was divided into 9 tasks (Task A to Task I), as shown in the project management plan in Figure 2. All of the project objectives were achieved. Battelle, as the prime contractor, executed Tasks A, B, D, E, F, G and I. PNNL, as the FFRDC subcontractor, executed Tasks C and H. Domtar Paper Company provided significant quantities of biomass to the project under Task A, and Marathon Petroleum Company provided FCC catalyst as well as conducted analysis of hydrocarbon fuel product under Task G. Marathon Petroleum also provided valuable insight into integration of hydrocarbon bio-fuel product into the transportation fuel value chain.

This report is also organized along the Task structure of project management plan. The progress and achievements under each Task are reported sequentially as they appear in the project management plan.

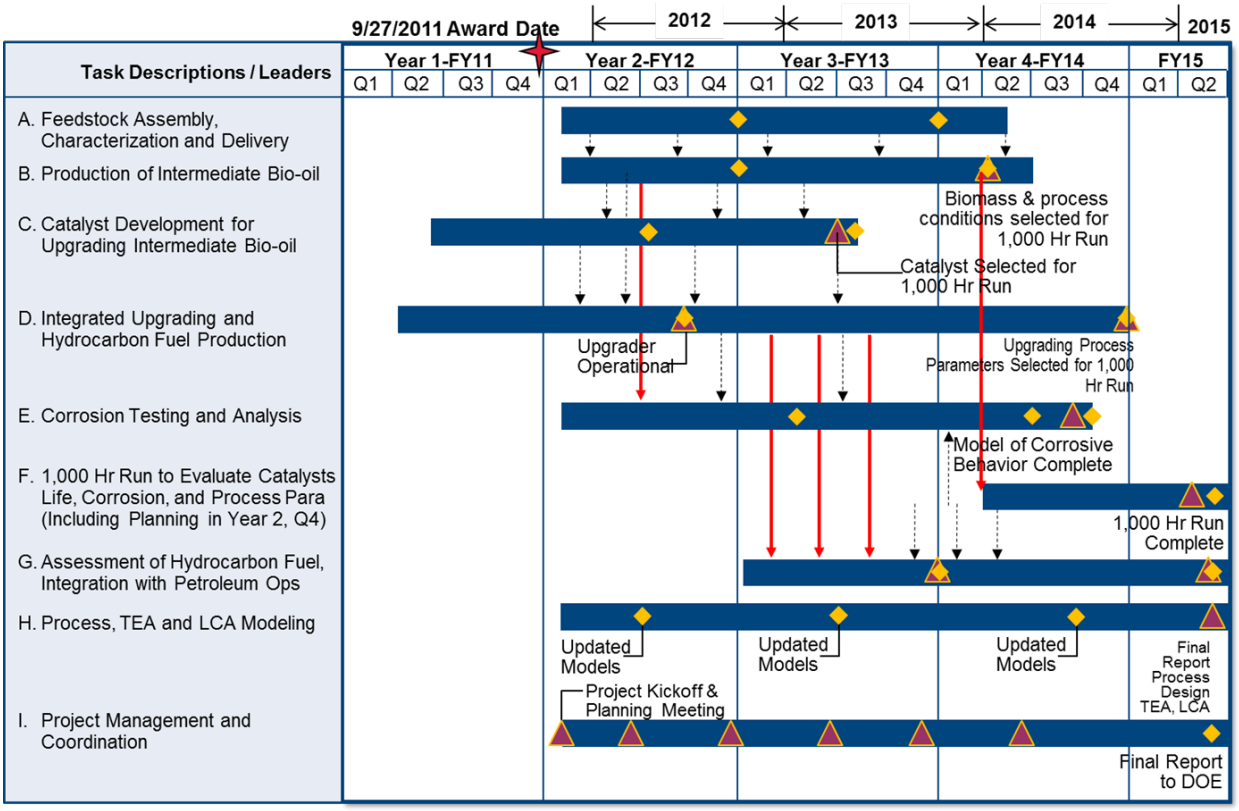

Figure 2. Project Management Plan showing the main tasks of the DOE project.

2.0 Task A: Feedstock Assembly

The objective of Task A was to acquire and process three types of biomass so that these could be tested for the production of bio oil and hydrocarbon fuel product. The project team worked with the following three types of biomass which were approved by the DOE:

1. Softwood
2. Miscanthus
3. Corn Stover

2.1 Softwood Biomass

Battelle has used two sources of softwood for our DOE program 1) softwood from local sawmills; and 2) softwood from pulp and paper mills.

2.1.1 Softwood from local sawmills

We have obtained Pine sawdust from local sawmills and used this feedstock as needed.

Figure 3. Pine sawdust obtained from local sawmills

Figure 3 shows the Pine which was used in the experimental work. Battelle has processed approximately 4 tons of pine from local sawmills.

Figure 4. Sawmill Pine dimension is in the 1/16" to 1/8" range

Figure 4 shows a close up of the pine biomass. After grinding and sifting, the biomass particle dimensions are generally in the range of 1/16" to 1/8", and sufficiently small to be used directly in our 50 lb./day and 1 ton/day pyrolysis systems. This biomass was dried to <3% moisture content prior to pyrolysis. Table 1 shows CHNS data for pine. Oxygen is determined by difference.

Table 1. Elemental Analysis of Pine Biomass

Carbon	Hydrogen	Nitrogen	Sulfur	Oxygen (by difference)
51.55	5.89	0.45	<0.005	42.11

Structural (Cellulose and Hemicellulose) carbohydrate compositions of two wood samples were determined by High Performance Anion Exchange Chromatography with Pulsed Amperometric Detection (HPAEC-PAD). The wood samples were air-dried, milled, sieved, solvent extracted with Dichloromethane and acid hydrolyzed prior to analysis. Results, reported on an extractives free oven dry weight basis, are summarized below. The bulk of the Glucan is derived from Cellulose. Depending on species, some Glucan may be associated with Hemicelluloses, as in Glucomannans. The Arabinan, Galactan, Xylan and Mannan are derived from the Hemicelluloses.

Table 2. Carbohydrate Analysis of Pine Biomass

	Arabinan (wt.%)	Galactan (wt.%)	Glucan (wt.%)	Xylan (wt.%)	Mannan (wt.%)	Carbohydrates (wt.%)
Replicate 1	1.11	2.74	43.13	5.21	9.78	61.97
Replicate 2	1.13	2.67	43.86	5.19	9.94	62.78
Average	1.12	2.70	43.49	5.20	9.86	62.38
Std. Dev.	0.01	0.05	0.51	0.01	0.12	0.58
%RSD	0.77	1.79	1.18	0.27	1.17	0.92

The acid insoluble lignin compositions were determined gravimetrically from the acid hydrozylates prepared for the carbohydrate determinations. The acid soluble lignin compositions were determined by measuring the absorbance of filtered aliquots of the acid hydrozylates at 280nm in a UV-VIS spectrophotometer. The ash content was determined gravimetrically after combusting the samples at 525^{o}C. Results are reported in Table 3 on an oven dry solids basis.

Table 3. Lignin and Ash Analysis of Pine Biomass

	Acid Insoluble Lignin (wt.%)	Acid Soluble Lignin (wt.%)	Total Lignin (wt.%)	Ash (wt.%)
Replicate 1	31.63	0.75	32.38	0.49
Replicate 2	30.02	0.74	30.76	0.43
Average	30.83	0.74	31.57	0.46
Std. Dev.	1.14	0.01	1.14	0.04
%RSD	3.69	0.78	3.62	8.81

The results above show that the pine biomass ~51% carbon, ~6% hydrogen, ~0.5% nitrogen and 42% oxygen. The biomass has 62% carbohydrate, 32% lignin and approximately 0.5% ash. These results are fairly typical for softwood pine.

2.1.2 Softwood from pulp and paper mills

Biomass was delivered in ½ ton canvas totes which are equipped with hooks, so that they can be lifted via a forklift, as shown in Figure 5 and Figure 6. The material is quite fine with particle size ranging from 1/8" to 1/2", as shown in Figure 7.

Figure 5. Half ton biomass tote being loaded up on forklift

Figure 6. Biomass totes stored at Battelle before use

Figure 7. Particle size distribution from pulp and paper mills is in the range of 1/8" to ½"

The softwood biomass was ground up and analyzed for carbohydrate, lignin and ash content. Table 4 and Table 5 show the results. The mixed biomass from Domtar appears to have slightly higher lignin content and correspondingly lower carbohydrate content (see Table 2 and Table 3).

Table 4. Cellulose and Hemicellulose Content of Domtar Mixed Pine Biomass Sample

	Arabinan (wt.%)	Galactan (wt.%)	Glucan (wt.%)	Xylan (wt.%)	Mannan (wt.%)	Carbohydrates (wt.%)
Replicate 1	1.97	3.12	37.16	5.19	8.08	55.53
Replicate 2	1.92	3.17	37.62	5.27	8.17	56.15
Average	1.95	3.15	37.39	5.23	8.12	55.84
Std. Dev.	0.04	0.03	0.32	0.06	0.07	0.44
%RSD	2.03	0.95	0.87	1.17	0.81	0.79

Table 5. Lignin and Ash Content of Domtar Mixed Pine Biomass Sample

	Acid Insoluble Lignin (wt.%)	Acid Soluble Lignin (wt.%)	Total Lignin (wt.%)	Ash (wt.%)
Replicate 1	33.73	0.83	34.56	1.07
Replicate 2	33.26	0.82	34.09	1.09
Average	33.50	0.83	34.32	1.08
Std. Dev.	0.33	0.01	0.33	0.02
%RSD	0.98	0.71	0.97	1.88

RSD = Relative Standard Deviation
na = not applicable

2.2 Miscanthus Biomass

Battelle acquired approximately 100 lbs. of Miscanthus. Figure 8 and Figure 9 show the biomass. The material is quite fine with particle size ranging from 1/8" to 3/4". The larger dimension is in length only; from a heat transfer perspective we do not feel that there is any need for size attrition. However with long, narrow particles, there is a chance of bridging in the feedstock delivery system.

Figure 8. Miscanthus biomass

Figure 9. Particle size distribution of Miscanthus is in the range of 1/8" to 3/4"

Table 6 shows Carbon, Hydrogen, Nitrogen and Sulfur (CHNS) content for Miscanthus. Oxygen is determined by difference.

Table 6. Elemental Analysis of Miscanthus Biomass

Carbon (%)	Hydrogen (%)	Nitrogen (%)	Sulfur (%)	Oxygen (by difference, %)
47.65	5.62	0.66	<0.022	46

The structural (Cellulose and Hemicellulose) carbohydrate compositions of two grass samples were determined by High Performance Anion Exchange Chromatography with Pulsed Amperometric Detection (HPAEC-PAD). The wood samples were air-dried, milled, sieved, solvent extracted with Dichloromethane and acid hydrolyzed prior to analysis. Results, reported on an extractives free oven dry weight basis, are summarized in Table 7 below. The bulk of the Glucan is derived from Cellulose. Depending on species, some Glucan may be associated with Hemicelluloses, as in Glucomannans. The Arabinan, Galactan, Xylan and Mannan are derived from the Hemicelluloses.

Table 7. Carbohydrate Analysis of Miscanthus

	Arabinan (wt.%)	Galactan (wt.%)	Glucan (wt.%)	Xylan (wt.%)	Mannan (wt.%)	Carbohydrates (wt.%)
Replicate 1	1.98	0.68	40.17	14.85	<0.01	57.68
Replicate 2	2.00	0.69	41.33	15.20	<0.01	59.22
Average	1.99	0.68	40.75	15.03	<0.01	58.45
Std. Dev.	0.01	0.00	0.82	0.25	na	1.09
%RSD	0.71	0.61	2.01	1.68	na	1.87

The miscanthus biomass has no Manan and higher Xylan relative to pine. The total carbohydrate content is similar to that of pine. The acid insoluble lignin compositions were determined gravimetrically from the acid hydrozylates prepared for the carbohydrate determinations. The acid soluble lignin compositions were determined by measuring the absorbance of filtered aliquots of the acid hydrozylates at 280nm in a UV-VIS spectrophotometer. The ash content was determined gravimetrically after combusting the samples at 525^{o}C. Results are reported in Table 8 on an oven dry solids basis.

Table 8. Lignin and Ash Analysis of Miscanthus Biomass

	Acid Insoluble Lignin (wt.%)	Acid Soluble Lignin (wt.%)	Total Lignin (wt.%)	Ash (wt.%)
Replicate 1	21.17	2.62	23.80	3.48
Replicate 2	21.28	2.59	23.87	3.43
Average	21.23	2.60	23.83	3.46
Std. Dev.	0.08	0.03	0.05	0.04
%RSD	0.36	1.02	0.21	1.06

RSD: Relative Standard Deviation
Na: not applicable

The results above show that the Miscanthus biomass has ~48% carbon, ~6% hydrogen, ~0.7% nitrogen, and 46% oxygen. The biomass has 59% carbohydrate, 24% lignin, and approximately 3.5% ash. These results are fairly typical for this type of feedstock, which tends to have higher nitrogen, higher sulfur, higher ash, and lower lignin relative to softwood.

2.3 Corn Stover Biomass

Battelle acquired Corn Stover from a local farm (see Figures below) for the project. This biomass was received and analyzed, milled and sieved to particle size of approximately 2mm and used in the program.

Figure 10. Corn field just northwest of Columbus, Ohio

Figure 11. Corn Stover removal

Figure 12. Corn Stover loaded on vehicle

Figure 13. Corn Stover being fed to the harvester

Figure 14. Corn Stover after being processed in the harvester

In addition to the corn stover biomass collected above, Battelle also received a 500 lb. bale of corn stover from a local Ohio farm. See Figure 15 below. This bale, along with the corn stover harvested during Q4 of FY12, was used to produce intermediate bio-oil for analysis.

Figure 15. Bale of corn stover received from local Ohio farm

Figure 16. Laboratory scale grinder to be used for corn stover

The corn stover was also milled using the grinder shown above in Figure 15 and sieved to a particle size ranging from 1/8 “ to ½” with some lengths approaching 1” as shown in Figure 16 and Figure 17.

Figure 17. Milled and sieved corn stover

Figure 18. Particle size distribution for corn stover is in the range of 1/8" to ½" with some lengths approaching 1"

The structural (cellulose and hemicellulose) carbohydrate compositions of the corn stover biomass samples were determined by High Performance Anion Exchange Chromatography with Pulsed Amperometric Detection (HPAEC-PAD). The samples were air-dried, milled, sieved, solvent extracted with Dichloromethane and acid hydrolyzed prior to analysis. Results, reported on an extractives free oven dry weight basis, are summarized in Table 9 below. The lignin and ash content of the samples are shown in Table 10.

Table 9. Cellulose and Hemicellulose Content of Corn Stover Biomass Sample

	Arabinan (wt.%)	Galactan (wt.%)	Glucan (wt.%)	Xylan (wt.%)	Mannan (wt.%)	Carbohydrates (wt.%)
Replicate 1	2.63	1.09	37.80	15.81	<0.01	57.32
Replicate 2	2.70	1.17	37.41	15.59	<0.01	56.87
Average	2.67	1.13	37.60	15.70	<0.01	57.10
Std. Dev.	0.05	0.06	0.27	0.15	na	0.32
%RSD	1.98	4.98	0.72	0.99	na	0.56

Table 10. Lignin and Ash Content of Corn Stover Biomass Sample

	Acid Insoluble Lignin (wt.%)	Acid Soluble Lignin (wt.%)	Total Lignin (wt.%)	Ash (wt.%)
Replicate 1	16.75	3.30	20.06	3.99
Replicate 2	16.68	3.38	20.05	4.13
Average	16.72	3.34	20.06	4.06
Std. Dev.	0.05	0.05	0.00	0.09
%RSD	0.31	1.50	0.01	2.34

The corn stover is higher in ash content but significantly lower in lignin content when compared to the pine biomass samples and also higher in ash content and lower in lignin content when compared to miscanthus, but to a lesser degree.

2.4 Biomass Drying

In general, biomass has approximately 20% to 50% moisture. Biomass is dried prior to use in Battelle's pyrolysis systems to approximately 5%-10% moisture content. For the 50 lb/day pyrolysis system, the biomass dryer is a forced air convection oven purchased from Cascade TEK, model number TFO 10 (5,300 W). The oven is designed to operate within a temperature range of 5º C above ambient to 260º C and contains an independent over temperature controller to prevent overheating. Wet biomass is manually loaded onto twelve aluminum trays which are then placed in the oven to dry. The oven is generally set at a temperature of 90-110°C during the drying cycle. Drying times are on the order of 1-3 hours to achieve biomass moisture contents below 5%. Figure 19 shows a photograph of the biomass being loaded into the dryer. Moisture measurement is shown in Figure 20.

Figure 19. Biomass being loaded into Cascade TEK dryer

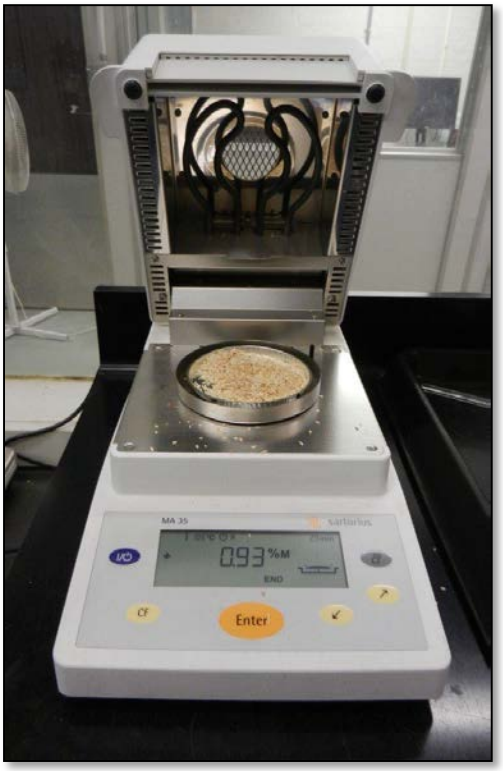

Figure 20. Biomass moisture measurement

3.0 Task B: Production of Intermediate Bio-Oil

The purpose of this task is to supply intermediate bio-oil for catalyst development for upgrading (Task C), integrated upgrading and hydrocarbon fuel production (Task D), corrosion testing and analysis (Task E), and 1,000 hour trial (Task F).

3.1 Biomass pyrolysis system

Over 14 separate bio oil production trials were conducted to produce bio oil for hydrotreatment. Two different biomass pyrolysis systems were used:

3.1.1 Battelle's 50 #/day bench scale pyrolysis system:

Approximately 1 gallon per day of intermediate bio-oil can be produced using Battelle's pilot scale ex-situ catalytic pyrolysis system (50 pounds of biomass per day). The pyrolysis system is an auger-based technology that thermochemically converts biomass feedstock into vapor phase. This pyrolysis system was purchased from ABRI-Tech based in Namur, Quebec, Canada. This system uses steel shot to pyrolyze the biomass in a horizontally configured auger system. The pyrolysis vapor is directed to an ex-situ catalytic reactor before it is condensed to form a bio oil. We have developed several types of ex situ vapor phase catalysis reactors, including (moving and fixed) packed bed reactors, catalyst- coated ceramic monolith type reactors, catalyst-coated ceramic foam type reactors and a novel moving bed reactor. The latter is a proprietary Battelle design which mechanically moves granular catalyst and contacts it with the pyrolysis vapor. Our data has shown that our downflow catalytic reactor has more flexibility compared to the other reactor designs: it is more resistant to coking and carbon accumulation, does not plug up, performs well with our 50 pounds of biomass per day auger based system, and provides easy in-situ catalyst regeneration. We are primarily using the moving bed reactor in the present program. Our condenser train features two single pass counter flow 'shell and tube' condensers and a wet electrostatic precipitator. We set our condensation conditions such that the bulk vapor phase temperature is in the range of 70^{o}C to 90^{o}C downstream of the first condenser. The second condenser is set to very low temperature, approximately 3^{o}C and the electrostatic precipitator operates at ambient temperature. We find that under these conditions, a relatively heavier oil phase condenses in the first condenser, an aqueous phase condenses in the second condenser and a relatively lighter oil phase is recovered in the electrostatic precipitator. Other co-products from the process include non-condensable gas (CO, CO_2, H_2, and light hydrocarbons) and a carbon rich char.

The intermediate bio-oil product was evaluated for water content, density, viscosity, elemental composition, acid content, and functional groups using NMR to determine extent of deoxygenation. The non-condensable gas stream was monitored online for carbon monoxide (CO), carbon dioxide (CO_2), and oxygen (O_2). Periodic GC samples were also taken of the non-condensable gas stream to monitor for hydrogen (H_2) and light hydrocarbons in addition to CO, CO_2, and O_2. Different feedstocks (pine, miscanthus and corn stover), reaction conditions (temperatures and residence time), and catalysts were studied for their effect on intermediate bio-oil properties. Table 11 summarizes the operating conditions of the catalytic pyrolysis system, including biomass feedstocks, feed rates and temperatures.

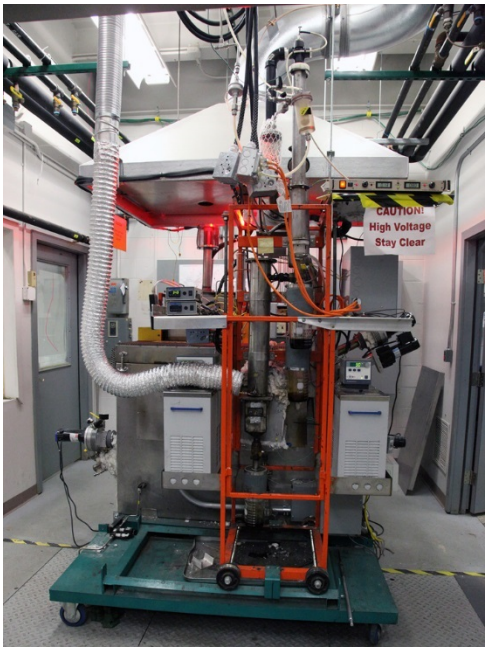

Figure 21. Photograph of the 50 lb/day catalytic pyrolysis system.

Table 11. Operation conditions of the 50 lb/day catalytic pyrolysis system

Conditions	Ranges
Temperature	450-550 ^{o}C
Biomass supply	White Pine, Miscanthus, corn stover
Sweep gas	Nitrogen, 2-3 slpm
Biomass feed rate	1.5 to 2.0 lbs/hr
Catalyst volume	1 to 1.2 liters
Catalyst pretreatment	Calcined for 2 hrs at 600 ^{o}C
Sampling	Solid, liquid, and gas samples
Product analysis	Water content, elemental composition, density, viscosity, total acid number (TAN), NMR, GC-MS

Commercial catalysts were used for the vapor phase catalytic reactor and included spent Fluid Catalytic Cracking (FCC) granular catalyst and a mixture of spent FCC and zeolite HZSM-5. Runs were conducted with four different forms of spent FCC catalyst 1) non-calcined spent FCC catalyst (as received), 2) calcined spent FCC catalyst (calcined in a box furnace for 2 hours at 600^{o}C), 3) in-situ calcined spent FCC catalyst (calcined in the vapor phase catalytic reactor), and 4) a mixture of 80 wt% spent FCC and 20 wt% HZSM-5.

3.1.2 Battelle's 1 ton/day truck-mounted system

In addition to the catalytic pyrolysis runs, fast pyrolysis runs were also conducted using Battelle's 1 ton/day truck-mounted system. This system features Battelle's proprietary down flow reactor technology which has the advantages of requiring no carrier gas, lower parasitic losses and self-sustaining operation in which the energy required for pyrolysis is supplied by char combustion.

Multiple campaigns were conducted over this project to produce intermediate bio-oil for Task C, Task D, and Task E. These campaigns are summarized in the following:

1. The first campaign was conducted on December 30, 2011 and January 4, 2012 to optimize the catalytic pyrolysis system on pine biomass feed using a new vapor phase catalytic reactor based on the Battelle's concept. This campaign produced approximately 1.7 pounds of bio-oil (~0.6 liters) from a total of 6.2 pounds of pine biomass processed. Pine biomass was dried to 2% moisture and fed to the pyrolysis reactor at the rate of 1½ to 2 lbs./hr. A mixture of 80 wt% calcined spent FCC and 20 wt% HZSM-5 catalyst was used in the vapor phase catalytic reactor.
2. The second campaign was conducted February 29, 2012 to evaluate in situ catalyst regeneration. This campaign produced approximately 1.6 pounds of bio-oil (~0.6 liters) from a total of 4.5 pounds of pine biomass processed. Pine biomass was dried to 2% moisture and fed to the pyrolysis reactor at the rate of 1½ to 2 lbs./hr. Uncalcined spent FCC catalyst (as received) was used in the vapor phase catalytic reactor.
3. The third campaign was conducted March 30, 2012 to April 11, 2012 to produce pine bio-oil for the hydrotreater. This campaign produced approximately 17 pounds of bio-oil (~6.3 liters) from a total of 60 pounds of pine biomass processed. Pine biomass was dried to 1-3% moisture and fed to the pyrolysis reactor at the rate of 1½ to 2 lbs./hr. Calcined, spent FCC was used in the vapor phase catalytic reactor.
4. The fourth campaign was conducted June 7, 2012 to June 13, 2012 to produce pine bio-oil for the hydrotreater. This campaign produced approximately 7.7 pounds of bio-oil (~2.9 liters) from a total of 27 pounds of pine biomass. Pine biomass was dried to <2% moisture and fed to the pyrolysis reactor at the rate of 1½ to 2 lbs./hr. Calcined, spent FCC was used in the vapor phase catalytic reactor.
5. The fifth campaign was conducted June 22, 2012 to June 27, 2012 to produce pine bio-oil for the hydrotreater. This campaign produced approximately 16 pounds of bio-oil (~6 liters) from a total of 52 pounds of pine biomass. Pine biomass was dried to 1-3% moisture and fed to the pyrolysis reactor at the rate of 1½ to 2 lbs./hr. Calcined, spent FCC was used in the vapor phase catalytic reactor.
6. The sixth campaign was conducted July 10, 2012 to July 13, 2012 to optimize the catalytic pyrolysis system on miscanthus biomass feed. This campaign produced approximately 4.6 pounds of bio-oil (~1.7 liters) from a total of 18 pounds of miscanthus biomass. Miscanthus biomass was dried to <2% moisture and fed to the pyrolysis reactor at the rate of 1½ to 2 lbs./hr. Calcined, spent FCC was used in the vapor phase catalytic reactor.
7. The seventh campaign was conducted July 19, 2012 to July 26, 2012 to produce pine bio-oil for the hydrotreater. This campaign produced approximately 17 pounds of bio-oil (~6.3 liters) from a total of 58 pounds of pine biomass. Pine biomass was dried to <2% moisture and fed to the pyrolysis reactor at the rate of 1½ to 2 lbs./hr. Calcined, spent FCC was used in the vapor phase catalytic reactor.
8. The eighth campaign was conducted July 27, 2012 to July 31, 2012 to optimize the catalytic pyrolysis system on miscanthus biomass feed. This campaign produced approximately 4.5 pounds of bio-oil (~1.7 liters) from a total of 19 pounds of miscanthus biomass. Miscanthus biomass was dried to <2% moisture and fed to the pyrolysis reactor at the rate of 1½ to 2 lbs/hr. Calcined, spent FCC was used in the vapor phase catalytic reactor.
9. The ninth campaign was conducted August 2, 2012 and August 14, 2012 to August 17, 2012 to support hydrotreater catalyst development. This campaign produced approximately 7.4 pounds of bio-oil (~2.8 liters) from a total of 30 pounds of pine biomass. Pine biomass was dried to <2% moisture and fed to the pyrolysis reactor at the rate of 1½ to 2 lbs./hr. Calcined, spent FCC was used in the vapor phase catalytic reactor.
10. The tenth campaign was conducted to produce intermediate bio-oil for catalyst studies at PNNL and hydrotreater optimization. This campaign produced approximately 50 pounds of intermediate bio-oil (~19 liters) from pine biomass using FCC catalyst. The pine biomass was dried to <3% moisture and fed to the pyrolysis reactor at the rate of 1½ lbs/hr.
11. The eleventh campaign was conducted to produce non-catalytic bio-oil for catalyst studies at PNNL. This campaign produced approximately 4 pounds of non-catalytic bio-oil (~1.6 liters) from

pine biomass. Pine biomass was dried to <2% moisture and fed to the pyrolysis reactor at the rate of 1½ lbs./hr.

12. The twelfth campaign was conducted to produce intermediate (catalytic) bio-oil from pine biomass to support catalyst development in Task C in Q2FY13. A sufficient amount of intermediate (catalytic) bio-oil was also produced to support hydrotreater development (Task D) and corrosion analyses (Task E).
13. The thirteenth campaign was conducted to produce intermediate bio-oil from corn stover. This campaign produced approximately 2.4 pounds of intermediate bio-oil (~0.9 liters) from corn stover biomass using Fluid Catalytic Cracking (FCC) catalyst. Corn stover biomass was dried to <2% moisture and fed to the pyrolysis reactor at the rate of 1½ lb./hr.
14. The fourteenth campaign was conducted to produce catalytic pyrolysis bio oil to finally assess the benefit of using catalytic bio oil vs non catalytic bio oil during hydrotreatment. This run was conducted in Q4FY14.
15. The fifteenth campaign was conducted to produce regular pyrolysis bio oil for the 1,000 hr. run. Bio-oil was produced using Battelle's 1-Ton-Per-Day (TPD) pyrolysis system. The pyrolysis temperature was between 450°C and 500°C. The feedstock was pine saw dust with a particle size between 2 to 5 mm. The yield was approximately 65-70%. The bio-oil was filtered via a two filter system. The first filter was inline during bio-oil production just after condensation (10 micron) and the other was ex-situ (0.8 micron and conducted at high pressure up to 80 psi).

Table 12. Example data for intermediate bio-oil for hydrotreatment

Run ID	Run Time (min)	Feedstock	Feed Amt (lbs)	Feed Moisture %	Type of Catalyst	Avg Pyro Temp (°C)	Avg VPR Temp (°C)
J221	289	White Pine	7	2.9	Calcined FCC	476	518
J251	479	White Pine	13	1.6	Calcined FCC	480	517
J261	655	White Pine	18	1.5	Calcined FCC	480	520
J271	542	White Pine	14	1.5	Calcined FCC	483	520
U101	220	Miscanthus	6	1.5	Calcined FCC	485	519
U111	216	Miscanthus	6	1.6	Calcined FCC	480	521
U311	208	Miscanthus	6	1.2	Calcined FCC	481	518
3 Runs	54 to 256	Corn Stover	1 to 6	1 to 1.6	Calcined FCC	476 to 525	

3.2 Bio-oil product analyses

For campaigns 1-14, bio-oil is collected in three condenser stages, condenser 1 (C1), condenser 2 (C2), and electrostatic precipitator (C3). The general operational strategy is to maintain the temperature between C1 and C2 below 100C to reduce the amount of water that condenses in C1. C2 is operated at 3C which causes significant condensation and collection of water in the second condenser. The electrostatic precipitator is operated at ambient temperature (~20C) to capture bio-oil aerosol particles. Figure 22 shows that fairly dry oil is collected in C1 and C3 and a transparent aqueous phase is collected in C2.

The water content in C1 and C3 ranges from 5% to 33% and in C2 averages around 70%. The liquid collected in C2 is not miscible with the product collected in C1 and C3; however C1 and C3 are miscible

with each other. Total liquid yields using spent FCC catalyst is fairly consistent and generally ranges from 44% to 49%.

Use of FCC catalyst in the vapor phase catalytic reactor also significantly reduces the liquid product viscosity, the Acid Value, and the Hydroxyl value of the bio-oil. With conventional non-catalytic pyrolysis, the Acid Value is approximately 100, and the Hydroxyl Value is approximately 400. With FCC vapor phase catalysis, the Acid Value drops to approximately 30 to 40, and the Hydroxyl Value drops to an average of 250.

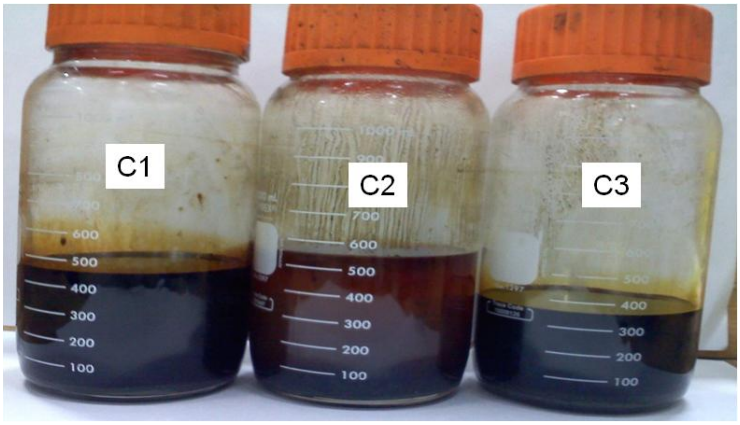

Figure 22. Bio oil collected in three stages, condenser 1 (C1), condenser 2 (C2), and electrostatic precipitator (C3).

For most of the above campaigns, the bio-oil was filtered with 0.45 µm nylon filter media using a Millipore pressure filtration system prior to using the bio-oil as a feedstock in the hydrotreater or for catalyst development. The pressure filtration was conducted up to 60°C and at pressures ranging from 10 psi to 50 psi. The bio-oil filtration flow rate averages 30 g/min at ΔP= 35 psig and T= 50°C.

3.3 Bio-oil molecular weight characterization by Gel Permeation Chromatography (GPC):

The bio oil produced in Run #12 was evaluated by GPC. The bio-oil weight average molecular weight ($\overline{M}_w$) and number average molecular weight ($\overline{M}_w$) was determined by gel permeation chromatography (GPC). This was accomplished by dissolving the bio-oil samples in THF (3.0 mg/mL) and then analyzed by GPC.

Molecular weight determination was conducted using a Polymer Standards Service (PSS) GPC SECurity 1200 system equipped with four Waters Styragel columns (HR0.5, HR2, HR4, HR6) at 30°C, an Agilent isocratic pump, Agilent auto-sampler, Agilent degasser, Agilent refractive index (RI) detector, and Agilent UV detector (270 nm) using THF as the mobile phase (1.0 mL/min) with injection volumes of 35 µL.

The molecular weight of the bio-oil samples was determined using a relative calibration curve. The calibration curve was created by fitting a second order polynomial equation to the retention volumes obtained from a series of narrow molecular weight distribution polystyrene standards (7.21 x 10^3, 4.43 x 10^3, 2.17 x 10^3, 1.11 x 10^3, 0.58 x 10^3 g/mol), phenol (94 g/mol), and acetone (58 g/mol). The curve fit had an R^2 value of 0.9941.

Table 13 summarizes the characterization results of the bio-oil. The molecular weight distribution (index of polydispersity, PDI) was obtained by dividing M_w by M_n. The intermediate bio-oil appears to contain some lower molecular weight components that the GPC graph detected as a peak that overlapped with another

low molecular weight component. Because the two main peaks overlapped with each other, it is not possible to accurately integrate the two peaks independently, therefore the molecular weight of the bio-oil was calculated based on the integration of whole sample. Figure 23 below shows the molecular weight distribution of the intermediate bio-oil and the overlap of the two peaks.

Table 13. GPC characterization results of three bio-oil samples.

Sample	M_w (g/mol)	M_n (g/mol)	PDI = M_w / M_n
intermediate bio-oil	326	143	2.28

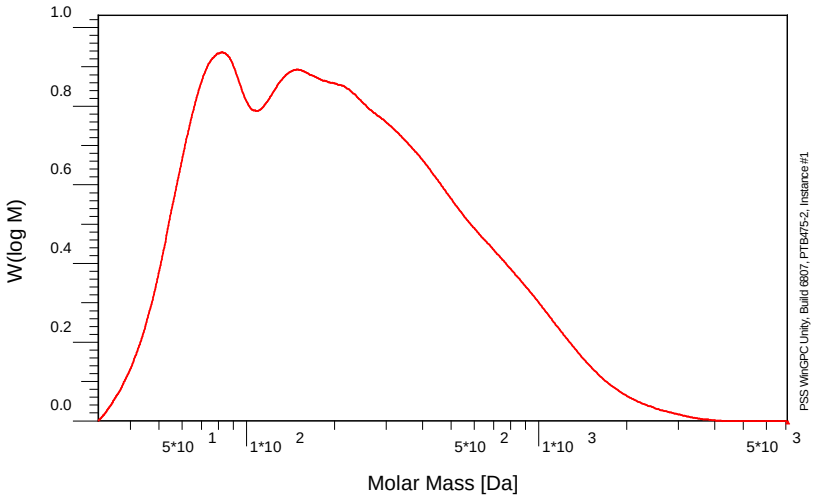

Figure 23. Molecular weight distribution of intermediate bio-oil

3.4 Effect of ex situ vapor phase catalysis

Table 14 summarizes the elemental analysis results for bio-oil produced from pine biomass with and without use of FCC catalyst. As shown in Table 14, the catalyst increases carbon concentration in dry bio-oil, promotes de-oxygenation of bio-oil (water formation) and decreases the acidity of bio-oil (conversion of carboxylic acid to esters and other components). Based on the elemental composition, the empirical formulation of catalytic and non-catalytic bio-oil is respectively: $C_{12}H_{12.5}O_{2.8}$ and $C_{12}H_{16.4}O_{5.5}$. There is a considerable decrease in oxygen content.

Table 14. Elemental composition of non-catalytic and catalytic bio-oil made with pine biomass

	C (wt%)	H (wt%)	N (wt%)	S (wt%)	O (wt%)	Water (wt%)	TAN	H/C Ratio	H/C Ratio (corrected for H2O)	Empirical Formula
Non-catalytic bio-oil	51.6	7.1	0.1	0.005	41.2	11	110	1.65	1.37	$C_{12}H_{16.4}O_{5.5}$
Spent FCC catalytic bio-oil	58.6	7.1	0.0		34.3	18	75	1.45	1.04	$C_{12}H_{12.5}O_{2.8}$

4.0 Task C: Catalyst Development for Upgrading Intermediate Bio-Oil

4.1 Catalyst Development and Testing using Model Compounds and Small Scale Trials:

Under this task, model compounds were first used to identify non carbon supported metal catalysts with low coke formation

A Ru/TiO_2 bifunctional catalyst with both metallic and acidic active was selected. This catalyst showed much higher deoxygenation activity than catalysts with only metallic active sites. The final products of HDO of oxygen-containing model compounds on the catalyst were a mixture of hydrocarbons, instead of a mixture of hydrocarbon and alcohols produced by metal alone. This catalyst showed good stability and there was no deactivation of HDO activity during a 220 hour stability test. A non carbon TiO_2 support with sufficient surface area was also selected. The non carbon based support can allow for oxidative or reductive de carbonization without support deterioration.

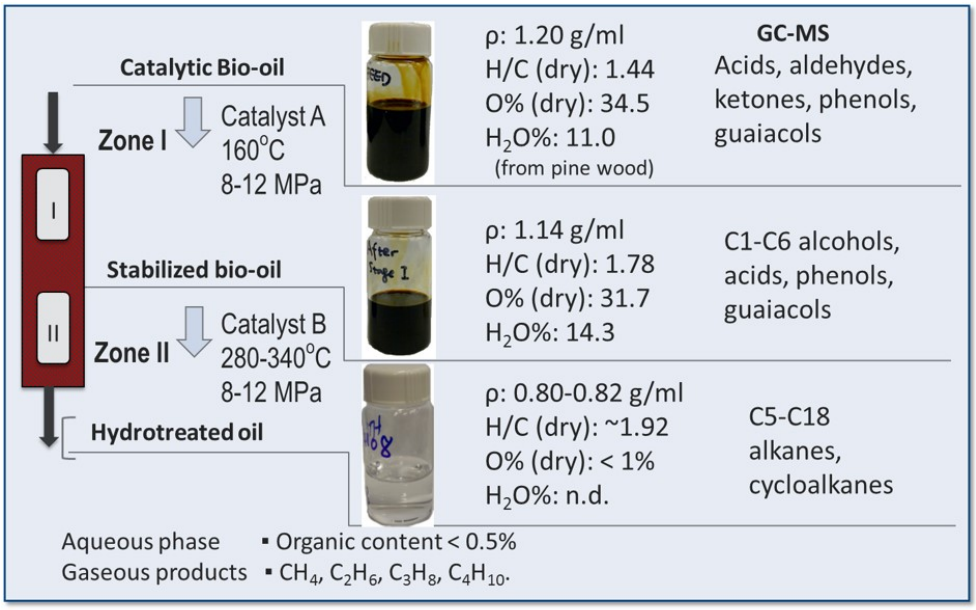

Figure 24. Performance of Zone I and Zone II bi functional catalysts

Figure 24 (above) shows the performance of the Zone I and Zone II catalysts when used for bio oil hydrotreatment. The Zone I, non carbon supported metal catalyst is effective in converting the aldehydes and ketones to alcohols. The Zone II catalyst is also a non carbon supported metal catalyst, but has additional acidity incorporated in it, which makes it effective at hydrogenation and cracking. These catalysts have a low coking rate and were used for more than 200 hrs. TOS before deactivation was noted. We were also successful in decoking these catalysts using H_2 and diluted O_2.

5.0 Task D: Integrated Upgrading and Hydrocarbon Fuel Production

5.1 Fabrication and Commissioning of Hydrotreaters (Battelle Cost Share):

An integrated upgrading pilot hydrotreatment system was designed and built. Battelle Laboratory facilities were modified to accommodate the upgrader. An extensive hazard analysis was conducted and the recommendations were implemented. Since H_2 is used at 2,000 PSIG, a powerful ventilation system was installed. This system consists of a complete enclosure around the skid, a hood and a dedicated fan. Battelle's cost share funds were used for this task. Figure 25 shows the hydrotreater system as installed at Battelle Columbus.

Figure 25. Front and Rear views of the Battelle Hydrotreatment System, shown fully installed with ventilation system and enclosure

The reactor has two heating zones, a low temperature zone for bio oil stabilization and a higher temperature zone for hydrogenation / cracking. The temperature in the zones is maintained by two molten salt baths. Figure 26 is a schematic of the hydrotreater reactor and shows the location of the heating zones and the internal reactor thermocouples. The active reactor volume in the heated zones is approximately 300 ml.

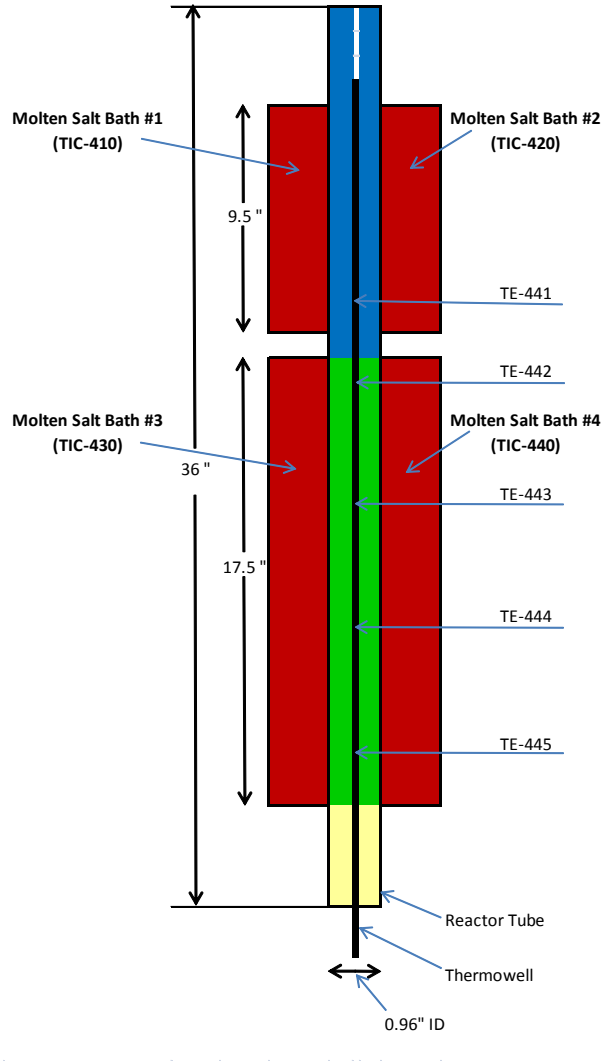

Figure 26. Schematic of reactor temperature zones

In addition to the above, large hydrotreater which has the capacity to produce approximately ½ gallon of product per day, a smaller hydrotreater was also built for rapid catalyst screening and testing. The operating cost of the smaller hydrotreater are also significantly lower than that of the larger unit. This hydrotreater has a production capacity of 200 ml/day.

Figure 27 shows a diagram of the smaller hydrotreater. The test rig consists of four sections:

a) Gas distribution: This section feeds H_2 and N_2 at high pressure. The flow is controlled with mass flow controllers (flow rate range: 50- 2000 ml/min)
b) Liquid distribution: In this section bio-oil is injected in the reactor with a high pressure pump (flow rate range: 0.001-100ml/min)
c) Reactor: This is a 316 stainless tube with 0.5 inch OD, 0.045 inch wall thickness and equipped with a thermo-probe that has 6 thermocouples
d) Sampling system: This section consists of a back pressure regulator, 150 ml liquid receiver and series of valves to bypass the reactor during liquid sampling and/or gas sampling for gas chromatography (GC).

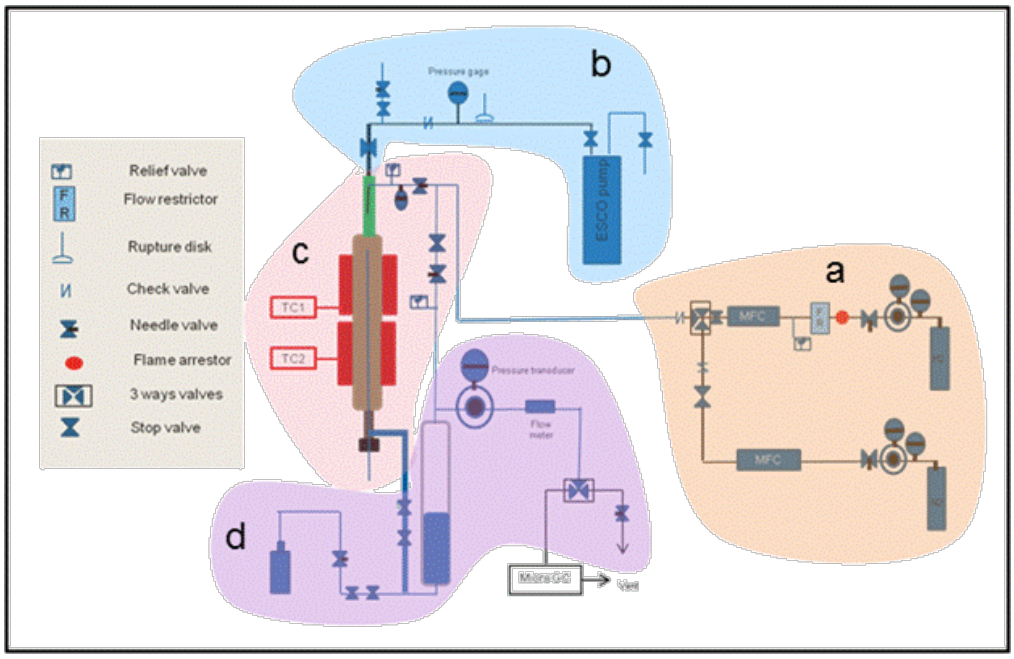

Figure 27. Mini hydrotreatment System at Battelle Columbus

5.2 Development of a catalyst regeneration method:

Catalyst deactivation, and bed plugging because of coking is a known problem during hydrotreatment of bio oil. Coke removal can be accomplished via oxidation or reduction, and in order to use these methods, a non carbon supported, Ru/TiO_2 catalyst was developed. This catalyst was described in the previous section. In this project, a method was developed to de coke and regenerate this catalyst after use. This method can be summarized by the following steps:

1. Remove loosely bound carbon via rinsing with solvent. The fouled catalyst is first rinsed with solvent to remove un reacted bio oil and soluble organic material before decoking. This is accomplished by first reducing the temperature to ambient and then de pressurizing the reactor down to atmospheric pressure. Following cool down and depressurization, the reactor is flushed with acetone or methanol. Following flushing with solvent, the reactor is dried by nitrogen.
2. Remove bound carbon (coke) via chemical reaction. Following rinsing, the catalyst is exposed to an excess of hydrogen at ~350C to 380C and this process is continued until production of CH_4 is reduced to a few ppm level. This process completes regeneration.

The procedure described above was tested with hydrotreatment of bio oil. The bio-oil used in this run was produced using Battelle's one ton per day pilot plant and filtered via a 1 micron filter. The pyrolysis reaction conditions were: biomass (pine sawdust with moisture content approximately 10%) and pyrolysis temperature of 480°C to 520°C.

Hydrotreatment of this bio-oil was performed at a LHSV of 0.2, H_2/bio-oil volume ratio of 4,000:1, and pressure of 1,700psi.

The hydrotreatment catalyst was divided into two zones. Catalyst in Zone I consisted of Ru/TiO2, and catalyst in Zone II was Ru/TiO2 blended with ZSM5. The temperature of Zone I was 160°C and of Zone II was 320°C. After 50 hrs time on stream (TOS) the catalysts were regenerated with H_2 as per the procedure described above. This was repeated for 5 cycles. Figure 28 reports the density of the organic phase as a function of time on stream after each regeneration cycle with methanol rinsing and reduction with hydrogen at 380°C.

The following observations were made:

1. The initial catalyst activity is recovered completely up to 4 cycles and partially on cycle 5.
2. The pressure drop across the reactor remains the same for all cycles. This indicates that there is no plugging of the reactor, even with catalyst being partially active after cycle 5.
3. The products obtained from all the cycles have two phases: a light organic phase and an aqueous phase.

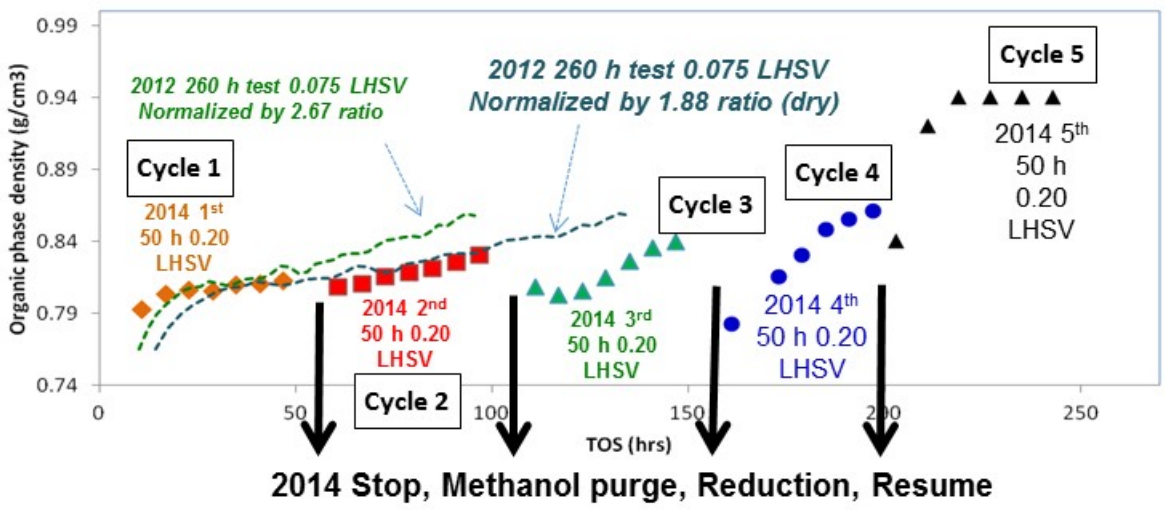

Figure 28. Organic phase density on fresh and regenerated catalysts for 5 cycles

Figure 28 shows the evolution of organic phase density variation for 5 cycles of hydrotreatment. After each cycle, the reaction is stopped, the catalyst bed is rinsed with methanol and the catalyst is reduced. This catalyst cleaning procedure appears to recover the initial activity of the catalyst, however the rate of deactivation increases during each successive cycle, as shown by the increase of the slope of the organic density variation vs. TOS.

5.3 Characterization of the catalyst to determine its deactivation mechanism

5.3.1 Formulation and evaluation of hypotheses for catalyst deactivation

To investigate the deactivation mechanisms of the catalyst, we developed several hypotheses for the phenomena, and then tested these hypotheses against characterization data of the catalyst. The following hypotheses for catalyst deactivation were evaluated:

1. There is residual carbon left on the catalyst after regeneration with hydrogen. This residual carbon plugs the active sites on the catalyst, and accumulates from cycle to cycle, thus decreasing the activity.
2. Ru metal is lost either by methanol washing or under reaction conditions. The loss of Ru results in reduction of activity.
3. Ru sintering by agglomeration: under reaction conditions (high pressure, high temperature, and presence of water) Ru can agglomerate and lose its dispersion.
4. Ru poisoning with heteroatoms: Ru is poisoned by metals or other heteroatoms carried by the bio oil.
5. Decomposition of ZSM5 structure due to presence of water. This would lead to loss of surface area and pore volume. This results in catalyst deactivation.
6. There is significant loss in the acidity of the catalyst. This results in catalyst deactivation.

The detailed catalyst characterization was conducted and is summarized and ranked as shown in Table 15 below. The ranking shows that the most likely cause of catalyst deactivation after five cycles of regeneration is accumulation of heteroatoms on the Ruthenium. The poisoning by the heteroatoms can explain the significant loss of activity, as well as the loss in acidity of the catalyst. There also is some loss of Ruthenium due to either leaching or agglomeration; however, this appears to be secondary to poisoning by heteroatoms from the perspective of loss of activity. There is some decomposition of the ZSM5 structure, but this is also not large enough to explain fully the significant loss in activity.

Table 15. Catalyst deactivation mechanisms ranked by order of importance

Rank	Hypothesis	Justification
1	4: Ru poisoning by heteroatoms	ICP data clearly shows heteroatoms on catalyst.
2	2: Ru lost by washing or reaction	ICP data shows some loss of Ru, but not sufficient to justify loss of activity.
2	3: Ru agglomeration	TEM analysis conducted previously did not show agglomeration, however chemisorption data indicates loss of dispersion. We presently are repeating the TEM analysis. Chemisorption data also may be showing the effect of heteroatom poisoning.
3	5: Decomposition of ZSM5 structure.	XRD shows presence of SiO_2, which can originate from ZSM5. BET area reduction indicates loss of ZSM5. However, the loss of ZSM5 is not sufficient to justify loss of activity.
4	6: Loss in acidity	There is some loss in acidity, but it does not appear to be sufficient to explain the significant loss in activity. The loss in acidity may be due to decomposition of ZSM5, or poisoning by heteroatoms.
5	1: Residual carbon on the catalyst	Our catalyst cleaning procedure can remove most of the carbon from the catalyst.

It is concluded that the most likely mechanism was poisoning of the catalyst due to heteroatoms carried through and deposited on to the catalyst with the bio oil. To confirm this conclusion, two synthetic bio oils, one without heteroatoms and one with heteroatoms, were prepared and hydrotreated. The heteroatoms were added at the same concentration as that in actual bio oil. It was demonstrated that the hydrotreatment catalyst was not deactivated when synthetic bio oil without heteroatoms was hydrotreated. However the hydrotreatment catalyst deactivated rapidly when synthetic bio oil with heteroatoms was hydrotreated.

5.4 Bio oil cleaning using Ion Exchange Media:

The bio-oil produced in Task B was processed with ion exchange media at 40°C and at atmospheric pressure in a slurry bed reactor. Figure 29 is a photo of the ion exchange system used to clean the bio-oil of heteroatoms.

Figure 29. Photo of ion exchange system

Table 16. Inorganic elemental concentration (ppm) by ICP analysis of bio-oil before and after inorganic removal by ion exchange batch reactor

Element	bio-oil filtered	Resin treated bio-oil at 40°C
Al	5.11	<3
Ca	17.98	<3
Fe	15.76	<3
K	57.24	6.02
Mg	5.05	<3
Na	3.83	2.80
Si	10.62	0.84
S	10.16	8.92

The concentration of the heteroatoms in the bio-oil before and after resin treatment are presented in Table 16, above. The concentration of inorganic species such as Al, Ca, Na, Mg, and Fe decreased to < 3.0 ppm, which is the detection limit for the analytical equipment. The concentration of potassium was 6 ppm, which is still very low. These results show significant removal of these inorganic compounds from the bio-oil using ion exchange. Unfortunately, the ion exchange process does not appear to significantly remove the sulfur. This sulfur does not appear to be present as a salt, and for this reason, could not be removed via an ionic exchange process.

Figure 30 is a NMR spectrum of the ^{1}H proton before and after resin treatment. There were no changes to the functional groups associated with the bio-oil. The two spectrums look identical. This indicates that with resin treatment the heteroatoms are reduced as shown in Figure 30 but there are no other significant chemical modifications to the bio-oil.

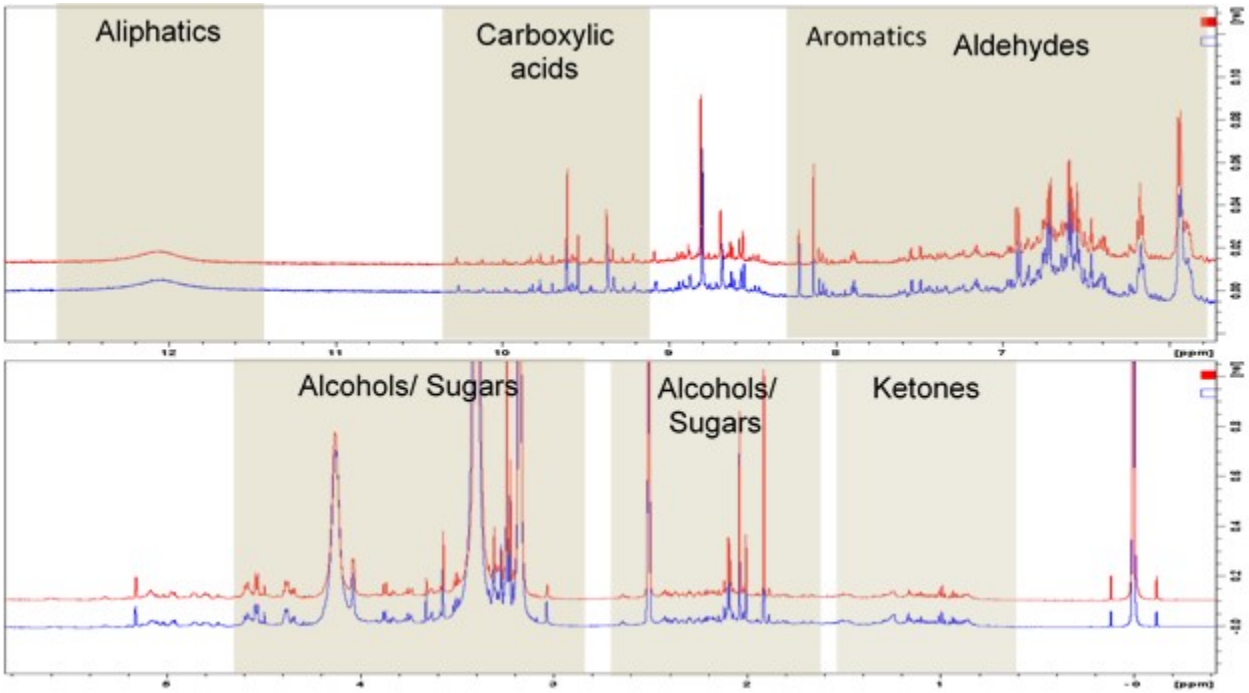

Figure 30. 1H NMR of bio-oil-methanol before (blue) & after (red) resin treatment of 'dirty' bio-oil at 40 °C. The resin treatment had no effect on the bio-oil as the functional groups were identical before and after resin treatment.

Conventionally, bio-oil hydrotreatment is done in a dual zone reactor. The first zone (Zone I) is intended for bio-oil stabilization, and the second zone (Zone II) is intended for hydrogenation and cracking. Generally, Zone I is operated at a lower temperature (~150 to 300 °C) and Zone II is operated at a higher temperature (~300 to 400 °C). Battelle's experience has been that in a dual zone reactor, significant axial heat transfer takes place from the higher temperature Zone II to the lower temperature Zone I. This results in excessively high temperatures in Zone I and poor temperature control, which can cause accelerated coking and catalyst deactivation. Also, it is not possible to characterize the post Zone I, stabilized bio-oil in a dual zone reactor. Characterization of the stabilized bio-oil is necessary at this stage of research into hydrotreatment. In addition, if a sulfided catalyst is used in Zone II and not in Zone I, then there is a risk that sulfur from Zone II will contaminate the catalyst in Zone I. To address these issues, Battelle elected to conduct bio-oil stabilization and hydrogenation/cracking separately in its hydrotreatment operation. This allowed better control of the operating conditions, including temperature and also characterization of the post Zone I stabilized bio-oil.

Given the above, the following process was selected for Task F, 1,000 hr. run. Bio oil from Battelle's pyrolysis system was first pressure filtered through a 0.2 micron filter. Following the filtration, the ion exchange process was used to clean the bio oil. Following the ion exchange process, the bio oil was blended with solvent and fed to Zone I hydrotreatment step. A solvent was used because Battelle used a high pressure syringe pump in their hydrotreater system. This pump does not have a stirring system, and because it is well known that bio oil tends to stratify, a solvent was used to keep the feed more uniform. Battelle confirmed that the solvent does not participate in Zone I reactions.

A Ru/TiO_2 catalyst was used in Zone I. Following Zone I, a sulfided Cobalt Molybdenum catalyst was used in Zone II.

6.0 Task E: Corrosion Testing and Analysis

6.1 Introduction

The objective of this task was to characterize the relative performance and susceptibility of different stainless steel alloys to corrosion in pyrolysis oil. This study involved a laboratory-scale investigation over a range of temperatures to mimic conditions as might be expected throughout a biomass upgrading system and specifically the hydrotreater portion of the process. These efforts will help move towards materials selection to ensure safety and performance at a minimum in terms of cost. Ultimately, this task culminated in a simplified model that can be used to make judgments about alloy suitability for a given set of operating and environmental conditions experienced in the upgrading process, as well as, general pyrolysis oil handling, transport, and storage. Additionally, this task highlighted and catalogued critical considerations in terms of metallurgical or environmental factors that operational engineers need to be aware to prevent potential materials failures should operation conditions or feedstock change dramatically. A combination of literature review and testing at both “low” and “high” temperature regimes was used to achieve the task’s objectives.

6.1.1 Pyrolysis Oil Composition and Compositional Space

An understanding of the compositional space that pyrolysis oils occupy is critical to successful materials selection. The composition of pyrolysis oils can vary widely with water, acid, and oxygen content depending on the exact feedstock and production parameters. Within our experiments and the literature, water content is reported to range from 14 percent to 50 percent and has a direct impact on how aggressive a bio-oil is to a metal surface with aggressiveness increasing with water content. Further, both increased temperature and oxygen content, which can be as high as 50 percent by mass, are associated with more aggressive conditions. The pH of bio-oils is typically between values of 2 and 3. This is an important consideration, as many materials will depassivate in acidic electrolytes. The acidic pH is due to the presence of carboxylic acid compounds, which vary depending on feedstock and processing. When these components segregate to the aqueous phase of the oil, conditions conducive to corrosion are created with contacting metal surfaces. The complexity of these systems makes the use of “realistic” surrogate test electrolytes for development of meaningful results difficult, especially given the outsized effect that small amounts of contaminants can have on overall susceptibility. Consequently, testing in “real” pyrolysis oil has a number of advantages for long-term performance prediction. Despite this, analysis has shown the primary components across a number of different pyrolysis oils and feedstock are formic and acetic acid; and materials selection for these systems can provide some guidance. There are ranges of organic acid concentrations in different pyrolysis oils. However, as an example, acetic acids can exist at concentrations on the order of 3.5 percent, while formic acids are typically present at lower concentrations and can be present at concentrations on the order 1.5 percent[i].

6.1.2 Environmental Variability within the Upgrading Process

Of central importance to whether a given materials will undergo attack are the reactions and interactions that occur in the hydrotreater as the pyrolysis oil undergoes upgrading. Materials selection is particularly challenging for this type of process in that conditions and chemical constituents change as a function of time and location within the reactor. This creates a gradient of conditions in which the entry point into the reactor may be the most aggressive in terms of oxygen, acid content, and water, while the lower portion of the reactor experiences the most extreme conditions in terms of temperature. A simplified schematic of the hydrotreater is shown in Figure 31. As shown, pyrolysis oil and H_2 gas are fed into the top of the reactor at rates of approximately 1 mL/min and 3.4 L/min, respectively. These components enter the reactor at a temperature of approximately 100ºC. The hydrotreater itself can be divided into two distinct regions, which contain different catalysts and operate at different temperatures. The top of the reactor is typically filled with a stabilization catalyst. Temperatures in this section range from approximately 100ºC to 250ºC. In the lower portion of the reactor a different catalyst is used that may contains sulfur species

as a component. Temperatures in this section can reach 450ºC. Throughout the reactor, pressures in the range of 1000 to 2,200 psi are maintained. From a corrosion engineering perspective this system contains not only highly aggressive species and water at elevated temperatures but may also present an H_2S corrosion risk through the presence of both H_2 and S species. This means that a wide range of different local environments and temperatures are experienced along the length of the hydrotreater and the selected material must be sufficiently resistant to the entire spectrum of conditions.

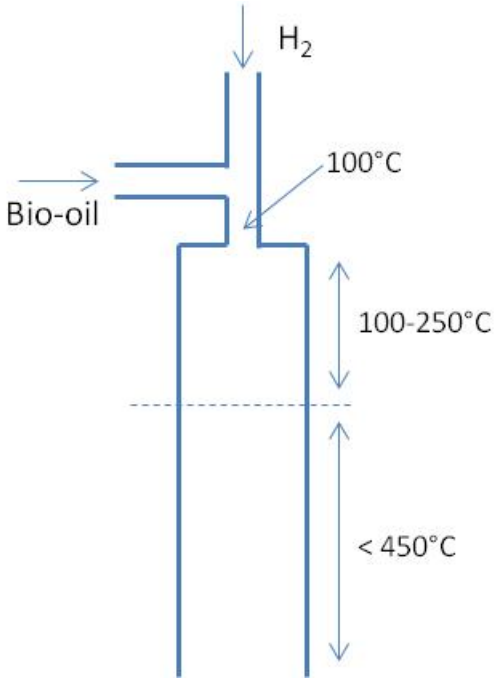

Figure 31. Simplified schematic of the hydrotreater.

6.1.3 Materials for Organic Acid Handling

Although pyrolysis oils are highly complex combinations of different acidic species some materials selection guidance can be taken from industrial environments used for processing and handling organic acids. In particular, materials used for corrosive species like acetic and formic acids that are prevalent in pyrolysis oil. Generically, stainless steels and nickel-based alloys are used in the bulk of organic acid production and handling activities. As the environmental severity increases there is a continuum of stainless steels with increasing alloy content (usually increasing amounts of Cr, Ni, and Mo) that can provide enhanced passivity. Stainless steels like 304L and 316L are the workhorses for organic acid production and handling with additional recommendations to use low carbon and stabilized grades for any application that requires exposure to organic acids at temperatures above 60ºC. High-nickel alloys including C-276 are recommended for in the most severe environments or to provide the highest margin for safety. The literature emphasizes that generalization assumptions of corrosiveness across organic acid environments is difficult and dangerous – small amounts of contaminants, changes in environment, or ratios of component acids can render otherwise passive materials highly susceptible to attack. Specifically, pH, chloride content, temperature and oxygen content can have a significant impact on corrosion[ii]. In the context of this work this means testing needs to be conducted in as realistic conditions as possible and sufficient safety margins need to be factored into the final materials selection to account for process variability.

6.1.4 Critical Metallurgical and Corrosion Issues for Consideration

The combination of high-temperatures and aggressive aqueous conditions can result in a number of different corrosion modes and failure mechanisms. In particular, for stainless steels failure may involve in isolation or combination both general and localized attack (chloride stress corrosion cracking (SCC),

pitting, intergranular, and sulfide-SCC). There have been few quality studies of corrosion in pyrolysis oils. However, one exception is work that was conducted at Oak Ridge National Laboratory, which determined that SCC can be an issue in low-Cr stainless steels exposed to bio-oil at moderately elevated temperatures such as 50°C[iii]. Although all alloys tested in this task are more heavily alloyed it is salient to note that SCC can be an issue in these systems.

Additionally, given that process temperatures may approach 450°C there are a number of metallurgical phenomena, including embrittlement and sensitization that must be recognized as their occurrence could result in rapid and catastrophic failure. Even if absolute operation temperatures do not reach 450°C it is important to be cognizant of these issues as they can occur in isolated areas around welds that may have experienced excess heat. An abbreviated, and by no means comprehensive, summary of some of these issues is provided below:

- **Sensitization** – Occurs when chromium carbides precipitate at grain boundaries after exposure to elevated temperatures. This effectively removes Cr from the surrounding matrix and results in areas adjacent to grain boundaries which are more susceptible to attack. The temperature at which this phenomenon occurs varies by alloy and the effect is largely confined to austenitic stainless steels.

- **475°C Embrittlement** – The formation of brittle second phases in the microstructure from heat treatment or prolonged exposure at elevated temperature leads to a decrease in toughness. Ferritic stainless steel alloys can become susceptible to this embrittlement from prolonged exposures to temperatures of approximately 350°C. The effect becomes more pronounced with increasing chromium content of the alloy.

- **Chloride SCC** – It is not expected that this mechanism will play a major role as chlorides are not expected to be present in the pyrolysis oils used in this study. However, chlorides can lead to failure at moderately elevated temperature at parts per million (ppm) concentrations. Given that small concentrations of chloride are essential for metabolic processes in plants and that atmospheric chloride and chlorides in water are ubiquitous, contamination of feedstock is within the realm of possibility.

- **Hydrogen Embrittlement** – This occurs when atomic hydrogen penetrates into the metal matrix leading to embrittlement. Hydrogen diffuses into the metal matrix and combines with carbon to form methane, which leads to voids, embrittlement, and cracking. The effect becomes less critical at higher temperatures and this effect increases with increasing hardness of the alloy.

- **Sulfide SCC** – Is a variant of hydrogen embrittlement in which S poisons the recombination of atomic hydrogen to form H_2 at the surface. This leads to increased quantities of atomic hydrogen that are available to diffuse into the matrix.

- **Microbial Induced or Influenced Corrosion (MIC) –** MIC is caused by the proliferation of microbial species, which produce or compound an aggressive environment. This is likely only an issue for relatively low temperatures and perhaps long-term storage of pyrolysis oil – this mode of attack is not likely critical for upgrading. MIC can be cause or enhance localized attack on 304 and 316 stainless steels.

6.2 Low Temperature Testing

Low temperature testing was used to identify corrosion rates and materials incompatibilities at temperatures as might be experienced in the handling, transport, or storage, of pyrolysis oil. Specifically, exposure experiments of coupons in actual pyrolysis oil were used to assess general corrosion rates and susceptibility to stress corrosion cracking.

6.2.1 Materials Selection

A range of stainless steels were chosen for evaluation including: 304L, 316L, 904L, 444, and 2205. Table 17 provides a summary of alloys, compositions, and other information for each alloy tested at low temperatures.

Table 17. Stainless steel alloys selected for low temperature pyrolysis oil exposures. Primary alloying additions, steel type, and maximum suggested use temperature are indicated.

Alloy	Type	Max T °C	Cr	Ni	Mo	Cu	Mn
304L	Austenitic	425	18-19	9-10			2.0
316L	Austenitic	425	17-17.5	12-13.5	2.5		2.0
904L	Austenitic	400	19-23	23-28	4-5	1-2	
444	Ferritic	320	17.5-19.5	1.0	1.8-2.5		1.0
2205	Duplex	320	22	5-6	3		0.7

Among alloys selected, were three austenitic steels with increasing general resistance to corrosive environments (304L, 316L, and 904L). These alloys generally have good corrosion resistance across a range of environments; however, they are known to be susceptible to SCC in the presence of chloride at ppm-type concentrations at elevated temperatures. Additionally, a ferritic stainless steel (444) and a duplex stainless steel (2205) were selected for testing. Both alloys are generally more resistant to SCC than austenitic stainless steel. An abbreviated summary of some of the advantages and disadvantages of each alloy in terms of corrosion resistance and metallurgy are described below:

- **304L** – 304L is assumed to have similar, but lower, corrosion resistance as 316L, especially in terms of pitting.
- **316L** – 316L is susceptible to sensitization if held for long periods of time at temperatures between 425°C and 800°C creating a risk for intergranular attack. The alloy is susceptible to chloride SCC at a few ppm Cl^- concentrations in combination with low pH, oxygen, and elevated temperature. Additionally, 316L is resistant to pure acetic acid but at high temperatures, pressures, and in the presence of formic acids will corrode.
- **904L** – 904L is in some ways a higher alloy content version of 316, but with greater resistance to SCC, pitting, and crevice attack. The higher alloying content means the risk of sensitization increases and the alloy is not recommended for long term use at temperatures above 400°C.
- **444** – 444 is more resistant to chloride SCC relative to 304 and 316, but can be susceptible to embrittlement at temperatures above approximately 340°C. Type 444, like other ferritic stainless steels, is often not compatible with hydrogen-rich environments due to susceptibility to hydrogen embrittlement.
- **2205** – 2205 has filled many of the applications for which 904L has been formerly used. 2205 can have issues with embrittlement due to the ferritic portion of the microstructure at temperatures as low as 340°C and consequently is often not recommended for service above 300°C (especially for pressure vessels). The alloy is resistant to chloride-SCC in comparison to 304 and 316 but can be susceptible to hydrogen embrittlement. 2205 is resistant to low concentrations of organic

acids but should be used with caution at higher temperatures and concentrations. Also, the alloy tends to be resistant to sulfide stress cracking.

Based on the above alloys, 444 and 2205 are likely not appropriate for use in the 'hot' portion of the reactor but may have utility in lower temperature regions. The austenitic steels can likely be used over the range of temperatures experienced in the hydrotreater, but if some feedstock contain chlorides or additionally corrosion resistance is needed a range of higher performance Ni-based alloys are available.

6.2.2 Corrosion Samples

Samples for low temperature experiments were obtained from a combination of Metal Samples Company and existing stock within Battelle. Both U-bends and corrosion coupons were tested in triplicate for each material. Images of typical U-bend and corrosion mass loss coupons can be found in Figure 32 below.

Coupon samples: Coupon samples provide an indication of the general corrosion rate a material experiences in a given test solution. Sample coupons were polished to 120 grit by hand, cleaned in ethanol, and weighed. After exposure samples were removed, wiped, and then cleaned in ethanol using an ultrasonic bath. The samples were then dried and weighed again to determine if any generalized corrosion had taken place.

SCC U-bend samples: U-bend samples provide an indication of susceptibility to SCC by exposing a sample with a tensile stress (through deformation of a metal sheet / bar around a mandrel) to an electrolyte of interest. These particular samples were also fabricated to have a weld at the apex of the bend, which provides an even more conservative estimate of SCC susceptibility. Samples were stressed with the aid of a vice and stress was maintained with the use of 316 stainless steel hardware and Teflon fittings. After exposure, samples were removed, wiped, and then cleaned in ethanol using an ultrasonic bath. The samples were then dried and inspected optically for evidence of cracking.

(a)

(b)

Figure 32. Sample (a) U-bend and (b) coupon specimens used for low temperature pyrolysis oil testing to assess susceptibility to SCC and general corrosion rate.

6.2.3 Pyrolysis Oil / Test Solution

In this study, White Pine biomass was used as the feedstock material to produce the pyrolysis oil (internal reference 53633-24A C1+C3) used for the “low” temperature corrosion testing. Analyses of pyrolysis oil of this type and similar to the oil used for experimentation described below indicated a water content of approximately 20% by mass with primary organic acids including acetic and formic acids. For these and other tests to be self-consistent, it was necessary to run entire series of experiments in a single sourced electrolyte / pyrolysis oil. This means that results would be a fair comparison amongst each other, however, will not necessarily be comparable across different experimental runs (i.e. the corrosion rates are only strictly valid for the specific electrolyte in which they were tested).

6.2.4 Low Temperature Experimental

Samples of each material were exposed for 1,000 hours in pyrolysis oil heated to 50ºC to assess general corrosion and susceptibility to SCC at elevated but relatively low temperatures. All the samples (U-bend and coupons) for a given material were exposed in a single 500 mL glass beaker. The samples were arranged and suspended to not be in contact with each other during testing as shown in Figure 33a. Approximately 330 mL of bio-oil was poured into each beaker to completely cover each sample. Over time the bio-oil separated and the coupons and apex portions of the U-bends were left exposed in the aqueous phase of the solution. Efforts were made to seal the beakers to create closed systems with a combination of plastic and Parafilm covers. Each beaker was then placed into a water bath, which was used to regulate and maintain the temperature at 50ºC as seen in Figure 33b. The top of the water bath was insulated and the entire setup was placed into a fume hood for the duration of the 1,000 hour test run.

Figure 33a. Samples arrangement in a beaker prior to pyrolysis oil addition and b) hot water bath used to heat solution to 50ºC.

6.2.5 Low Temperature Results and Discussion

In general, none of the five alloys physically showed significant corrosion after 1,000 hours of exposure. Samples exhibited a “shiny” appearance and polishing marks were still evident. To illustrate, before and after images of a 444 coupon are shown in Figure 34. Again polishing marks are clearly evident and little to no observable change was apparent after 1,000 hours of exposure. The physical observation was corroborated by the mass change results. The average mass changes (three samples / alloy) for all tested alloys are presented in Table 18. Interestingly, in four of the five alloys tested, samples on

average gained a small amount of mass (in the fifth sample an outlier data point was largely responsible for an average mass loss). This result was somewhat unexpected and could be an indication of a thickening passive film. In any case, it does not appear that significant general corrosion occurred in any of the five alloys evaluated.

Figure 34. Before (left) and after (right) image of a 444 sample coupon after 1,000 hours of exposure to pyrolysis oil heated to 50ºC.

Table 18. Average mass change for each alloy after 1,000 hours of exposure to pyrolysis oil heated to 50ºC.

Alloy	Initial mass (g)	Final mass (g)	% change
304L	20.7133	20.7134	0.00088
316L	6.3630	6.3635	0.00788
904L	4.2992	4.2997	0.01144
444	8.0690	8.0690	-0.00011
2205	8.3365	8.3368	0.00352

Similar results were observed from the SCC U-bend samples. In all instances the samples appeared pristine after 1,000 hours of exposure. In no instances was any indication of cracking observed. Example images of a 2205 U-bend specimen before and after exposure are provided in Figure 35. Prior works at Oak Ridge National Laboratories had shown, unexpectedly, that some low Cr-content steels were susceptible to SCC in pyrolysis oils at 50°C[iii]. However, it appears that all alloys testing in this task were sufficiently resistant to SCC to not exhibit cracking in the bio-oil used for this study.

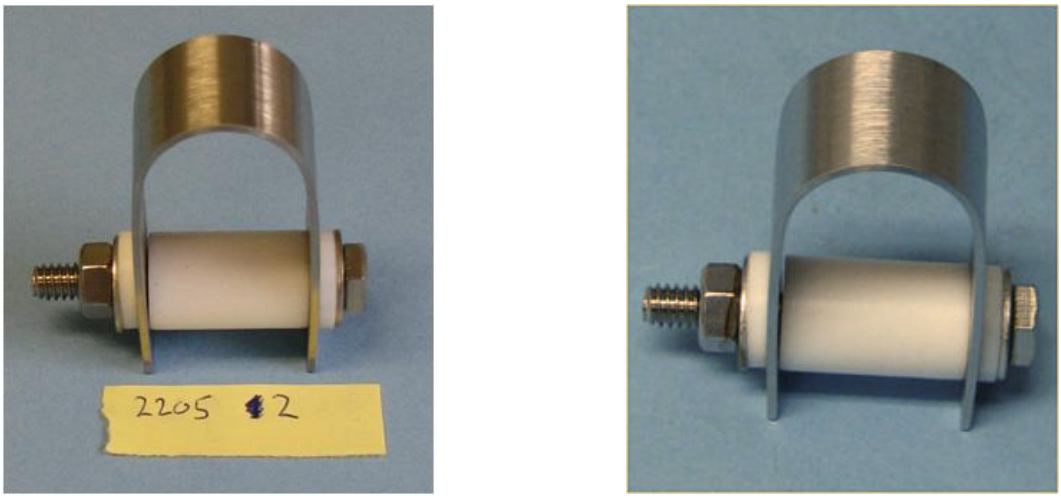

Figure 35. Before (left) and after (right) image of a 2205 U-bend sample after 1000 h of exposure to pyrolysis oil heated to 50ºC.

6.3 High Temperature Testing

The primary concerns about material-environment incompatibility and corrosion are in the hydrotreater, which will simultaneously experience an aggressive corrosive environment, a range of high temperatures, and high pressures. Two different approaches for assessing materials performance can be taken, 1) in-situ testing during actual bio-oil to bio-fuel production runs, or 2) simulated testing using an autoclave. Both approaches have advantages and disadvantages in terms of creating realistic and experimentally controlled conditions to make fair performance assessments. An attempt at in-situ testing was made in 2012 before deciding to pursue simulated autoclave testing throughout 2013. Two different 1,000-hour autoclave tests were conducted at target temperatures of approximately 155°C and 265°C, respectively. During each test, three different stainless steel materials were evaluated using duplicates of two types of samples, namely those for general corrosion assessment (coupons) and those for stress corrosion cracking (SCC) assessment (teardrop). Both types of samples were evaluated in the submerged condition and in the vapor space of the test vessel. Total test specimens was forty-eight. Table 19 provides a test matrix for each tested material that shows the number of samples tested, temperatures, and phases to which samples were exposed.

Table 19. Test matrix for each material under evaluation. Three different alloys (304L, 316L, and 904L) were evaluated.

Test Temperature	Vapor Phase		Liquid Phase	
	Coupons	**Teardrop**	**Coupons**	**Teardrops**
155°C	2	2	2	2
265°C	2	2	2	2

6.3.1 Materials Selection

As previously mentioned, three stainless steels were chosen for high temperature autoclave test evaluation: Types 304L, 316L, and 904L. In general, these alloys have good corrosion resistance to a number of environments, with general resistance to corrosive environments increasing as alloy content increases from 304L to 316L to 904L. The number of tested alloys was limited due to space restraints presented by the test vessel and a desire to test materials at least in duplicate. Table 20 provides a summary of alloys, compositions, and other information for each evaluated alloy.

Table 20. Stainless steel alloys selected for high temperature autoclave testing. Primary alloying elements, microstructure type, and maximum suggested use temperature are indicated.

Alloy	Type	Max T ºC	Cr	Ni	Mo	Cu	Mn
304L	Austenitic	425	18-19	9-10			2.0
316L	Austenitic	425	17-17.5	12-13.5	2.5		2.0
904L	Austenitic	400	19-23	23-28	4-5	1-2	

While these alloys have good general corrosion resistance across a range of environments, they are known to be susceptible to SCC in the presence of chlorides at ppm-level concentrations at elevated temperatures. Austenitic steels can likely be used over the range of temperatures experienced in the hydrotreater, but if some feedstock contains chlorides or additional corrosion resistance is needed, a range of higher performance Ni-based alloys are available. Additionally, the potential for environments that are conducive to sulfide stress corrosion cracking (SSC) and or hydrogen embrittlement (HE) may be present broadly in hydrotreater-type systems. Unless they are heavily cold-worked, austenitic stainless steels (like the alloys listed in Table 20) generally have some resistance to SSC and less susceptibility to hydrogen embrittlement in comparison to ferritic stainless steels. However, the possibility of this type of attack warrants mention. An abbreviated summary of some of the advantages and disadvantages of each alloy in terms of corrosion resistance and metallurgy are described below:

- **304L** – 304L is assumed to have similar, but lower, corrosion resistance as 316L, especially in terms of pitting.
- **316L** – 316L is susceptible to sensitization if held for long periods of time at temperatures between 425°C and 800°C creating a risk for intergranular attack. The alloy is susceptible to chloride SCC at a few ppm Cl^- concentrations in combination with low pH, oxygen, and elevated temperature. Additionally, 316L is resistant to pure acetic acid, but at high temperatures, pressures, and in the presence of formic acids, it will corrode.
- **904L** – 904L is in some ways a higher alloy content version of 316, but with greater resistance to SCC, pitting, and crevice attack. The higher alloying content means the risk of sensitization increases and the alloy is not recommended for long term use at temperatures above 400°C.

6.3.2 Corrosion Samples

Samples for high temperature experiments were obtained from a combination of Metal Samples Company and existing stock within Battelle. For each autoclave test, both teardrop and corrosion coupons were tested in duplicate for each of the above materials and in both the vapor and liquid phases

within the test vessel. Images of typical teardrop and corrosion mass loss coupons can be found in Figure 36 below.

Coupon samples: Coupon samples provide an indication of the general corrosion rate a material experiences in a given test solution. Sample coupons were polished to 120 grit by hand, cleaned in ethanol, and weighed prior to testing. After exposure, samples were removed, wiped, cleaned, and weighed for mass change. Cleaning involved a first step exposure to acetone for 120 seconds in an ultrasonic bath at ambient temperature and a second step cleaning using an ASTM-specified 10 percent nitric acid solution at 60ºC for 20 minutes.

Teardrop weld samples: Teardrop-type samples provide an indication of susceptibility to SCC by exposing a sample with a tensile stress (through deformation of a metal sheet / bar around a mandrel) to an electrolyte/environment of interest. The use of teardrop samples was made to 1) eliminate the need for hardware associated with traditional U-bend SCC samples, and 2) take advantage of the smaller profile to allow duplicate testing during the autoclave testing. Also, these particular samples were fabricated to have an autogenous weld at the apex of the bend, which provides an even more conservative estimate of SCC susceptibility, as well as an indication of attack near weld regions. After exposure, samples were removed, wiped, and then cleaned in acetone. The samples were then dried and inspected optically for evidence of cracking.

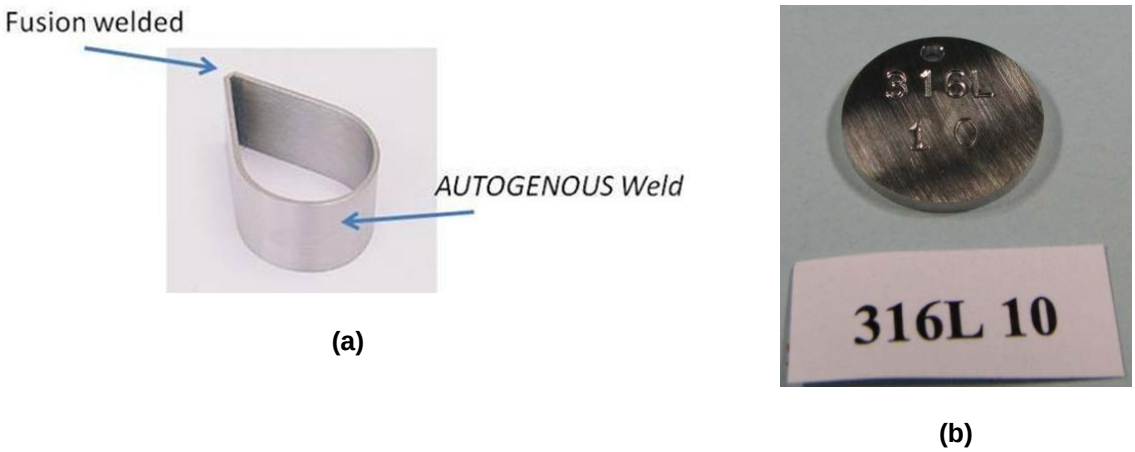

(a) **(b)**

Figure 36. Sample (a) teardrop and (b) coupon specimens used during autoclave testing to assess susceptibility to SCC/cracking and general corrosion rate, respectively.

6.3.3 In-situ Testing

An attempt at collecting meaningful corrosion data from samples placed inside the reactor and exposed to actual service environments during the upgrading process was pursued. In order to prevent disruption / clogging of the process, 304L stainless steel samples were machined into thin rings (low profiles), which were affixed to the thermo well that runs down the centerline of the reactor. These samples are shown in Figure 37 and had a nominal ID of 0.25 inch. During a trial, three separate samples were positioned at different locations along the thermocouple to sample different temperatures along the length of the hydrotreater.

Figure 37. Two views of machined "ring" specimens which were used in trial in-situ hydrotreater tests.

An initial feasibility trial was performed on three ring samples during a short test run using sulfided CoMo catalyst at temperature range 350 to 400°C. On removal of samples from the reactor the surface appeared tarnished but largely intact. As with the low temperature tests the polishing / machining marks were still evident on the surface. Table 21 provides initial and final masses determined from the tested specimens. Definitive conclusions cannot be made based on a single short test run, but it should be noted that small mass losses were observed in the middle and lower portions of the reactor. Although this result is interesting the test would need to be replicated to add confidence of an effect. The intention was to perform similar tests over longer durations. However, during a subsequent run it was found that the ring samples had a tendency to slide down the thermocouple and clog the exit port for the reactor (Figure 38) – creating a situation in which pressure increased and the run had to be terminated. Although this type of testing had value it was difficult to make performance comparisons across different test runs (each run is its own unique catalyst and conditions) or replicate results. For this reason and due to the risk of rings slipping down the thermo well and plugging the reactor outlet, it was decided to abandon this approach in favor of autoclave-based tests.

Table 21. Mass change of in-situ ring samples obtained from a short test run.

Sample Location	Initial Mass (g)	Final Mass (g)	% Change
Top	0.1739	0.1740	0.0575
Middle	0.1856	0.1850	-0.3233
Bottom	0.1825	0.1819	-0.3288

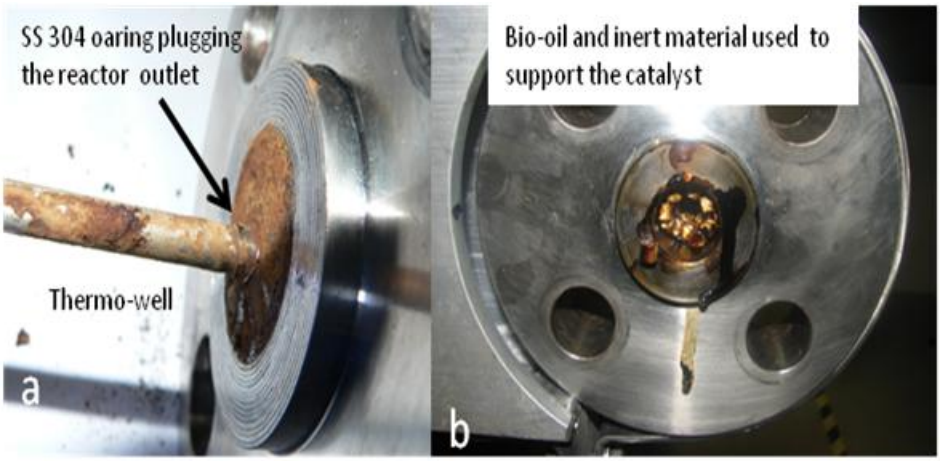

Figure 38. Photo of the thermo-well showing the o-ring/ring coupon plugging the reactor outlet.

6.3.4 Autoclave Testing

Autoclave experiments were an attempt to mimic environmental conditions as might occur in the hydrotreater. The advantage of using an autoclave is the simplicity in terms of setup and greater ability to exert experimental control than can be achieved with in-situ experimentation. The disadvantage of this approach is that it is an artificial and over simplified representation of the hydrotreater, which in itself is highly complex in terms of environment and temperature that vary along the length of the reactor.

A decision was made to perform the autoclave exposure tests using the separated aqueous phase from produced pyrolysis oil as the test solution. Analyses of pyrolysis oil of this type and similar to the oil used for experimentation indicated a water content of approximately 20 percent by mass with primary constituent organic acids including acetic and formic acids. The use of the aqueous phase removes concerns about polymerization and charring of the bio-oil during testing at high temperatures. Further, the aqueous phase is the portion of the pyrolysis oil that contains the most aggressive organic species and is believed likely to be the phase that promotes corrosion to the largest extent. These tests are potentially more aggressive than the conditions experienced in the actual hydrotreater, meaning the results could allow conservative recommendations to be made. To help account for and simulate the H_2 in the system, the autoclave was backfilled with H_2 gas prior to testing – the ratio of water vapor to H_2 in the vapor space is a rough order of magnitude approximation of conditions in the hydrotreater. It should be noted that another key difference between the autoclave testing and the actual hydrotreater is that the test contents in the autoclave are static (ignoring convection from heating) and not refreshed as opposed to the flow that is experienced during the actual upgrading process.

For the autoclave tests to be self-consistent it was necessary to run the entire series of experiments in a single sourced electrolyte / pyrolysis oil. The same separated bio-oil aqueous phase was used for both autoclave runs (internal reference of: FCC Bio-oil C2 Aq. Phase Ref 5366-B). This means that results would be a fair comparison amongst each other, however, will not necessarily be comparable across different experimental runs (i.e. the corrosion rates are only strictly valid for the specific electrolyte in which they were tested).

Autoclave tests were run at two different target temperatures (within the autoclaves' limit) to be representative of as large as possible temperature range as experienced in the hydrotreater. The two target test temperatures were 155°C and 265°C. The autoclave used for testing had a Hastelloy C-276 body and head with an approximate one gallon capacity. The autoclave, insulation, and temperature controller are shown in Figure 39 below. The autoclave could be run at a maximum pressure and temperature limit of 5,000 PSI at 600ºF (315ºC), however, actual tests were at pressures and

temperatures below these limits. Portions of the actual hydrotreater will experience temperatures during service in excess of the proposed maximum test temperature. However, empirical observations from PNNL's reactor suggest the most severe corrosive attack occurs between 250ºC and 300ºC and thus this autoclave should be able to approach a "worst case" environment as experienced during actual hydrotreater runs.

A Teflon liner was used during testing as well as 220 VAC heaters. Two type K thermocouples were used for control and overshoot temperatures, and a C-276 rupture disc was utilized for safety. The samples were mounted to a C-276 alloy test stand to allow different sets of samples to be exposed in both the vapor and submerged condition. The test stand with samples mounted prior to testing is shown in Figure 40. A small difference between the tests run at 155°C and 265°C was the method of sample suspension from the test rack. All tested samples were suspended using Teflon tubing except for the 316L mass loss coupons tested at 265°C. Those samples were fabricated with a hole that was too small to accommodate the Teflon tubing and as a result required that a chromel thermocouple wire was used. It is not believed this would impact results significantly, but the potential for galvanic interactions may have existed.

A generalized procedure for testing is as follows: 1) load the sample rack, 2) fill the autoclave with aqueous bio-oil-based test solution to approximately ½ inch above the samples mounted on the bottom of the rack, 3) close the autoclave, 4) backfill with H_2 and 5) slowly heat the autoclave to a target temperature. Prior to testing, the aqueous phase of the bio-oil was measured to have a pH value of approximately 2.4 - 2.5. The exposure tests were for 1,000 hours.

Figure 39. The autoclave test setup with temperature controller.

Figure 40. Test stand used to suspend samples during the autoclave exposure. The samples at the top of the sample rack were exposed to the vapor space while samples at the bottom were submerged.

6.3.5 Results and Discussion

Autoclave exposures of coupon and teardrop samples to the separated aqueous phase of a bio-oil were conducted for 1,000 hours at both 155°C and 265°C. The following sections present summary results from the 155°C and 265°C tests, respectively.

6.3.5.1 Autoclave testing 155°C

The 155°C temperature autoclave run went smoothly with no observed leaks or problems. The pressure of the system was observed to slowly decline throughout the testing from approximately 175 psi initially to approximately 130 psi. The reason for the slow steady decrease in pressure was unclear and conceivably could be related to a reaction or breakdown of the test solution. There was no evidence of autoclave leaking in terms of observed liquid or smell. After the 1,000-hour test, the test rack was removed from the test vessel. Figure 41 shows the test rack at the time of removal. The samples exposed to the liquid phase were covered with a layer of bio-oil-based product, while the samples exposed to the vapor phase were observed to be relatively clean although tarnishing was evident.

Figure 41. The appearance of the sample rack and samples after the 1,000-hour autoclave test conducted at 155°C.

Sample images of before and after test specimen from the 155°C 1,000-hour test are provided in Figure 42. Both vapor and liquid samples experienced observable damage. For the vapor phase, attack was concentrated at the bottom of the sample (samples suspended by the hole), while attack (and removal of polishing marks) was more uniformly distributed on samples exposed to the liquid phase.

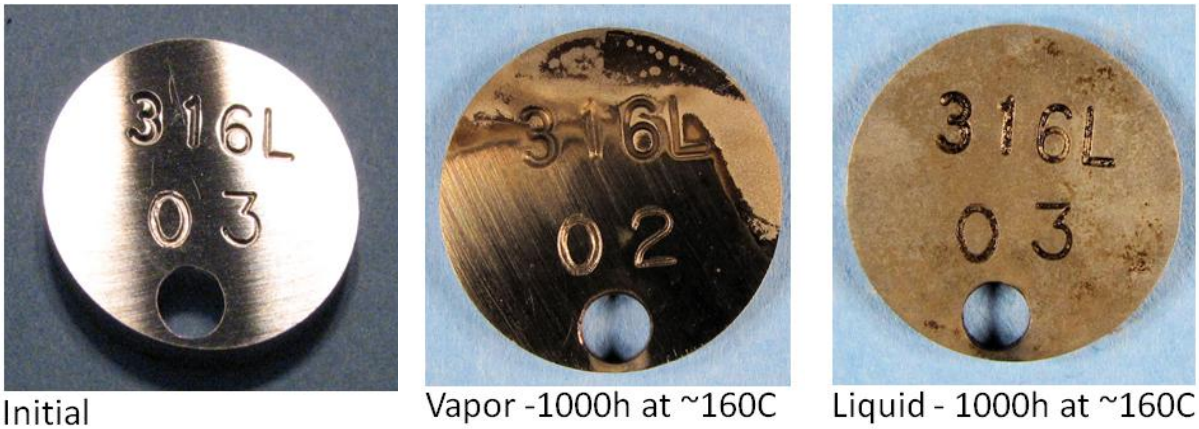

Figure 42. Images of samples before and after tests at 1,000 hours at approximately 155 ºC. Tarnishing and attack was evident.

Table 22 presents corrosion rates determined from the 1,000-hour autoclave test at 155ºC for samples exposed in the vapor and aqueous phases. The data is presented as a horizontal bar chart in Figure 43. The observed corrosion rates from both the liquid and vapor phase are roughly as would be expected from a metallurgical standpoint, with corrosion rates for 304L > 316L > 904L. The mass changes in the vapor space were observed to be higher in magnitude than observed in the liquid phase with the highest corrosion rate being observed from a 304L coupon that showed a rate of approximately 0.18 mm per year. It should be noted that corrosion rates observed at 155°C were in general observed to be one-to-two orders of magnitude larger than corrosion rates observed from the autoclave test performed at 265°C.

Visual inspection of the teardrop samples did not reveal any evidence of cracking. Selective etching at the weld was observed in a number of samples. Additionally, some end grain attack was observed at one side of a 304L teardrop exposed to the vapor space.

Table 22. Corrosion rates determined from mass change measurements of samples exposed to the aqueous separated phase of bio-oil after 1,000-hour exposure at approximately 155ºC.

Material	Phase	mm per year
304L	V	0.158
304L	V	0.178
304L	L	0.023
304l	L	0.022
316L	V	0.056
316L	V	0.055
316L	L	0.014
316L	L	0.014
904L	V	0.012
904L	V	0.017
904L	L	0.006
904L	L	0.007

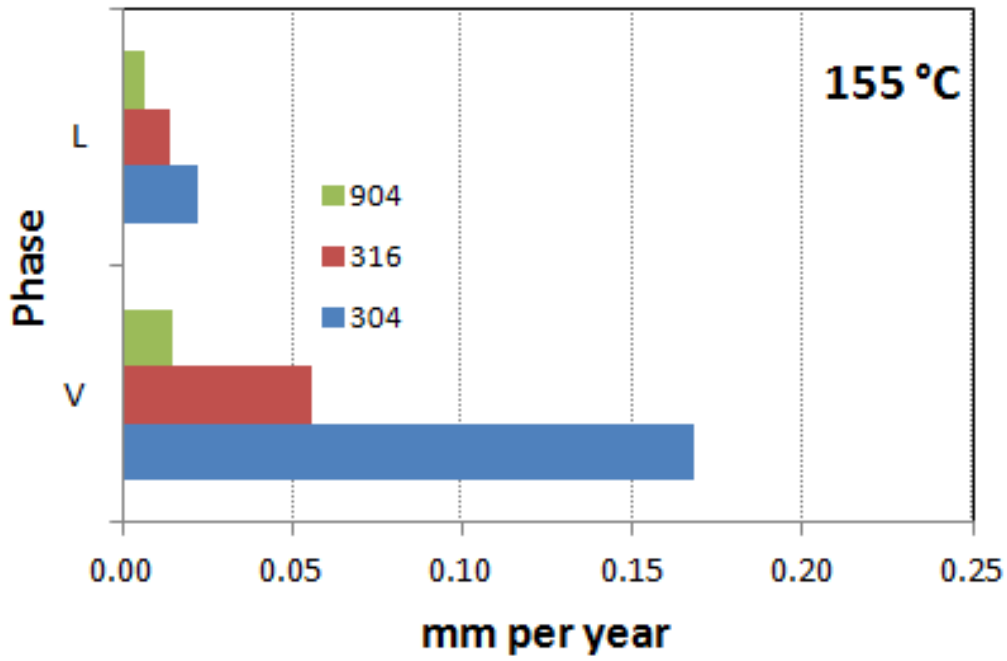

Figure 43. Average corrosion rates of tested materials after 1,000-hour exposure to liquid and vapor phases of bio-oil-based aqueous liquid held at approximately 155°C.

6.3.5.2 Autoclave testing 265°C

Autoclave testing at 265°C proved to be more difficult than the testing conducted at lower temperature. For example, during the initial temperature ramp a leak was detected from the autoclave. This required the test to be postponed overnight while a Hastelloy plug was machined and fit into the head of the autoclave. The following day the autoclave was again prepped and charged with H_2 before the temperature was ramped upward. The autoclave reached pressure and temperature of 740 psi and 504°F (262 °C) and these temperatures and pressures held for two days. After two days the pressure dropped to approximately 710-720 psi (at 262°C) where it remained for approximately 5 weeks. A few small droplets of bio-oil were observed on the insulation at the rear of the autoclave but the pressure remained steady. Additionally, at approximately 17 days into the test, moisture was observed inside the pressure gauge. Again, the pressure remained steady at ~710 psi. However, this is likely an indication that water was escaping the autoclave. A decision was made to allow the test to run until completion provided the temperature and pressure remain steady near 265ºC and 710 psi, respectively. On completion of the 1,000-hour test, the liquid phase samples were still submerged (indicating water loss was minimal). However, given that a leak was potentially present it is possible or even likely that the backfilled H_2 escaped from the test vessel.

Sample images of before and after test specimen from the 265°C 1,000-hour test are shown in Figure 44.

Samples removed from the autoclave were observed to be tarnished and have undergone some level of attack. Attack was largely uniform over the sample surface.

Initial Vapor -1000h at ~265°C Liquid -1000h at ~265°C

Figure 44. Images of samples before and after tests at 1,000 hours and 265ºC. Tarnishing and attack observable by eye.

Corrosion rates determined from samples exposed in both the vapor and aqueous phase during the 1,000-hour autoclave test at 265ºC are provided in Table 23. Figure 45 presents the corrosion rates from the 265°C autoclave experiment. The observed corrosion rates from the liquid phase are roughly as might be expected with corrosion rates for 304L > 316L > 904L, similar to rates observed form the 155°C exposure. However, in the vapor phase the 304L was observed to have the lowest corrosion rates among similarly tested samples. Additionally, the 316L was observed, unexpectedly, to have significantly higher corrosion rates than either the 304L or the 904L in the vapor phase. In this instance, the 316L samples were not insulated from the chromel wires used to suspend the samples from the test rack. It is conceivable that some sort of galvanic interaction between the different alloys occurred during testing which could have played a role in the increased corrosion rates that were observed. Galvanic corrosion is not expected, but it is a plausible explanation for the dramatic difference in behavior displayed by 316L (however, it does not explain why the 304L outperformed the 904L).

Table 23. Corrosion rates determined from mass change measurements of samples after 1,000-hour exposure at 265ºC in the aqueous separated phase of bio-oil.

Material	Phase	mm per year
304L	V	0.003
304L	V	0.003
304L	L	0.006
304l	L	0.006
316L	V	0.033
316L	V	0.014
316L	L	0.003
316L	L	0.005
904L	V	0.010
904L	V	0.008
904L	L	0.003
904L	L	0.003

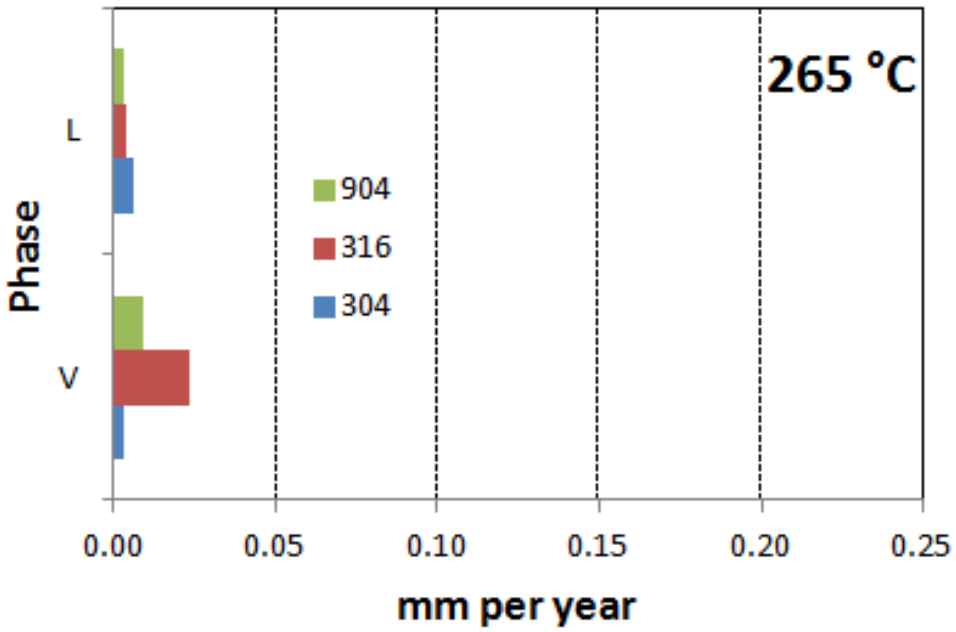

Figure 45. Average corrosion rates of tested materials after 1,000-hour exposure to liquid and vapor phases of bio-oil-based aqueous liquid held at approximately 265°C.

Visual inspection of the teardrop samples did not reveal any evidence of cracking. Selective etching at the weld was observed in one of the 904L samples exposed to the liquid phase. In general, less etching near weld areas was observed compared to samples exposed at 155°C.

Also, it should be noted that over the course of 1,000-hour at 265ºC the test solution underwent a change in pH and appearance. The initial solution was measured to have a pH value of approximately 2.4-2.5. However, after testing the solution pH value had shifted to values of approximately 3.4. This change in pH was also accompanied by clarifying of the solution as shown in Figure 46. A similar solution color change was observed in the before and after solutions for the 155°C test. An increase in pH indicates a decrease of the hydrogen ion concentration in solution, which could occur during chemical reactions of the bio-oil during heating. The change in color is also likely due to chemical reactions of the bio-oil from the heating process.

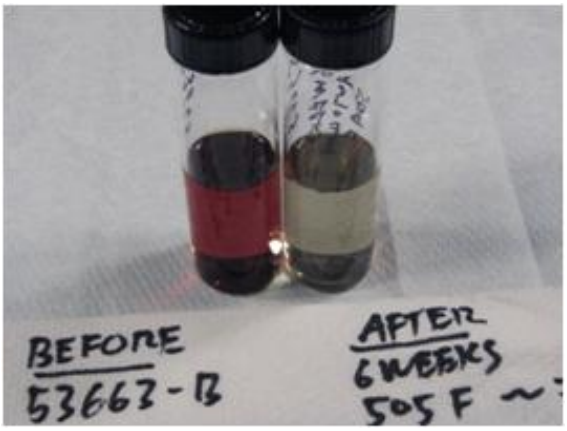

Figure 46. Test solutions before and after the 1,000-hour autoclave test at 265ºC.

6.3.5.3 Scanning Electron Microscopy and Energy Dispersive Spectroscopy

(This work was conducted by Jim Keiser's group at ORNL under DOE funding)

In addition to in-house testing and sample analysis, Battelle was able to collaborate with researchers at ORNL who have been working on related systems for a number of years. After analysis at Battelle a subset of samples was provided to collaborators at Oak Ridge National Lab (ORNL) for metallographic and microscopy analysis. This effort involved an information exchange meeting in Columbus Ohio, as well as, scanning electron microscopy and energy dispersive spectroscopy analysis at ORNL of some of the sample coupons from the 265°C autoclave run. Sample SEM images of cross-sectioned coupons are shown in Figure 47. In large part, the SEM analysis corroborates the mass loss results with the thickness of observed scale correlating well with measured mass change. The samples exposed in the liquid phase generally showed a thin passive film on the order of a couple of microns or less. The scales observed on the surfaces of samples exposed to the vapor phase were generally thicker than scales observed from samples exposed to the liquid phase. In particular, the 316L and 904L samples exposed to the vapor phase were observed to have thicker oxide films compared to all other samples analyzed. The 316L sample was observed to have an oxide approaching 10 microns in thickness in some locations and cracks in the layer were evident in some locations. Additionally, slight grain boundary attack was observed on the 316L vapor sample. The thickness of the oxide observed from samples exposed in the vapor phase scaled with the observed mass loss (316L>904L>304L).

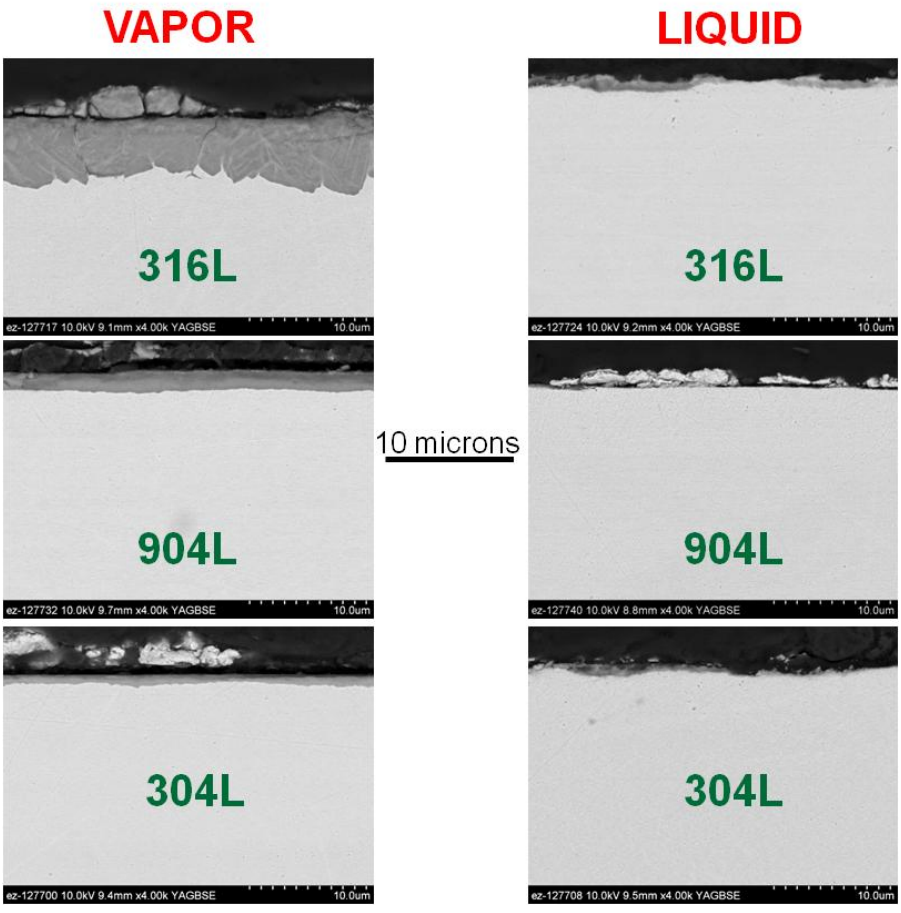

Figure 47. Sample SEM images of samples after 1,000-hour exposure at 265ºC in the aqueous separated phase of bio-oil.

Figure 48 provides SEM-EDS spectra of 316L coupons after the 1,000-hour autoclave exposure at 265°C showing the base alloy, the surface oxide formed in the liquid phase, and the surface oxide formed in the vapor phase. EDS is a semi-quantitative characterization technique that allows identification of the elemental composition and relative proportions of identified species. Analysis was performed on the base alloys as well as the oxides formed on the surface after different exposures. Chromium-rich surface oxides were observed from surfaces exposed to both liquid (b) and vapor (c) phases. Due to the interaction volume of the electron beam and the thin cross-section of the oxides it is difficult to draw conclusions about possible differences in chemistry being associated with thick oxide films and or increased corrosion rates.

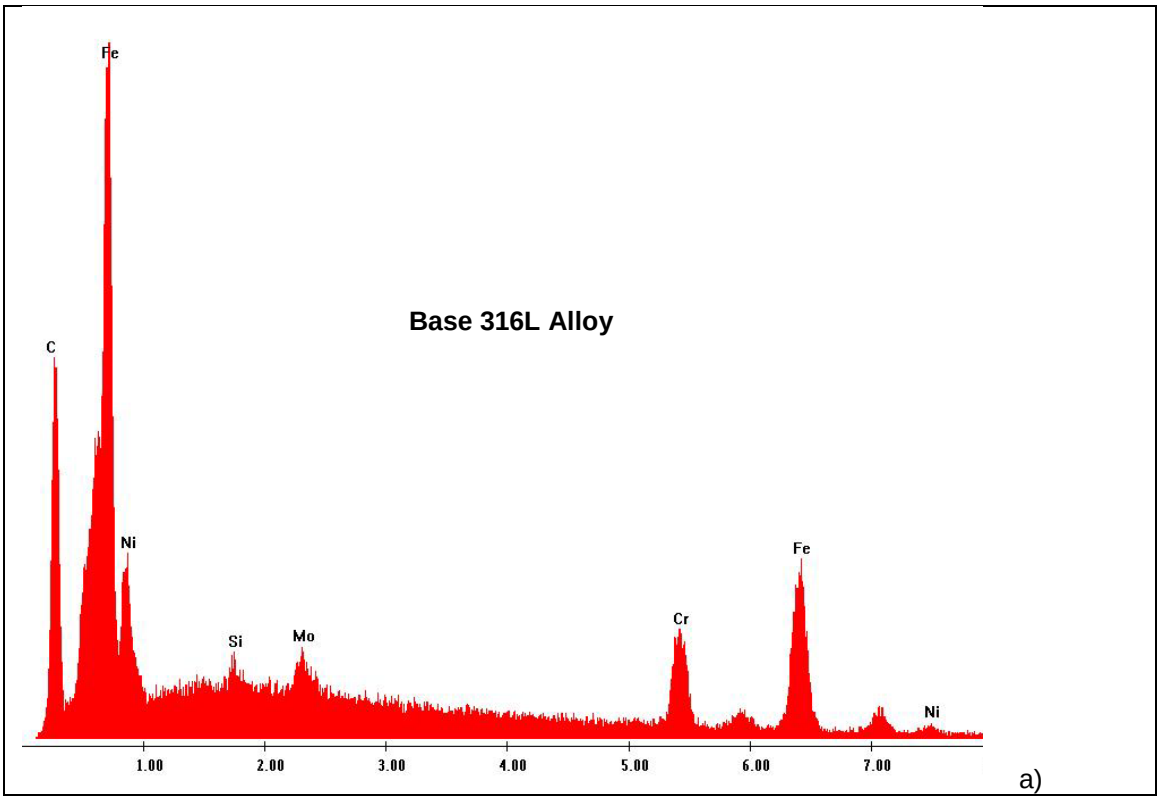

a)

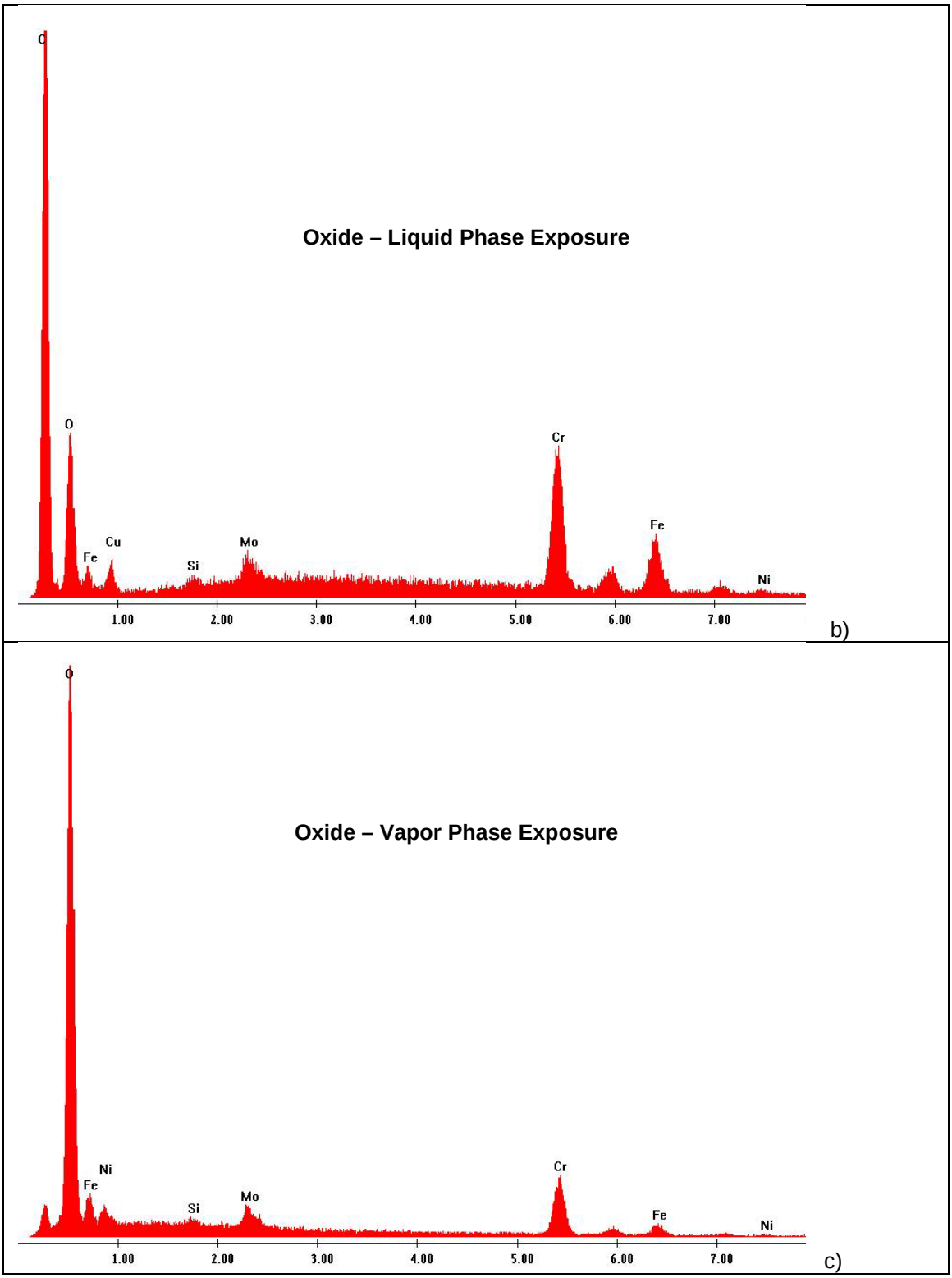

Figure 48. EDS spectra of 316L after the 1,000-hour autoclave exposure at 265°C showing the a) base alloy, b) the surface oxide formed in the liquid phase, and c) the surface oxide formed in the vapor phase.

6.3.5.4 Corrosion Models

The models that follow are based on data obtained from 1,000-hour exposure tests in bio-oil-based test solutions. The models predict general corrosion rates for 304L, 316L, and 904L in bio-oil or separated aqueous bio-oil-type environments from 50°C to 265°C in both the liquid (submerged) and vapor phases. Coupon data used to construct the model included:

1) A 1,000 hour "low" temperature exposure at 50°C to bio-oil. Data was collected in triplicate and corrosion rates were essentially zero in comparison to the magnitude of rates determined in higher temperature tests.

2) A 1,000 hour "intermediate" temperature exposure at 155°C to the separated aqueous phase from a bio-oil. Each data point represents the average of two samples.

3) A 1,000 hour "high" temperature exposure at 265°C to the separated aqueous phase from a bio-oil. Each data point represents the average of two samples.

Curve fittings were performed with a second-order polynomial function using Microsoft Excel®. The fittings yield a perfect fit because only three data points were available for the model. Assumptions and limitations are listed below. Figure 49 shows the data fit and fit equations of 304L, 316L, and 904L coupon exposed to the liquid phase of bio-oil-based test solutions. The equations for corrosion in the liquid phase are listed after the figure.

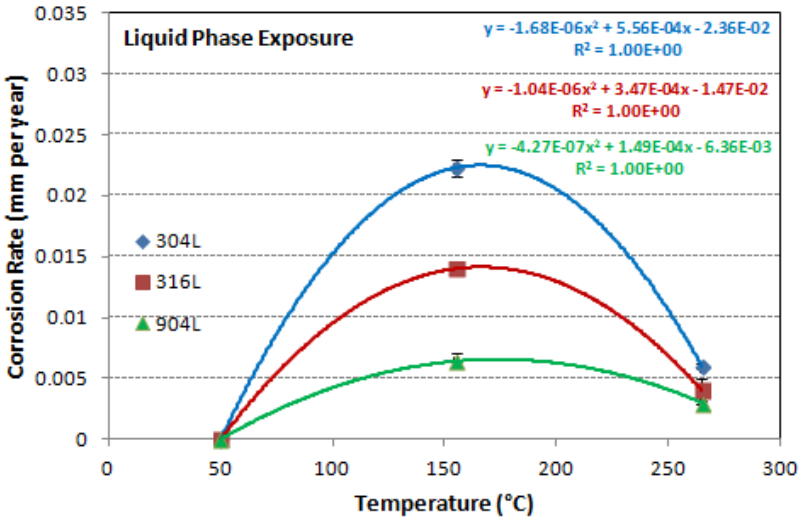

Figure 49. Predictive fits and equations for the general corrosion rates in the liquid phase of bio-oil-based test solutions of 304L, 316L, and 904L over temperatures ranging from 50°C to 265°C. Error bars indicate range in measurements.

304L Liquid Phase:

$$Corrosion\ Rate\ \left(\frac{mm}{yr}\right) = -1.68 \cdot 10^{-6}T^2 + 5.56 \cdot 10^{-4}T - 2.36 \cdot 10^{-2}$$

316L Liquid Phase:

$$Corrosion\ Rate\ \left(\frac{mm}{yr}\right) = -1.04 \cdot 10^{-6}T^2 + 3.47 \cdot 10^{-4}T - 1.47 \cdot 10^{-2}$$

904L Liquid Phase:

$$Corrosion\ Rate\ \left(\frac{mm}{yr}\right) = -4.27 \cdot 10^{-7}T^2 + 1.49 \cdot 10^{-4}T - 6.36 \cdot 10^{-3}$$

where T is temperature in °C.

Figure 50. shows the data fit and fit equations of 304L, 316L, and 904L exposed to the vapor phase of bio-oil-based test solutions. The equations for corrosion in the vapor phase are listed after the figure.

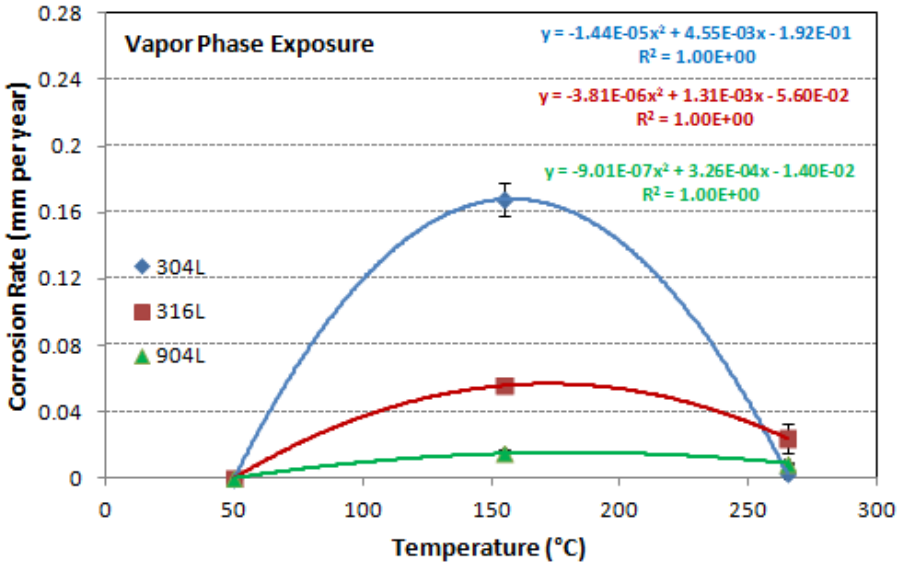

Figure 50. Predictive fits and equations for the general corrosion rates in the vapor phase above bio-oil-based test solutions of 304L, 316L, and 904L over temperatures ranging from 50°C to 265°C. Error bars indicate range in measurements.

304L Vapor Phase:

$$Corrosion\ Rate\ \left(\frac{mm}{yr}\right) = -1.44 \cdot 10^{-5}T^2 + 4.55 \cdot 10^{-3}T - 1.92 \cdot 10^{-1}$$

316L Vapor Phase:

$$Corrosion\ Rate\ \left(\frac{mm}{yr}\right) = -3.81 \cdot 10^{-6}T^2 + 1.31 \cdot 10^{-3}T - 5.60 \cdot 10^{-2}$$

904L Vapor Phase:

$$Corrosion\ Rate\ \left(\frac{mm}{yr}\right) = -9.01 \cdot 10^{-7}T^2 + 3.26 \cdot 10^{-4}T - 1.40 \cdot 10^{-2}$$

where T is temperature in °C.

Assumptions and Limitations: These data and model should be viewed as preliminary as tests to-date have involved a limited number of samples and test runs. Additional data is required to help confirm preliminary results to-date as well as provide an idea about corrosion rates at intermediate (non-tested) temperatures. Tests at temperatures higher than 265°C would be of value.

- The data and equations only cover temperatures ranging from approximately 50°C to 265°C.
- The data points used for fitting are only based on single test runs using either duplicate (155°C and 265°C) or triplicate samples (50°C).
- It is assumed that the autoclave tests conducted in a static, separated bio-oil aqueous phase accurately mimic the test environments in the hydrotreater. It is also assumed that the test

solutions used are broadly representative of the chemistries that might be experienced in hydrotreater/bio-oil systems using a range of feedstock materials.

- It is assumed the maximum corrosion rate occurs at or near approximately 155°C. Additional tests would be required, but the highest corrosion rate could occur at another temperature – which would change the profile of the fit.

- The model is only for general corrosion (as opposed to SCC, pitting, SSC, or hydrogen embrittlement). At this point, it is not known what the primary failure mode of stainless steel materials is in bio-oil/hydrotreater-type environments. This means if the dominant mechanism of failure is something other than general corrosion, these models cannot be used to estimate service life as wall thinning will not be the limiting factor for service.

- There is possibly a step change in behavior/rate at 100°C associated with the phase change of water which is not accounted for in the model. Additionally, corrosion rates approaching zero may persist at temperatures above 50°C. For model development, given the small magnitude of mass change observed at 50°C, relative to that observed at higher temperatures, the corrosion rate at 50°C was assumed to be effectively zero.

- It is assumed that the small amount of leakage (and presumed loss of hydrogen) during the 265°C autoclave run did not significantly alter observed corrosion rates. Again, additional testing in this temperature range would be useful to confirm or amend prior results.

6.4 Conclusions and Recommendations

To our knowledge, no other studies have reported results of corrosion evaluation of pyrolysis oil on various metals at elevated temperatures. Prior works at Oak Ridge National Laboratories studied the corrosion of various metals in pyrolysis oil at 50°C and observed minimal corrosion in stainless steels at this temperature[iii]. The work herein reported, hence, represents an extension of previous work at the upper end of expected pyrolysis oil storage temperatures to temperature regimes representative of pyrolysis oil hydrotreating process conditions. Conclusions from the autoclave experiments are as follows:

1. In general, corrosion rates appeared to be higher for materials exposed to the 155°C environment compared to materials exposed to the 265°C environment.

2. In general, corrosion rates appeared to higher for samples exposed to the vapor phase compared to samples exposed to the liquid phase

3. For the samples exposed to the vapor and liquid phase at 155°C and for samples exposed to the 265°C liquid, corrosion rates increased going from 904L to 316L to 304L – as would be expected from a metallurgical perspective. For samples exposed to the 265°C vapor phase, corrosion rates increased from 304L to 904L to 316L. It is unclear if this difference is real or an anomaly associated with either the 304L or 316L data.

4. Visual assessment of teardrop samples did not show obvious cracking, although preferential etching of the welds was observed in a number of cases.

5. SEM analysis of samples exposed at 265°C showed the formation of thin oxide films on most samples. The 904L and 316L vapor exposed samples were found to have thicker oxide films. Incidentally, these two materials also had relatively high corrosion rates compared to other specimens exposed at 265°C

The testing conducted to-date should be viewed and used only as preliminary guidance for future materials decisions. It is strongly recommended that additional testing be performed to confirm the results found within this work, as well as provide data across the range of temperatures experienced in a

hydrotreater environment which were not explored in this exercise. In particular, the potential for embrittlement and cracking phenomena in these types of service environments is not well understood and testing should be carried out in these areas. Additionally, it would be prudent to account for this uncertainly when future materials selection choices are made or until a better understanding of possible failure mechanisms is developed.

7.0 Task F: 1,000 Hr. Run to Evaluate Catalyst Performance

7.1 Introduction

Based on the work done under Tasks C and D, the following process parameters were selected for the 1,000 hr. run:

1. Biomass: Pine biomass was used, because the dry bio oil yield associated with it is the highest.
2. Pyrolysis process: Fast pyrolysis (with no vapor phase catalysis) was used. Use of bio oil from catalytic pyrolysis resulted in some benefits, but there was significant reduction in dry bio oil yield.
3. Zone I catalyst: Ru/TiO_2 developed by PNNL.
4. Zone II catalyst: Sulfided Co/Mo. This catalyst has already been shown (at PNNL) to perform long term hydrogenation and cracking if the bio oil provided to it is stable.
5. Bio oil cleanup: Ion exchange method developed by Battelle.
6. Space velocity: LHSV: 0.2 hr^{-1}

The Zone I stabilization run was conducted at Battelle Columbus. Ru/TiO_2 catalyst was used at 170°C. This run was very successful, and over 1,200 hrs TOS were achieved. The Zone II hydrotreatment run was conducted at PNNL using a sulfided CoMo catalyst for 1,200 hrs.

7.2 Zone I Stabilization Run at Battelle Columbus

Battelle started a Zone I stabilization/hydrotreatment run under Task D in FY15Q1. The feed bio-oil used for the run was produced by Battelle under Task B, and cleaned via ion exchange methods under Task D. The objective of the Zone I stabilization/hydrotreatment run was to convert aldehydes and acids and to partially hydrogenate the bio-oil. This reaction was conducted at high pressure in the presence of hydrogen. Table 24 presents the reaction conditions and the catalyst used. Hydrotreatment was conducted in three cycles using the same catalyst. The catalyst was regenerated two-times during the testing. The total Time On Stream (TOS) achieved was 1,200 hrs at a LHSV of 0.2 hr-1. More than 3.5 liters of bio-oil produced was processed. The liquid yield (stabilized bio-oil product / cleaned bio-oil feed), as shown in Figure 51, was approximately 100%.

Table 24. Reaction conditions and catalyst used for Zone I stabilization/hydrotreatment at Battelle

Catalyst	Ru/TiO_2
	17.8 ml (20.3 g)
	350<Ø<800mm
Temperature	170 ˚C
Total pressure	1,500 psi
LHSV	0.2 hr^{-1}, excluding methanol
Activation	H_2 at 300°C , 3 hrs
Bio-oil	Resin process, filtered via 0.2 µm
co-solvent	30% (wt)
total bio-oil feed (ml/min)	0.1 (ml/min)
H_2 flow rate	400 ml/min
H_2/bio-oil volume ratio	4,000

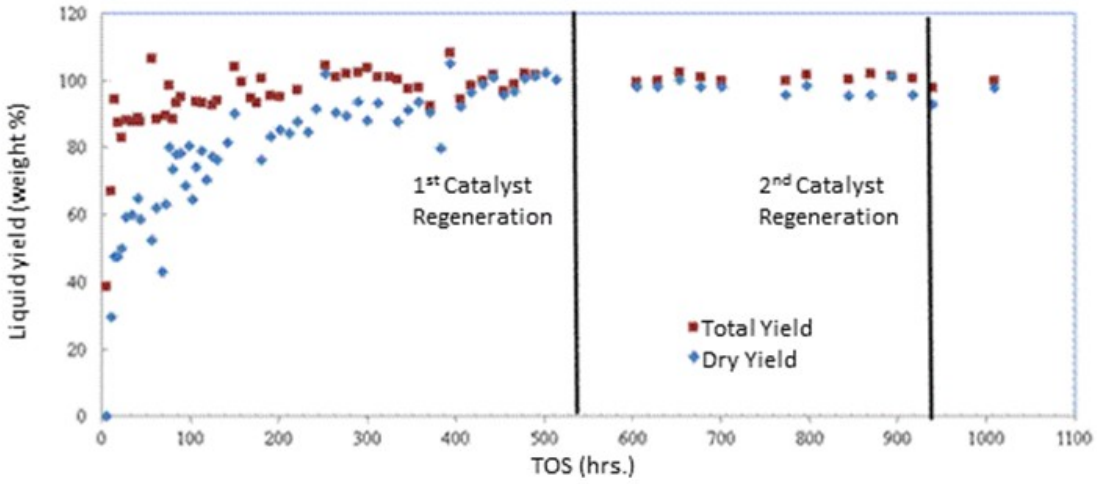

Figure 51. Liquid (stabilized bio-oil product / cleaned bio-oil feed) yield: The treatment of bio-oil with methanol at a pressure of 1,500 psig in the presence of hydrogen at 170°C. Dry yield is the total yield excluding water.

Figure 52. shows the pH of the stabilized bio-oil product versus the TOS. The pH of the liquid product increased from 2.4 (in the 'cleaned' bio-oil feed) to 3.7 after treatment in Zone I.

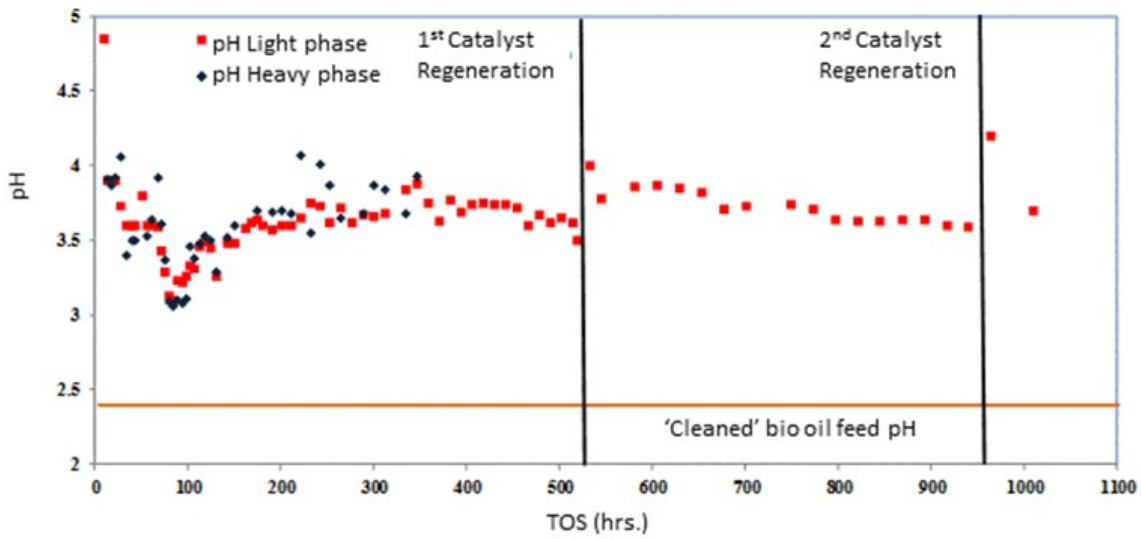

Figure 52. pH of stabilized bio-oil product: light phase (red) and heavy phase (blue). The pH of the 'cleaned' bio-oil feed is 2.4.

7.3 Zone II Hydrotreatment Run at PNNL

The bio oil produced in the run described in Section 7.2 above was shipped to PNNL, where it was hydrotreated using a sulfided CoMo catalyst. Figure 53 shows the density variation with TOS. The product density is low, at 0.78 g/ml for the first 400 hrs. TOS, because the catalyst is still 'fresh'. After approximately 500 hrs. TOS, the product density is stable, at 0.82 g/ml. There was a failure of the building ventilation system at TOS just under 800hrs. TOS which caused the hydrotreater to trip. Hydrotreater startup procedures after a trip required rinsing and reconditioning the catalyst before introduction of bio oil. This resulted in higher activity for a short period just before 800 hrs. TOS.

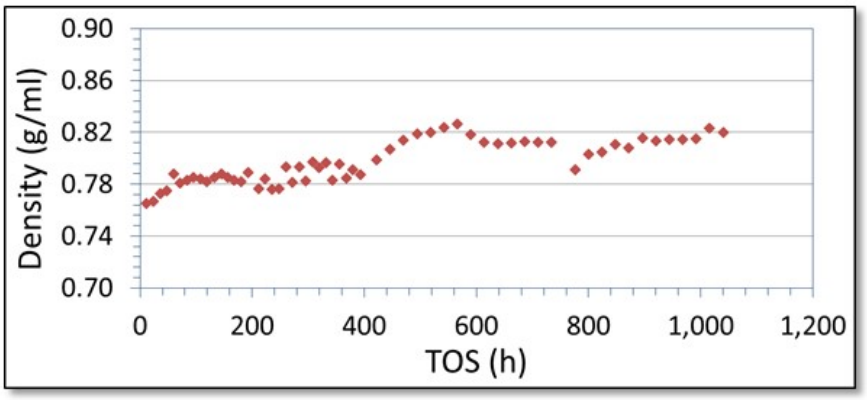

Figure 53. Density of final product after hydrotreatment - 1,000 hr. run

The overall liquid product yield during the operation was approximately 60 gals per dry ton of biomass.

8.0 Task G: Assessment of Hydrocarbon Fuel, Integration with Petroleum Operations

The purpose of this task is to analyze the hydrocarbon fuel product and assess its suitability for integration with petroleum operations.

8.1 Assessment of Hydrocarbon Fuel

A boiling point curve was generated with the product organic phase (Figure 54). The data are listed in Table 25. The cut-off for the gasoline fraction is 420 °F so approximately 70 percent of the bio-fuel was in the gasoline fraction and 30 percent was in the higher boiling diesel/kerosene fraction.

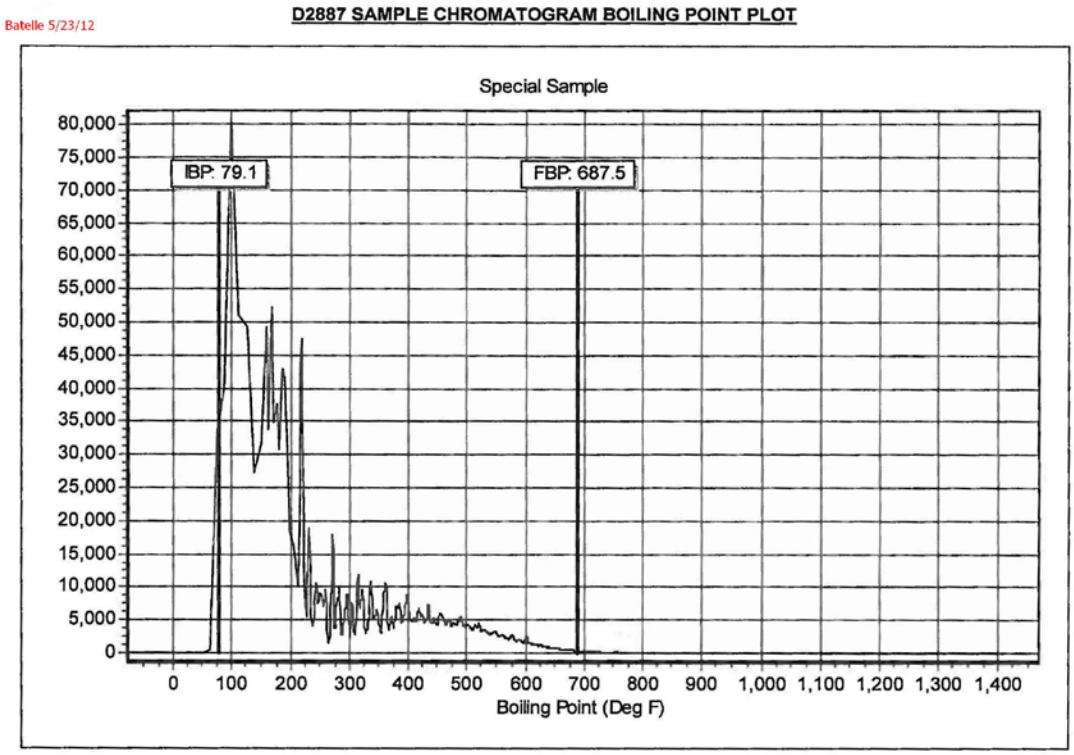

Figure 54. Boiling point curve for bio-fuel sample.

Table 25. Boiling point data.

Sample ID:	5251202 Battelle 5-23-12
	(new sample 2012)
Total Sulfur by D2622, ppm w/w	**340**
D3710 Simulated Distillation	
Vol% BoilOff	**Boiling Point, °F**
Initial boiling point (0.5%)	79
2%	90
5%	111
10%	159
15%	178
20%	201
25%	219
30%	238
35%	270
40%	291
45%	315
50%	336
55%	358
60%	380
65%	399
70%	421
75%	445
80%	471
85%	500
90%	534
95%	581
98%	627
Final Boiling Point (99.5%)	688

A summary of the major components in the naphtha fraction are shown in Table 26.

Table 26. Bio-fuel composition.

DETAILED HYDROCARBON ANALYSIS - Naphtha Fraction (IBP-420°F)				
Sample ID:	**Battelle 53576 23 ORG Rec'd 5-23-12**			
SUMMARY_BY_GROUP				
GROUP	%WGT	%VOL	%MOL	
Paraffin	16.26	19.44	22.18	
I-Paraffins	8.70	9.63	8.88	
Total Aromatics	17.50	15.18	15.96	
Mono-Aromatics	*15.11*	*13.15*	*14.10*	
Naphthalenes	*0.01*	*0.00*	*0.01*	
Naphtheno/Olefino-Benzs	*2.39*	*2.02*	*1.86*	
Indenes	*0.00*	*0.00*	*0.00*	
Total Naphthenes	57.38	55.59	52.85	
Mono-Naphthenes	*49.87*	*48.51*	*47.48*	
Di/Bicyclo-Naphthenes	*7.51*	*7.08*	*5.37*	
Total Olefins	0.00	0.00	0.00	
n-Olefins	0.00	0.00	0.00	
Iso-Olefins	0.00	0.00	0.00	
Naphtheno-Olefins	0.00	0.00	0.00	
Di-Olefins	0.00	0.00	0.00	
Total Oxygenates	0.00	0.00	0.00	
Unidentified	0.17	0.15	0.12	
Plus	0.00	0.00	0.00	
Total	100.00	100.00	100.00	

The estimated octane rating for the naphtha fraction is shown in Table 27. A comparison to the ASTM D4814 11b standards shows that the octane rating is also somewhat low, however this rating is acceptable for blending into conventional transportation fuels. Additional comparisons to the ASTM D4814 standards are presented in Table 30 below in the context of integration with petroleum operations.

Table 27. Estimated octane of naphtha fraction.

	Battelle 53576 23 (5-23-12)	ASTM D4814 11b Specification
Calculated RON	74	
Calculated MON	66	
Calculated Road Octane (R+M)/2	70	87 - 91

Table 28 shows the benzene volume percent measured in the naphtha fraction. It is slightly higher than the EPA allowable specification. We can address this by modification of the operating conditions of the hydrotreater.

Table 28. Benzene in naphtha fraction.

Component	Battelle 53576 23 (5-23-12)	Maximum Allowable EPA Specification
Benzene	0.88 volume percent	0.62 volume percent (pooled average)

Further analysis of the product showed that the density range was representative of what would be expected in a gasoline/diesel blend. The ratio of olefinic carbons/total hydrocarbon determined from $_{13}C$ NMR ranged from 0.34 to 0.56 which is two to three times the amount found in JP8. The average energy value for the product was 43.7 MJ/Kg. This is similar to both diesel and gasoline which have a net heating value of approximately 43.2 MJ/Kg.

8.2 Biofuel Insertion in the Transportation Fuel Distribution Network.

Figure 55 shows a generic transportation fuel production and distribution network. Crude oil from wells or from transport tanker ships is fed to refineries where it is converted into gasoline, diesel and other fuels. From the refineries, the gasoline/diesel and other fuel products are shipped, mostly by pipelines, rail or barge to blending terminals. There are approximately 1,500 blending terminals in the US. Ethanol and other proprietary branding components are added, which then convert the generic gasoline entering the terminal to a commercial branded fuel product ready for retail sale. A single blending terminal can produce branded retail gasoline product for several competitive brands. Gasoline is generally shipped by truck from the blending terminals to the retail gasoline stations.

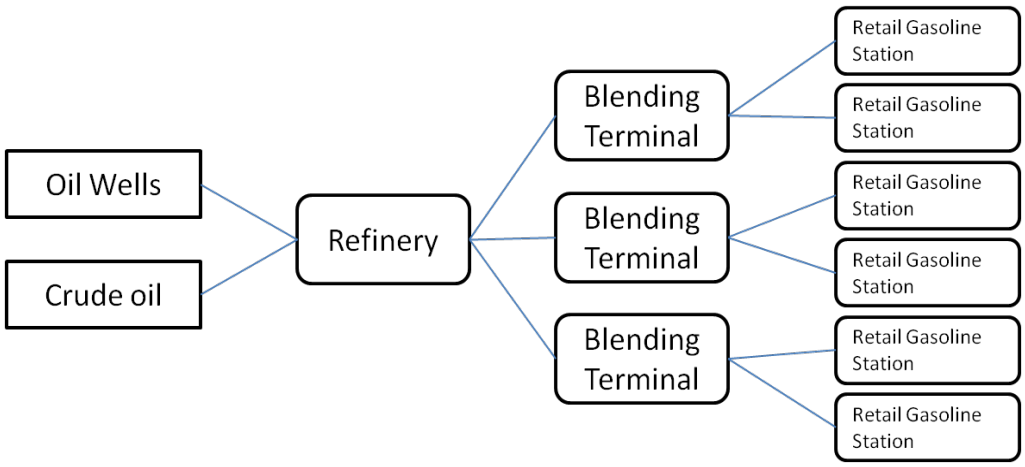

Figure 55. Typical transportation fuel distribution network.

Biofuel addition to hydrocarbon fuels was evaluated at several points along the value chain shown in Figure 55, above. The criteria used for the evaluation included economics, technical feasibility, and market receptiveness.

Biofuel addition upstream of refineries was not accepted mainly because of economics. The product value is the lowest at the upstream end of the value chain and because the ratio of biofuels volume to crude oil volume is extremely small, refinery operators will not easily be able to assign a fair market value to the biofuels.

Biofuel addition in processing streams inside refineries was initially considered, however this option was discouraged by our industrial partner. Petroleum refineries are precisely tuned for operations at large scale, high reliability and uptime, and because of very large capital investment and operating costs, unplanned downtime is extremely expensive. Since biofuels production technology is relatively immature, it was felt that the addition of biofuels at significantly smaller volumes into refinery streams might lead to unacceptable capital investments for the refiner (in terms of storage, pre-treatment, and other infrastructure changes) as well as possible risks to operations. Refineries strongly encouraged Battelle to consider addition of the biofuel at blending terminals. These facilities are already configured for blending gasoline with alcohol and additives, therefore addition of biofuels blending capability will be a natural extension of their function in the transportation fuel distribution chain.

8.2.1 Federal Regulatory Considerations:

Under section 211 of the Clean Air Act, the Federal Government requires any new fuel to be approved and registered by the EPA prior to commercial use in transportation vehicles. The EPA has two major regulations that must be met before a new biofuels can qualify to generate RINs under the EPA Renewable Fuels Program. Each is discussed below:

8.2.1.1. EPA Fuel/Fuel Additive Registration Requirements (Title 40 CFR Part 79):

For registration under this program, biofuels manufacturers are required to analyze the combustion and evaporative emissions generated by their fuel, conduct an analysis of the health effects, and provide this information to the EPA. The information requirements are categorized under:

> ***Tier 1 (Title 40, Section 79.52)***: This requires fuel manufacturers to conduct a survey of the existing scientific literature related to vehicle emissions from their fuel, and where adequate information is not available, conduct laboratory tests. The emissions include: total hydrocarbons, carbon monoxide, oxides of nitrogen, and particulates. The manufacturers are also obligated to provide any available information regarding the health and welfare effects of those emissions. This includes potential toxicological, environmental, and other public welfare effects of the emissions.
>
> ***Tier 2 (Title 40, Section 79.53)***: If the *Tier 1* information related to the toxicological, environmental, and health effects of the emissions is not sufficient (as described in Title 40, Sections 79.62-79.68), animal testing is required under *Tier 2*. This testing consists of trials using laboratory rats that are exposed to the exhaust of engines fueled with the fuel (subchronic exposure) for 90 days. After 90 days, the rats are dissected and examined for evidence of carcinogenicity (tendency to cause cancer), mutagenicity (tendency to cause genetic mutations-conducted on diesel particulate extract), teratogenicity (tendency to cause fetal abnormalities), reproductive toxicity (inability to reproduce), and neurotoxicity (nervous system problems).
>
> ***Tier 3 (Title 40, Section 79.54)***: If the information submitted under *Tier 1* and *Tier 2* is deemed to be insufficient, the EPA reserves the right to require further health effects testing. *Tier 3* testing may address details such as concentration-effect relationships, statistical significance of the results and severity of health effects.

8.2.1.2 EPA Requirements for Qualifying as a Renewable Fuel under the Renewable Fuel Standard.

New biofuels will need to be approved by the EPA to qualify as a Renewable Fuel under the Renewable Fuel Standard. This approval is necessary for the fuel to earn a Renewable Identification Number (RIN).

The biofuels produced by the Battelle process will qualify for a "D" value of 3 (Cellulosic biofuels) under the EPA categorization of conversion routes.

On May 7, 2013, Battelle's representatives met with EPA staff in the Office of Transportation and Air Quality in charge of the Alternative Pathway program for RFS2. The purpose of the meeting was to obtain guidance from EPA staff on how to expedite and streamline Battelle's application for a new fuel pathway.

EPA published its final rule entitled: "Identification of Additional Qualifying Renewable Fuel Pathways under the Renewable Fuel Standard Program" in the Federal Register on March 7, 2013. The rule became effective May 6, 2013. The new rule identified additional fuel pathways that EPA determined meet the biomass-based diesel, advanced biofuel or cellulosic biofuel lifecycle greenhouse gas (GHG) reduction requirements specified in Clean Air Act section 211(o), the Renewable Fuel Standard (RFS) Program, as amended by the Energy Independence and Security Act of 2007 (EISA). The final rule includes EPA's evaluation of renewable gasoline and renewable gasoline blendstocks, and clarifies EPA's definition of renewable diesel. EPA included Table 29, "Applicable D Codes for Each Fuel Pathway for Use in Generating RINs". Renewable gasoline blendstock is approved under category "M" as shown below:

Table 29. EPA Section 80.1426—Applicable D Codes for each fuel pathway for use in generating RINs. Battelle's process qualifies under category "M", D-code 3.

	Fuel type	Feedstock	Production process requirements	D-code
I	Cellulosic diesel, jet fuel and heating oil.	Cellulosic Biomass from crop residue, slash, pre-commercial thinnings and tree residue, annual covercrops, switchgrass, miscanthus, and energy cane; cellulosic components of separated yard waste; cellulosic components of separated food waste; and cellulosic components of separated MSW.	Any	7
M	Renewable gasoline and renewable gasoline blendstock.	Cellulosic Biomass from crop residue, slash, pre-commercial thinnings, tree residue, annual cover crops; cellulosic components of separated yard waste; cellulosic components of separated food waste; and cellulosic components of separated MSW.	Catalytic Pyrolysis and Upgrading, Gasification and Upgrading, Thermo-Catalytic Hydrodeoxygenation and Upgrading, Direct Biological Conversion, Biological Conversion and Upgrading, all utilizing natural gas, biogas, and/or biomass as the only process energy sources Any process utilizing biogas and/or biomass as the only process energy sources.	3
N	Naphtha	Cellulosic biomass from switchgrass, miscanthus, and energy cane.	Gasification and upgrading	3
O	Butanol	Corn starch	Fermentation; dry mill using natural gas, biomass, or biogas for process energy.	6

Source: EPA Final Rule "Identification of Additional Qualifying Renewable Fuel Pathways under the Renewable Fuel Standard Program" – published in Federal Register March 7, 2013

Battelle's process would be covered under the new alternative fuel pathway under category "M", D-code 3. This is highly significant, since Battelle would not be required to submit an alternative pathway application to EPA and/or conduct land use analysis and modeling to demonstrate GHG emission compliance with the RFS for RIN generation.

8.2.2 State Regulatory considerations:

Several states have adopted ASTM D4814 "Standard Specifications for Automotive Spark Ignition Engine Fuel" for drop in gasoline biofuels and ASTM D975 for drop in diesel. These specifications describe characteristics of motor fuels which include volatility, water tolerance, maximum vapor pressure, antiknock index and components such as sulfur, lead and phosphorous for all the states in the continental USA for all seasons. The specifications also describe various test methods needed to evaluate the fuel for compliance to the Standard.

Battelle characterized its fuel product against selected tests for a preliminary evaluation. Table 30 shows the results against ASTM D4814:

Table 30. Biofuel properties against ASTM specifications.

Test	ASTM Method per ASTM D4814	Result for Battelle's biofuel	ASTM D4814 Specification	Unit
Viscosity	D445	1.842		mm^2/sec
Flash Point	D93	<25.0		^oC
Sulfur	D5453	0.8 (TiO_2 catalyst)	<80	ppmw
Sulfur	D2622	24 (Sulfided Catalyst)	<80	ppmw
Vapor Pressure	D5191	1.44	9.0-15.0	PSI
Antiknock index		70	As agreed with customer	
Benzene		0.67-0.88	<0.62 Jan-2015 <1.3% Jul 2012	vol%
Distillation TiO_2 catalyst	D86			
10%	D86	101	50-70	^oC
50%	D86	199	110-121	^oC
90%	D86	311	185-190	^oC
Distillation Sulfided catalyst	D3710			
10%	D3710	69.4	50-70	^oC
50%	D3710	178.3	110-121	^oC
90%	D3710	289	185-190	^oC

The Sulfur in the Battelle biofuels is mainly from the catalyst; its concentration is very low (< 1ppmw) when the TiO_2 catalyst is used and 24 ppmw when the sulfided CoMo catalyst is used. This level is still below the ASTM specification, and can be reduced further by conditioning the sulfided catalyst if it is used.

The Antiknock index is relatively low at 70. Commercial fuel specifications require minimum Antiknock index of 87. Increasing the isoparaffin content would improve the octane rating and increase the antiknock index. Antiknock index can also be adjusted via blending into a large pool of gasoline and addition of additives such as ethanol.

The Benzene content is within the limits at the present time, but would be marginally out of compliance in January 2015. The Benzene in the Battelle biofuels is produced mainly by the partial cracking of the aromatic character of lignin. This can be reduced by tuning the hydrotreatment catalyst and the process conditions to further crack open the aromatic ring structure of lignin based components in the product.

The distillation curves show that the Battelle biofuel is less volatile than the specifications for gasoline. Distillation properties for kerosene and diesel overlap. In some cases, it is possible to certify a fuel as both kerosene and diesel. Finished kerosene and diesel typically have a final boiling point of about 316°C-321°C. The Battelle process does not yet employ fractional condensation or distillation. With those steps, the Battelle process will produce separate diesel and gasoline products which will be compliant with the ASTM 3710 distillation specifications.

The finished gasoline product must meet seasonal volatility and distillation requirements per ASTM D4814. There are also requirements related to gum formation, corrosion, etc. These can be addressed after the hydrotreatment process is optimized during commercial operational trials.

8.2.3 Other considerations related to blending.

8.2.3.1 Quality Assurance: Each shipment of biofuels will be tested by a third party laboratory against ASTM D4814 specifications agreed in advance with the blending terminal operator. The biofuels shipment will be accompanied by a Certificate of Analysis which will demonstrate compliance of the product against the ASTM specification.

8.2.3.2 Security: Since the biofuels will be chemically similar to gasoline, normal security procedures already in place at fuel blending terminals will likely be sufficient.

8.2.3.3 Blending infrastructure: Additives and ethanol are blended into gasoline at the terminal generally at the “rack”, i.e. the installation where the gasoline, ethanol and additives are actually pumped into the fuel transport trucks and the mixing takes place in the tank on the truck. The product after blending must comply with Federal, State and (if applicable) local regulations. Since biofuel volume is expected to be very small relative to conventional petroleum, it is likely that it will also be blended, like ethanol and additives at the rack, as this would be the lowest cost approach. The terminal operator will have to incur the cost of building a tank and related piping to store the biofuels and deliver it to the rack. Since the Battelle biofuels will be chemically equivalent to gasoline, traditional carbon steel metallurgy will be sufficient.

8.3 Conclusions

Battelle has analyzed the hydrocarbon fuel product and assessed its suitability for integration with petroleum operations. Battelle’s biofuels characterization data were compared against ASTM D4814 specifications and a case for suitability for blending was presented. Fuel blending terminals are identified as the most suitable locations for insertion of the biofuels into the value chain.

9.0 Task H: Techno-Economic Analysis of Catalytic Pyrolysis and Upgrading

9.1 Process Flow Sheet and Model Development

9.1.1 Base Case Process Model (2012)

The initial process model was developed in CHEMCAD©. To produce upgraded oil from wood, the process flow sheet is divided into three sections: catalytic pyrolysis, hydrotreating, and hydrogen and steam production. The process flow sheet is shown in Figure 56.

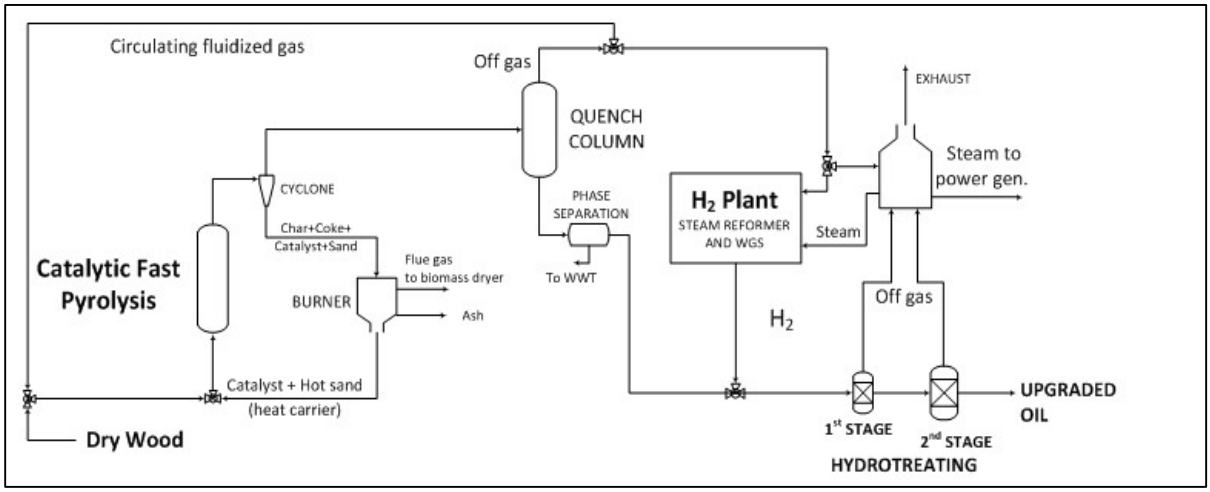

Figure 56. Process flow of catalytic pyrolysis and upgrading.

Catalytic pyrolysis experimental data (FP032) were adjusted to balance the elements which are necessary for process model development and simulation. Assumptions for the hydrotreating step were estimated based on experimental data that is in the publicly available literature[iv,v]. The assumptions are shown in Table 34 below, compared with those used in subsequent model iterations.

A portion of the off-gas from the catalytic pyrolysis stage is sent to the hydrogen plant which is comprised of a steam reformer and a water gas shift reactor. The rest of the off-gas is combined with the hydrotreating off-gas and burned to generate heat for the steam reformer and for steam generation. Steam is utilized on-site as well as used for electricity generation.

The modeling and economic assumptions are similar to those used in the OBP pyrolysis design case, Production of Gasoline and Diesel from Biomass via Fast Pyrolysis[vi]. The cost analysis was performed using a discounted cash flow method based on 2,000 metric ton per day (mtpd) wood feedstock. Key economic assumptions are n^{th} plant, 2007 USD (US dollars), 10% IRR (Internal Rate of Return), 90% stream factor and MACRS (Modified Accelerated Cost Recovery System) depreciation. Upgraded oil yields and the estimated minimum selling prices obtained from the model are shown in Table 31 below. The results of a sensitivity analysis of model inputs is depicted in Figure 57 below.

Table 31. Upgraded oil yield and minimum fuel selling price obtained from the model (base case process).

Yield	52	gallon/dry U.S. ton
Annual Production	37	MM gallon/year
Minimum Fuel Selling Price, MFSP	2.97	$/gallon

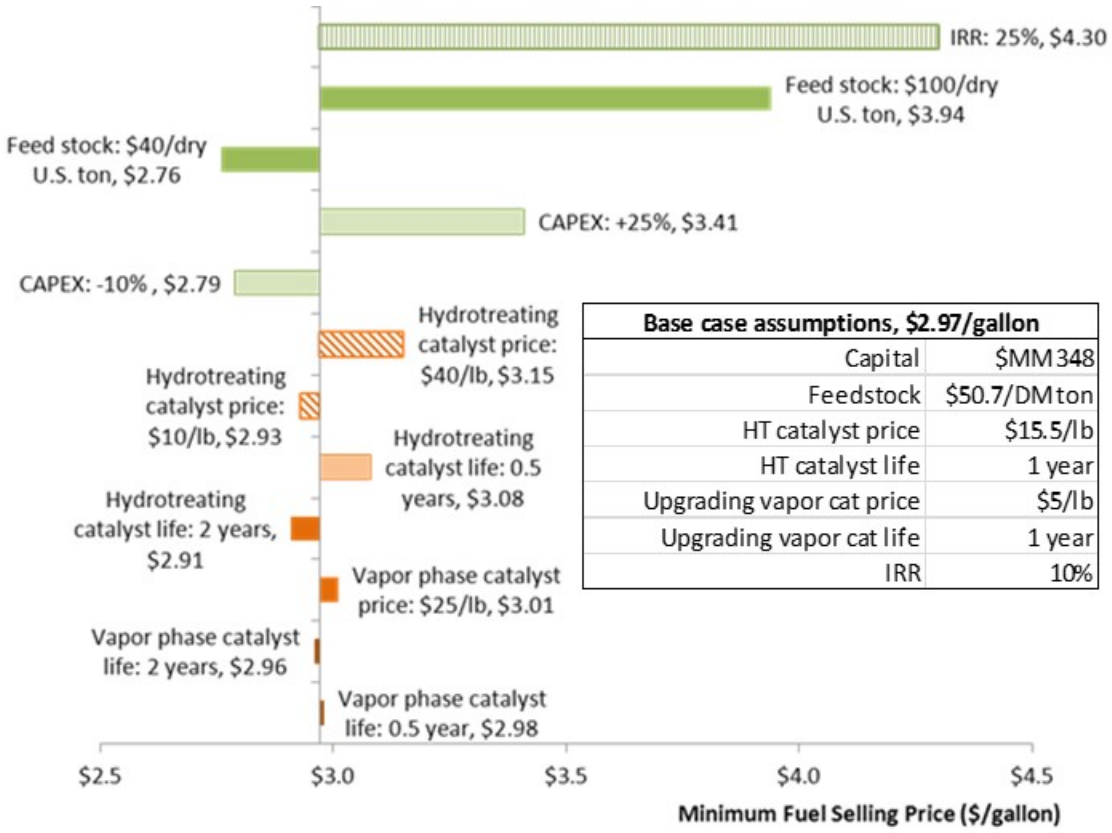

Figure 57. Sensitivity analysis (base case process).

There is a trade-off between pyrolysis oil yield and oxygen content in the oil. In Figure 58, the effect of oxygen content on oil yield is plotted, and was derived from various studies of catalytic pyrolysis of wood. Many catalysts are considered in this data plot and it shows that the oil yield increases with increasing oxygen content. Note that there is no natural gas brought into the hydrogen plant for the 2012 base case which yields 34% pyrolysis oil, because sufficient off-gas is available for hydrogen generation.

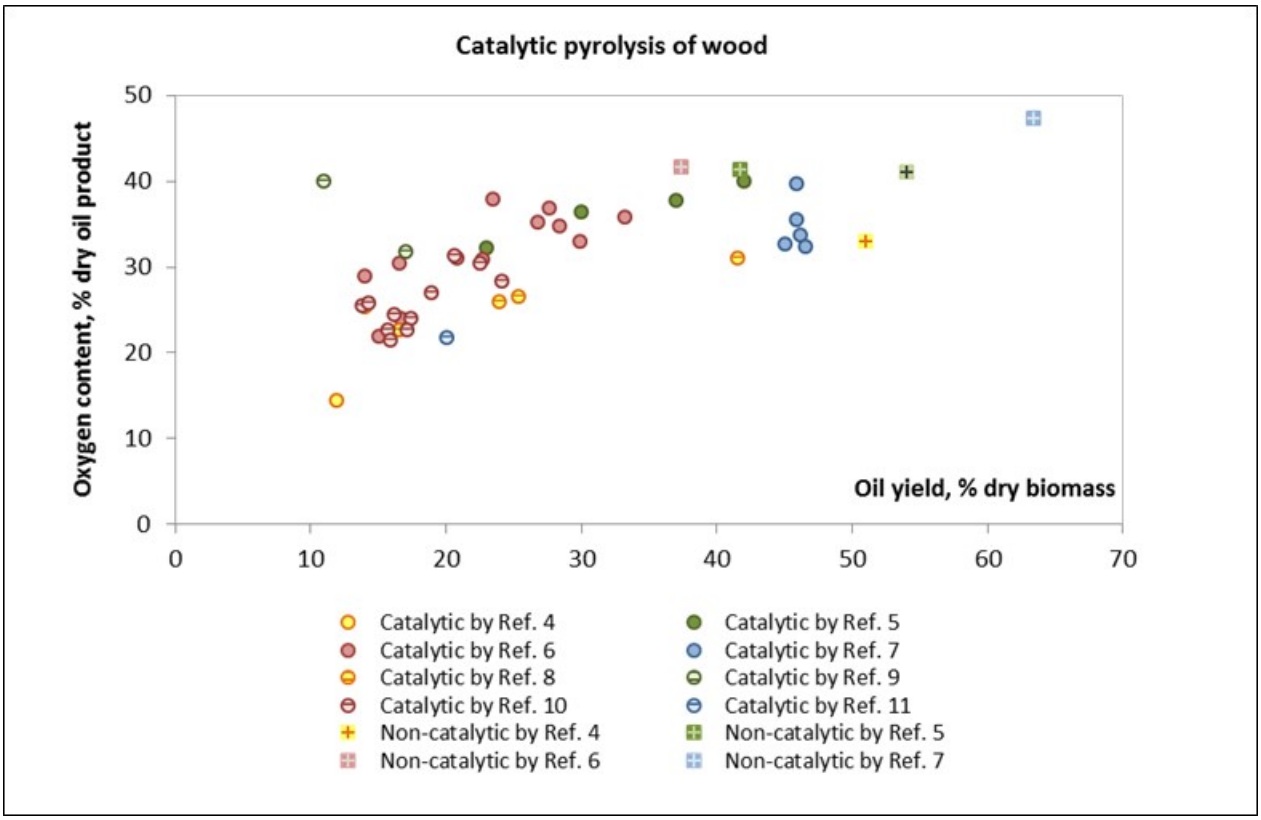

Refer-ences	Catalysts	Catalytic Pyrolysis	Biomass	Temperature (°C)	
				non-catalytic	catalytic
vii	HZSM-5	**Ex-situ:** Bubbling fluidized bed, flow reactor	Hybrid poplar - 200 g/h	450-475	425-450
viii	H-Beta Zeolite	**Ex-situ:** Bubbling fluidized bed, flow reactor	Pine wood, 15 g total	400	440
ix	Various	**Ex-situ:** Fixed bed, small catalyst tube	Commercial (Lignocel HBS 150-500) 1.5 g	500	500
x	HZSM-5	**Ex-situ:** Fixed bed, flow reactor	Saw dust - 3 kg/h	500	390-550
xi	Kaolin, FCC-L, FCC-H, Steamed FCCs	**In-situ:** Bubbling fluidized bed, flow reactor	Hybrid poplar - 150 g/h	450-475	
xii	CaY zeolite and catalyst M (by UOP)	**In-situ:** Bubbling fluidized bed, flow reactor	White oak	500	
xiii	FCC	**In-situ:** Recirculating fluidized bed, flow reactor	Hybrid poplar	475	
xiv	HZSM-5	**In-situ:** Bubbling fluidized bed, flow reactor	Hybrid poplar - 100 g/h	500	

Figure 58. Oxygen content and pyrolysis oil yields from recent literature.

Generating hydrogen, using a water gas shift reactor is inexpensive compared to a steam reformer; however, a steam reformer and a WGS reactor were used in the 2012 model because of the low CO/CO_2 ratio in the pyrolysis off gas as suggested by initial laboratory results. The capital cost could be significantly reduced if the CO/CO_2 ratio is improved and there is sufficient off-gas to meet the hydrogen demand. A simple comparison of installed equipment costs between using WGS alone and using a full hydrogen plant (a WGS and a steam reformer) is shown in Table 32. A previous analysis[vi] performed in 2009 assumed only WGS for hydrogen production and the installed equipment cost for hydrogen generation is approximately five times less expensive than having a full hydrogen plant as assumed in the current analysis.

Then-current available catalytic pyrolysis laboratory data were used in this economic analysis. Base case and the previous analysis (conducted in 2009) assumptions and results are compared in Table 32.

Table 32. Previous (2009) and base case (2012) analysis assumptions and results.

Update		2009 model based on literature			2012 model based on experiment (FP032)	Reason for update
		base case	improved case	advanced case		
✓	Upgraded oil ($/gallon)	$2.46	$2.02	$1.95	$2.97	
✓	Pyrolysis oil yields (% dry feed)	23%	29%	31.4%	33.7%	Updated numbers from experiment data (FP032)
✓	Oxygen content in bio-oil (% dry basis)	21%	21%	21%	37.60%	Updated numbers from experiment data (FP032)
✓	H_2 consumption in hydrotreating (lb/100 lb)	4.99	4.85	4.86	3.5	Estimated from oxygen content in the pyrolysis oil
✓	CAPEX ($MM)	$MM 167	$MM 164	$MM 164	$MM 338	Updated hydrogen plant, steam/power plant and wastewater treatment plants
	Feed stock price ($/dry U.S. ton)	$50.70				
✓	CO/CO2 mass ratio from catalytic pyrolysis	2.8			0.81	Updated numbers from experiment data (FP032)
✓	Hydrogen production	2 stage water gas shift (WGS)			reformer and water gas shift	Not enough CO in off gases
✓	Installed equipment cost for hydrogen production	$MM 14.2			$MM 75.6	Replacing 2 stage WGS with a reformer and a WGS
✓	Hydrotreating	1-stage: LSHV = 0.28			2-stage: LSHV = 1.1 (1st stage) and 0.3 (2nd stage)	
	Cost indexed	2007 US dollars				
	Feed stock	wood, 2000 mtpd, 5% moisture content				
	Stream factor, IRR and Depreciation assumptions	90%, 10 IRR and MACRS				

The minimum selling price increases from $2.50 (base case, 2009) to $3.00 per gallon fuel because of a higher capital cost. The laboratory results for pyrolysis oil yield and gas compositions suggest that the use of only water gas shift reactors are not able to generate enough hydrogen for upgrading the fuel. Therefore, a full hydrogen plant including a steam reformer and a water gas shift reactor are used in the 2012 process flow sheet. The steam and power plant design and capital costs are also updated as suggested by the laboratory analysis of the off gas compositions. In addition, two-stage upgrading rather than single-stage upgrading is more likely necessary due to the higher oxygen content in bio-oil product.

9.1.2 Interim Process Model (2013)

The process model was updated during the performance of the project. The process configuration and economic assumptions are the same as in the analysis work performed in 2012 to provide a consistent comparison. Hydrotreating conditions and hydrotreating yields in the process simulation are significantly different from the previous work since more detailed experimental results became available during the preceding year. The experimental data used in process modeling in 2012 and 2013 are compared in Table 34. Note that for the 2012 model, experimental data from bio-oil hydrotreating were not yet available, so assumptions were made based on best engineering judgment.

The process model was developed in CHEMCAD© and is divided into three sections: catalytic pyrolysis, hydrotreating, and hydrogen plant and steam production. Consistent with the previous work, the vapor phase upgrader was modeled as a fixed bed reactor with a 1-year catalyst life.

The cost analysis was performed using a discounted cash flow method. Key economic assumptions are n^{th} plant, 2007 USD (US dollars), 10% IRR (Internal Rate of Return), 90% stream factor and MACRS (Modified Accelerated Cost Recovery System) and 2000 mtpd wood feedstock processed. These assumption are unchanged from the 2012 analysis.

Experimental results in 2013 (Table 34) show a product yield of 17 g upgraded oil per 100 g dry wood, lower than what was assumed in the previous model (19 g upgraded oil per 100 g dry wood). However, the density of upgraded oil is different for each case (7.36 lb/gallon in 2012 model and 6.56 lb/gallon in 2013 model), and volumetric yields (gallon per dry ton biomass) turn out to be similar for the two cases. As experimental data for density and distillation curve of the upgraded oils were not yet available, the oil density was calculated in CHEMCAD and depended on the types of model compounds used in the simulation.

Table 33 shows the minimum selling price of the upgraded oil from previous model (2012) and updated model (2013). Annual upgraded oil yields in million (MM) gallon per year are comparable for the two models; however, the analysis results show that the upgraded oil price is more expensive for the 2013 model. This is because hydrogen consumption found from the hydrotreating experiment is higher than what was assumed in the 2012 analysis. As a result, a larger hydrogen plant is required, increasing the total capital cost by MM$34 and upgraded oil price by 17 cents/gallon. These results are substantially the same as the 2012 modeling results, given the level of experimental detail and associated error range of the analysis. Cost sensitivity to the major technical and economic assumptions is shown in Figure 59.

Table 33. Economic analysis results - 2013.

	2012 model	2013 model
Upgraded oil annual production (MM gallon/year)	37	38
Upgraded oil yield (gallon/dry US ton feedstock)	52	53
CAPEX ($MM)	$MM 338	$MM 372
Upgraded oil price ($/gallon)	$2.97	$3.14

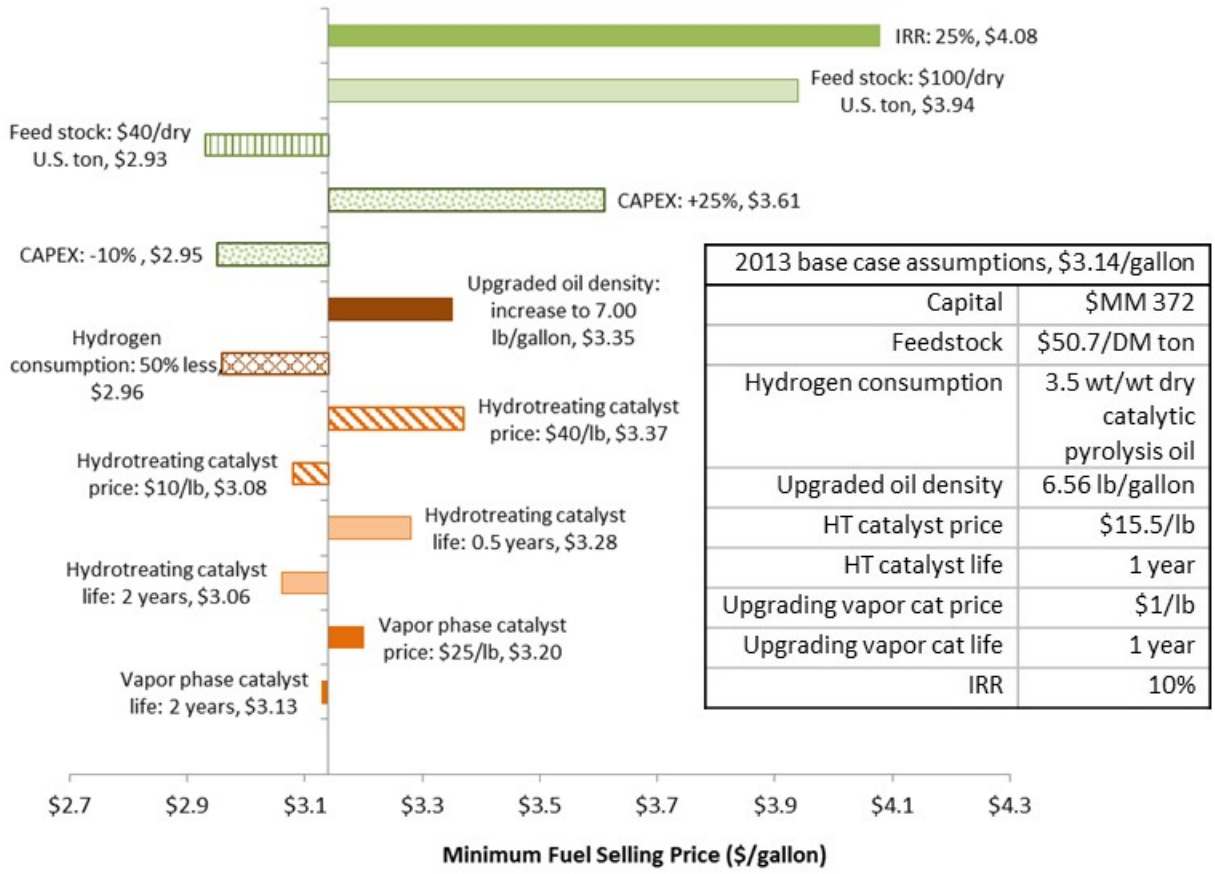

Figure 59. Sensitivity analysis (updated 2013 process).

9.2 Final Process Model (2015)

In the latter months of the project, the process model and economic analysis was refined to reflect experimental results and the evolution of the conversion processes, as well as to incorporate engineering design details developed by Battelle for its 100 ton per day commercial pyrolysis and hydrotreating system.

While maintaining consistency with the previous models and analysis, we developed models and capital cost estimates that reflect both experimental results and Battelle's small modular design concept. The pyrolysis model was developed using experimental data from Battelle's 1 ton/day pyrolysis system. The

hydrotreating model was developed in CHEMCAD© following the previous hydrotreating CHEMCAD model, but modified specifically to obtain an external cost estimate for a 100 ton/day system. Utilities and auxiliaries were scaled down from the previous process model and cost estimate. The hydrogen plant and steam production section cost estimate was derived from a DOE Hydrogen Program tool[xv].

The process modeling and economic analysis assumptions for each of the three model iterations are shown in Table 34 below. While individual assumptions and experimental values varied significantly across the models, the overall fuel yield remained remarkably similar. Hydrogen consumption was approximately ten percent higher than the 2013 model, reflecting the removal of the catalytic upgrading of pyrolysis vapor.

Table 34. Current and previous assumptions for process modeling and simulation.

Process	2012 model	2013 model	2015 model
Pyrolysis	**Experimental data (run# FP032, catalytic pyrolysis)**	**Experimental data (run# FP061 & FP062, catalytic pyrolysis)**	**Experimental data (Battelle 1 ton/day non-catalytic pyrolysis)**
	Yield (per dry woody feedstock)	Yield (per dry woody feedstock)	Yield (per dry woody feedstock)
	Oil 34%	Oil 36%	Oil 45%
	Gas 32%	Gas 32%	Gas 15%
	Solid 21%	Solid 20%	Solid 15%
	Water 14%	Water 12%	Water 25%
Hydrotreating	**Assumptions***	**Experimental data (run# HT2012-09-25 and HT2012-10-23)**	**Experimental data (Battelle Zone I and PNNL Zone II HT 1,000 hr run)**
	Hydrogen consumption (wt/wt, H2/dry catalytic pyrolysis oil) 3.5%	Hydrogen consumption (wt/wt, H2/dry catalytic pyrolysis oil) 7.5%	Hydrogen consumption (wt/wt, H2/dry pyrolysis oil) 8.3%
	Hydrotreating reactors 2-stage LSHV: 1.1 (1st stage) and 0.3 (2nd stage) Temp: 320 F (1st stage) and 608 F (2nd stage) Pressure: 2000 psia in both stages	2-stage hydrotreating reactors 2-stage LSHV = 0.4 in both stages Temp. =460 F (1st stage) and 734 F (2nd stage) Pressure: 1740 psia in both stages	2-stage hydrotreating reactors 2-stage LSHV = 0.4 in both stages Temp. =340 F (1st stage) and 680 F (2nd stage) Pressure (as tested): 1550psia (1st stage) and 1800 psia (2nd stage)
	Yield (per dry catalytic pyrolysis oil)	Yield (per dry catalytic pyrolysis oil)	Yield (per dry pyrolysis oil)
	Oil 55%	Oil 47%	Oil 40%
	Gas 22%	Gas 30%	Gas 31%
	Water 23%	Water 23%	Water 29%
Overall Yield	g upgraded oil per 100 g dry wood **19**	g upgraded oil per 100 g dry wood **17**	g upgraded oil per 100 g dry wood **18**

*Best estimate (not available experimental data) at the time of process model development.

9.2.1 Pyrolysis

Two significant changes to the process and economic model occurred between 2013 and 2015. First, vapor phase upgrading in the pyrolysis system, “catalytic pyrolysis,” was found to be unattractive and is no longer employed. Examination of the experimental results showed that the beneficial decrease in oxygen content achieved by vapor phase catalysis was more than offset by an unfavorable decrease in bio-oil yield and corresponding increase in non-condensable gas production. As shown in Table 34 above, the overall yield observed in experiments using non-catalytic pyrolysis oil are 18 g upgraded oil per 100 g of dry wood, an increase over the 2013 results with catalytic pyrolysis oil.

Second, the design basis was changed from a 2,000 ton/day system to a 100 ton/day system, specifically a cost effective, compact, small scale fast pyrolysis technology developed by Battelle. The material flow in the process is shown in Figure 60.

The technology features mechanical, auger based circulation of heating media (sand) between a proprietary down flow reactor and a fluidized bed char combustor. Use of mechanical circulation of heating media eliminates the need for fluidization gas, which then greatly reduces the capital costs, parasitic losses and complexity associated with blowers, preheaters, and oversized condensers needed for fluidized bed systems. Battelle’s down flow reactor technology uses gravity to augment the transport and mixing of the heating media and the biomass. The high heat transfer rates achieved in the down flow reactor result in high bio oil yield, comparable to that achieved by fluidized bed technology. Battelle’s system also features a novel, non-plugging condenser design which enables continuous operation without the ‘plungers’ and similar tar removal devices generally required by conventional systems. The benefit of eliminating fluidization gas and using down flow reactor technology is that a 100 ton/day system can be packaged into a small footprint. The system can be fabricated and tested off site, which will significantly reduce field work, errors and cost. This is in contrast to fluidized bed based systems of similar capacity being built on site using larger, taller and more expensive facilities.

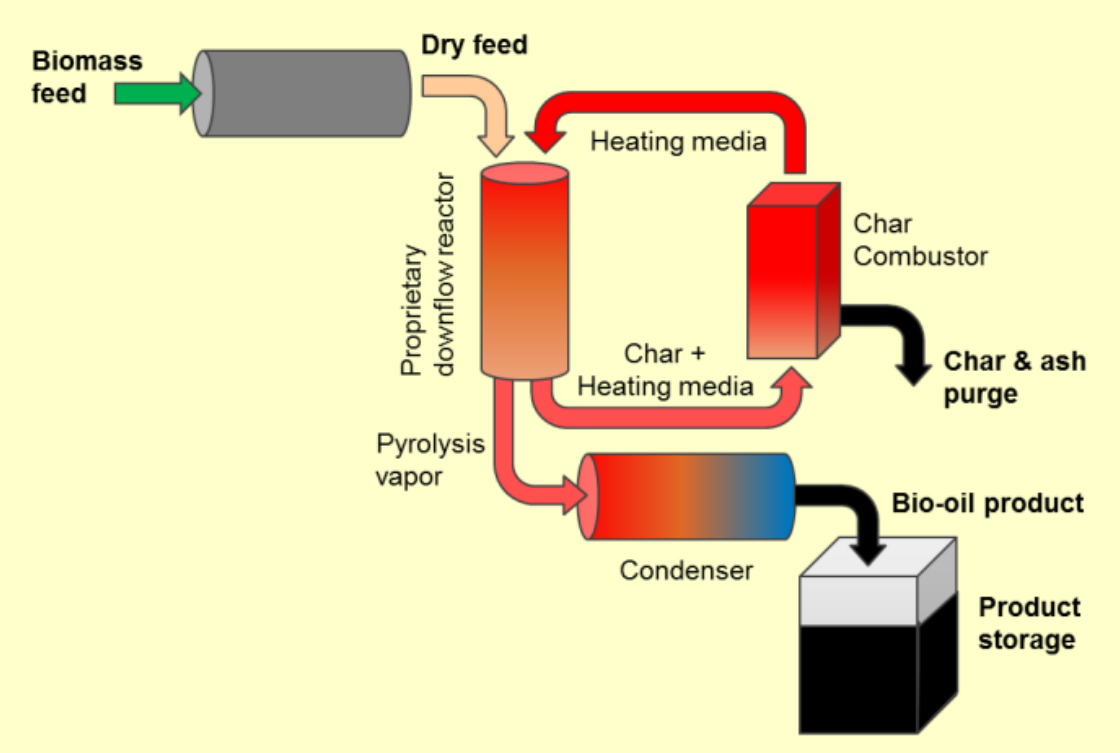

Figure 60. Pyrolysis process flow diagram.

Char produced by biomass pyrolysis is combusted within the system. The combustion heat is employed to provide process heat to drive the pyrolysis reaction and to dry the wet biomass feed. Under the assumed biomass feed condition of 30 wt% moisture, the char combustion heat alone is insufficient to fully dry the biomass. If the non-condensable gases were combusted along with the char, the biomass drying heat duty would be met. Battelle has evaluated this configuration for stand-alone pyrolysis system operation. However, as in the 2012 and 2013 process models, non-condensable gases are sent to the hydrotreating system to be utilized for hydrogen production. Excess heat from the hydrotreater is imported to the pyrolysis biomass dryer via steam or hot oil system included in the hydrotreater system. Pyrolysis vapors are condensed with the heat being dissipated by an air-cooled coolant loop. Bio-oil is collected and fed to the downstream hydrotreater for upgrading.

The capital cost estimate for the pyrolysis system is based on Battelle's internal financial model numbers. Total Purchased Equipment Cost (TPEC) was estimated from Battelle's equipment and fabrication cost estimates for a 20 ton/day pyrolysis system. The equipment includes the biomass dryer, pyrolysis reactor and fluidized bed combustor and steam generation unit, condenser system, and utilities. We scaled the TPEC cost estimate to 100 ton/day using a power law scaling factor of 0.65.

We then applied the general cost factoring approach as was done in the 2012 and 2013 cost estimates, which are similar to those used in the OBP pyrolysis design case, Production of Gasoline and Diesel from Biomass via Fast Pyrolysis[vi]. However, our approach deviated from the previous analyses in that different cost factor values were employed to reflect the small, modular plant model.

Battelle's business plan describes a massively distributed production model with a large number (eventually several hundred) of small pyrolysis-upgrading systems located near low-cost biomass sources. We exploit the fact that biomass availability significantly overlaps geographically the existing liquid petroleum pipeline network infrastructure, allowing for co-locating the system's blending stations.

The modifications to the cost factored approach reflect our business plan for modular systems. The rationale behind our use of lower factors is that installation of factory-built, skid mounted modules is expected to be significantly less costly than traditional field-built unit installation and construction. Site preparation costs are anticipated to be less, as well, owing to the small footprint and self-supporting modular construction. Our equipment cost estimates already reflect the factory-built costs necessary to realize these savings. The relatively small scale of our 100 ton/day systems will enable placement at existing facilities. As such, we have assumed the ability to leverage existing facility infrastructure in utilities and buildings.

The estimated Total Project Investment for the pyrolysis system is $5,163,966.

9.2.2 Hydrotreating

Battelle created a model of the hydrotreater portion of the pyrolysis system on a 100 TPD scale, for the purpose of generating a preliminary process flow diagram of the process and budgetary pricing for the system. A snapshot of the CHEMCAD flowsheet is shown in Figure 61 below.

The bio-oil feed stream is a mixture of expected compounds with a CHNO similar to that expected from the pyrolysis system. The bio-oil is mixed with the hydrogen recycle stream before it enters the Zone I hydrotreater. In practice this first stage will be split into two reactor in parallel such that one can be taken offline and the catalyst regenerated while the other stays in operation. The bio-oil is cooled and then a flash drum. These two unit operations represent a condenser, which removes water before the Zone II hydrotreater. At the time the model was built, two phase post-Zone I product was anticipated. The equipment was left in the system equipment list for capital cost estimating for conservatism, as well as to be utilized for solvent separation and recycling prior to Zone II, if required.

Next, bio-oil and the hydrogen-rich vapor phase together enter the Zone II hydrotreater, which converts the existing compounds to the final fuel. The product then enters two condensers, which splits the product into a C12+ heavy fraction and a C5-C11 rich fraction. The first condenser cools the stream to

175°C before the flash, while the second condenser cools the stream to 40°C. The non-condensable gases enter a splitter, which sends 10% of the flow to a purification process.

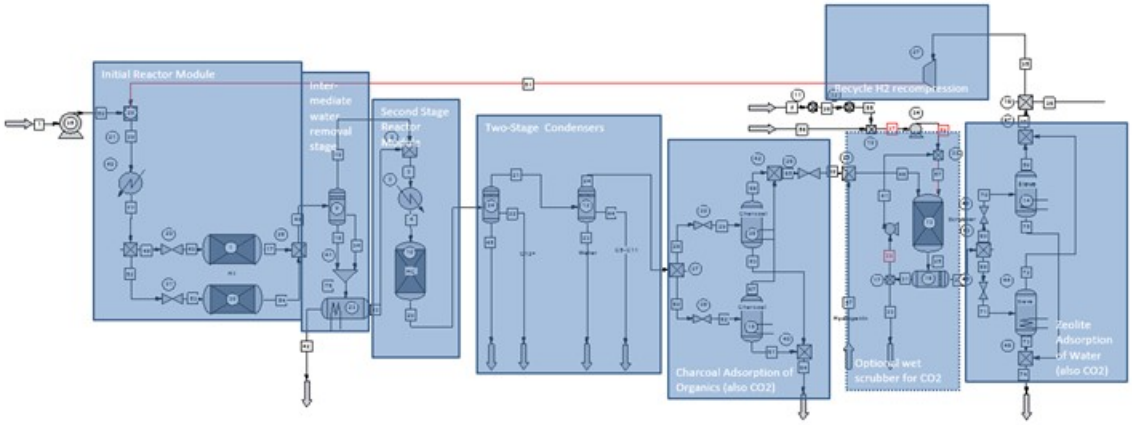

Figure 61. Hydrotreater process flow model.

The purification process has a guard bed of charcoal to prevent fouling of the pressure swing adsorption (PSA) system. These beds are duplexed in the model for clarity. The PSA is modeled to recover 80% of the hydrogen along with trace amounts of methane, CO, CO_2, and H_2O. The pressure of this stream is set to 1500 psi to represent pressure loss from the PSA, and fresh hydrogen is fed into the process from the hydrogen generation reformer discussed below. A small blowdown stream of recycle hydrogen is maintained to keep purity high. The recycle hydrogen is then recompressed to 2,000 psi with cooling to prevent damage to the compressor, and it is cooled again before mixing with the bio-oil feed to prevent coking in the first reactor.

The model depicted in Figure 61 above intentionally lacked a steam reforming system for hydrogen generation, but included a PSA system for hydrogen recovery. This was done to limit the scope of the hydrotreating system request for quotations aimed specifically at providers with expertise in hydrotreating process equipment. Not only did this avoid Battelle receiving inflated quotations for hydrogen generation equipment due reflecting vendor risk, but it also left options open as Battelle considered operational philosophies for its commercial systems. Options included an integrated system using pyrolysis NCG for H_2 generation; and a stand-alone pyrolysis operation where NCG would be burned in the pyrolysis unit, and natural gas would be reformed to provide make-up hydrogen to the hydrotreater. For the purposes of the present analysis, Battelle assumed integrated operation of the pyrolysis and hydrotreatment systems with pyrolysis NCG being utilized for hydrogen generation in a reforming unit in the hydrotreatment system. Hence, the analysis maintained the analysis approach employed in the 2012 and 2013 model iterations. The hydrogen plant cost estimate was derived from a DOE Hydrogen Program tool as described below.

As part of its internal commercialization efforts, Battelle obtained bio-oil hydrotreater process design services from a commercial engineering and construction firm. Our competitively-selected vendor developed a process flow diagram and equipment list, based on the Battelle-provided mode (Figure 61) land corresponding process narrative.

Battelle took its vendor's detailed cost breakdown and applied it to the capital cost estimating approach used for the 2015 pyrolysis system, as well as for previous 2012 and 2013 analyses. Specifically, Battelle summed the identified major equipment costs and added the modular skid frame construction cost to arrive at the TPEC. The vendor-quoted installation cost also included the Piping line item. The remainder

of the capital cost estimating followed the same modified cost factor approach described in Section 9.2.1 Pyrolysis, above with exceptions to account for capital costs that did not fit cleanly into the cost factored build as described below.

The Utilities and Auxiliaries section installed cost from the 2012 cost model[vi] was scaled from 2,000 ton/day to 100 ton/day using 0.65 scaling. This section was added to maintain the scope of the hydrotreatment system consistent with previous model iterations. Within the accuracy of the estimate, we assumed the respective scale systems to require the same utility duties per processed ton of biomass (or produced gallon of fuel).

The Hydrogen Supply System capital cost was derived from the H2A program developed for the DOE Hydrogen Program[xv]. The flow sheet from the "Forecourt" (distributed) hydrogen production case study is shown in Figure 62. The H2A distributed model was selected as the most appropriate for the current 100 ton/day scale, as opposed to the centralized hydrogen production models used in previous iterations. Applying the experimental results of 45% wt/wt yield of dry oil per dry woody feedstock and 8.3% wt/wt hydrogen consumption per dry pyrolysis oil listed in Table 34 gives a hydrogen consumption rate of 3,735 kg/day. We exercised the H2A "Forecourt" model for this design capacity. We omitted the engineering and design and up-front permitting costs and decreased the site preparation factor by half, since these items already are included in the hydrotreater system cost and would not be needed as assumed for the stand-alone hydrogen production facility intended in the H2A model. With the above assumptions, the H2A model total capital cost estimate is just under $2.5 million.

The ion exchange resign system costs were estimated based on equipment sizes calculated as described in Section 0 below.

We assumed that co-location at an existing facility would enable utilization of the host site's flare system.

The Total Project Investment for the hydrotreating system was $16,725,383.

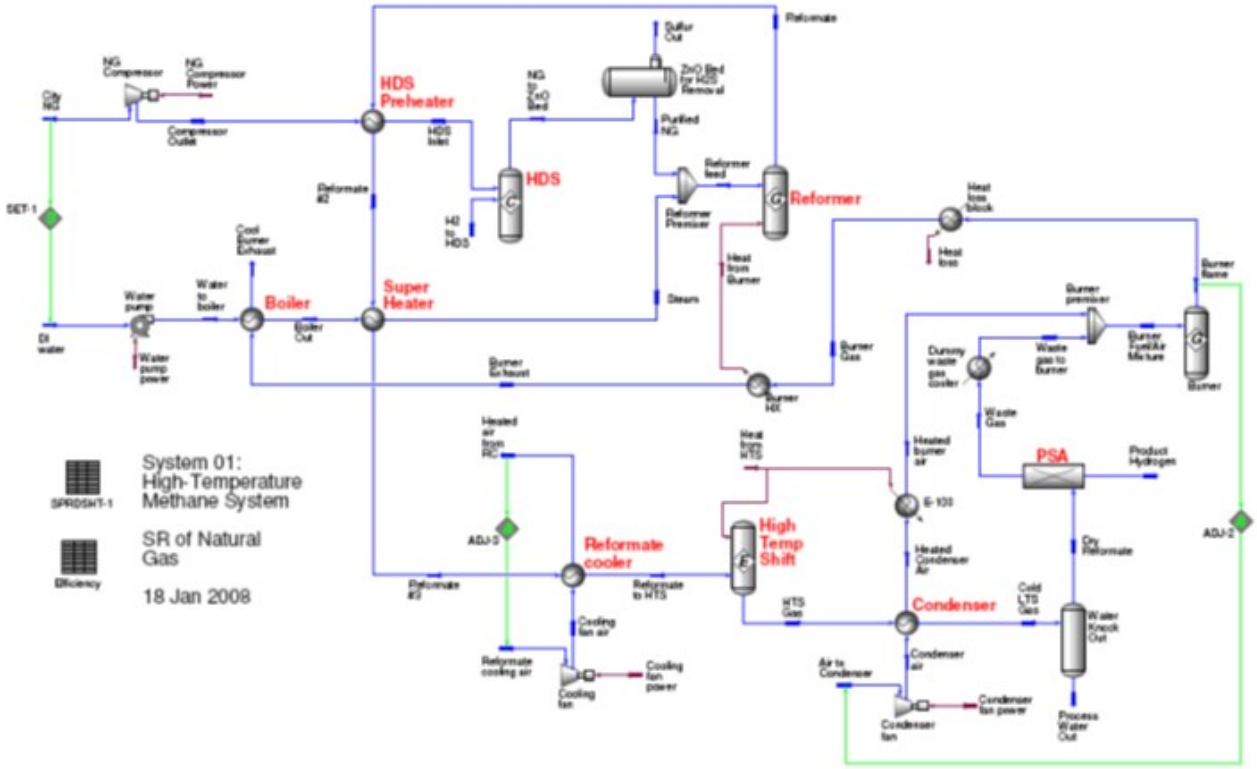

Figure 62. DOE steam methane reforming for hydrogen production flowsheet.xv

9.2.3 Catalyst Cost Estimates

Hydrotreating catalyst quantities and costs were estimated using the reaction liquid hour space velocities (LHSV) and catalyst compositions employed in the 1,000 hr demonstration run. The calculations and results are shown in Table 35.

For the Zone I, Ru/TiO_2 catalyst, costs were estimated based on the current market prices for the Ru metal and TiO_2 substrate materials. Full price was used for the initial catalyst charge, and a 75% credit was assumed for recycling of spent catalyst on catalyst replacement. Battelle staff have direct experience with catalyst recycling credit of up to 90% when noble metals such as Rh or Ru are replaced.

For the Zone II, sulfided $CoMo/Al_2O_3$ catalyst, Battelle obtained a budget quotation from a commercial sulfided hydrodesulfurization catalyst provider. We used the low end of the quoted price range—reflecting the Battelle model for wide-spread deployment of hydrotreaters and the associated volume pricing—and added the quoted price for sulfiding the catalyst. For catalyst replacement, Battelle assumed a 25% credit for recycling of spent catalyst.

Table 35. Hydrotreating catalyst cost estimate.

		Zone I	Zone II	Total
Catalyst		Ru/TiO_2	$CoMo/Al_2O_3$	
LHSV	h^{-1}	0.4	0.4	0.2
Catalyst volume	L	6,341	6,341	
Catalyst density	kg/L	1.0	1.0	
Catalyst mass	kg	6,341	6,341	
Catalyst composition				
Ru	wt%	3%		
TiO_2	wt%	97%		
$CoMo/Al_2O_3$	wt%		100%	
Catalyst component cost				
Ru	$/kg	$1,800[a]		
TiO_2	$/kg	$3.50[b]		
$CoMo/Al_2O_3$	$/kg	$11.35[c]		
Catalyst unit cost	$/kg	57.41	11.35	
Catalyst cost - initial reactor charge		$364,002	$71,969	**$435,971**
Catalyst recycling credit[d]		75%	25%	
Catalyst replacement cost		$91,000	$53,977	$144,977
Catalyst life	months	12	12	
Annualized catalyst replacement cost		$91,000	$53,977	**$144,977**

[a]$56/troy ounce, http://www.infomine.com/investment/metal-prices/ruthenium/, accessed March 13, 2015.
[b]TiO_2: $3,500/ton, http://www.discoveryinvesting.com/blog/2014/6/6/company-report-site-visit-to-argex-titanium, dated June 18, 2014, accessed March 13, 2015.
[c]Regenerated CoMo catalyst: $3 to $4/lb, plus sulfiding at $2.15/lb, vendor quote dated 11/15/2012.
[d]Assumed catalyst recycling credit based on Battelle experience with Rh catalyst where we received 90% credit for recycled catalyst; Ru is in same class of elements

9.2.4 Bio-oil Pretreatment Resin Cost Estimates

Ion exchange resin quantities for bio-oil pretreatment were calculated based on the heteroatom equivalents found by Inductively Coupled Plasma (ICP) elemental analysis of filtered bio-oil used in the project's experimental runs as summarized in Table 36.

We calculated the quantity of ion exchange resin based on its total exchange capacity against the required equivalents per gallon of bio-oil shown in Table 36. We employed the vendor-recommended resin bed conditions to size the resin regeneration system equipment, employing engineering oversizing margins, as shown in Table 37. Dilute acid regeneration rates followed vendor recommendations. Acid quantities were calculated by comparing acid normalities against ion exchange equivalencies. We assumed the use of sulfuric acid. Resin costs, shown in Table 38, were calculated using vendor quoted price per pound, assuming 30% annual loss of resin due to attrition or other mechanisms.

Table 36. Heteroatoms in Bio-oil.

Element	ppm	MW (g/mol)	mole/g of bio-oil	Valence	Eq/g bio-oil
Al	5.1				
Ca	18.0	40.0	4.49E-07	2.0	8.99E-07
Fe	15.8	55.8	2.82E-07	3.0	8.47E-07
K	57.2	30.1	1.90E-06	1.0	1.90E-06
Mg	5.1	24.3	2.08E-07	2.0	4.16E-07
Na	3.8	23.0	1.66E-07	1.0	1.66E-07
Si	10.6	28.1	3.78E-07	1.0	3.78E-07
S	10.2				
Total	125.73		0.0000034		0.0000046
Equivalents in bio-oil to be exchanged					
eq/g bio-oil	eq/g	4.61E-06			
eq/kg bio-oil	eq/kg	4.61E-03			
bio-oil density	kg/L	1.15			
eq/L bio-oil	eq/L	5.30E-03			
Eq/gal bio-oil	eq/gal	2.01E-02			

Table 37. Resin regeneration system equipment sizing.

Recommended bed size	gal	223
2 Resin vessels @ 1.2x+ recommended volume	**gal**	**300**
Regeneration cycle minimum frequency	days	7.3
Recommended regeneration flow rate	h^{-1}	20
	gal/min	74.44
Recommended regeneration time (minimum)	min	30
1 dilute acid circulation pump	**gal/min**	**100**
Yearly dilute acid requirement	gal	8,589
1 dilute acid tank[a]	**gal**	**1,000**

[a] Assumes monthly change out of dilute acid tank contents

Table 38. Resin cost estimate.

Resin to fill planned vessels	Gal	600
	L	2,271
	Kg	1,749
	Lb	3,856
Resin cost	$/lb	$37.25[a]
Initial resin vessels charge		**$143,620**
Resin attrition per year		30%
Resin make-up mass	lb	1,157
Annualized resin replacement cost		**$43,086**

[a]$37.25/lb budgetary pricing quoted by resin vendor, February 16, 2015.

9.2.5 2015 Economic Analysis Assumptions and Results

The following assumptions were made in the 2015 analysis, which built off of the 2012 FP032 base case model:

- Electric power requirement was scaled from the 2012 model, except that no power generation was assumed (conservative assumption increasing the power purchased).
- No capital equipment was included for power generation; instead all electrical power was purchased.
- Steam raised from the reformer system's syngas cooler is used for process heat, including biomass drying, instead of power generation.
- Pyrolysis NCG and hydrotreater tail gas are assumed to be sufficient to generate enough hydrogen to meet hydrotreating demands; no natural gas feed was required.
- Labor for the 100 ton/day plant was assumed to be two per shift: one shift supervisor and one shift operator; four additional personnel—plant manager, plant engineer, maintenance supervisor, and lab manager—were assumed to be shared across four plants (i.e., 0.25 FTE each).
- Overhead/Maintenance cost factor was assumed to be half that of 2012 FP032, owing to the small scale system.
- The hydrogen required in the 2012 FP032 case was scaled to match current hydrogen consumption rate and used to calculate the reformer catalyst quantity.
- One year construction with a six month startup was assumed with 50% production, 75% variable costs, and 100% of fixed costs during startup.
- 350 plant operating days per year
- Water requirement and WWT scaled from FP032 based on biomass feed rate ratio.

Process yields and economic analysis results are shown in Table 39. The results reflect the latest experimental results, which demonstrated an increase in yield over 2013 results to 60 gallons fuel per dry metric ton of biomass. The results of a sensitivity analysis of model inputs is depicted in Figure 63.

Table 39. Economic analysis results.

	2012 model	2013 model	2015 model
Feedstock capacity (dry metric tons wood/year)	2,000	2,000	100
Upgraded oil annual production (MM gallon/year)	37	38	2
Upgraded oil yield (gallon/dry US ton feedstock)	52	53	54*
CAPEX ($MM)	$MM 338	$MM 372	$MM 22
Upgraded oil price ($/gallon)	$2.97	$3.14	$3.62

*60 gallons per dry metric ton

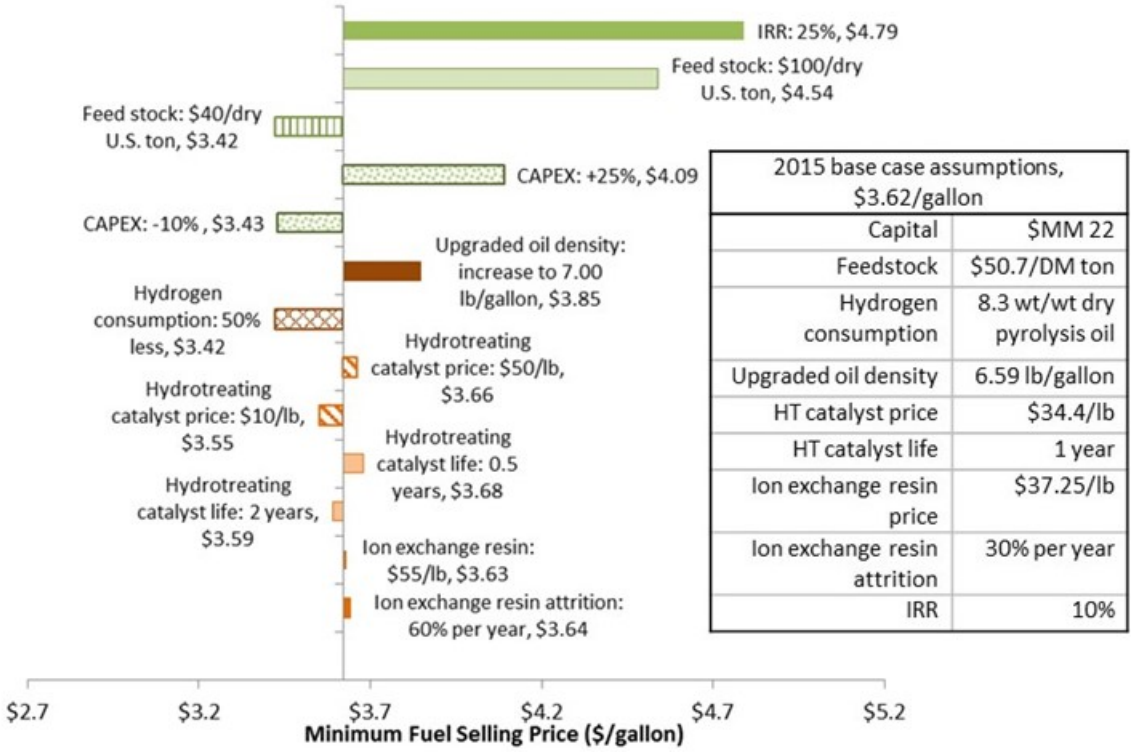

2015 base case assumptions, $3.62/gallon	
Capital	$MM 22
Feedstock	$50.7/DM ton
Hydrogen consumption	8.3 wt/wt dry pyrolysis oil
Upgraded oil density	6.59 lb/gallon
HT catalyst price	$34.4/lb
HT catalyst life	1 year
Ion exchange resin price	$37.25/lb
Ion exchange resin attrition	30% per year
IRR	10%

Figure 63. Sensitivity analysis (2015 process).

9.3 Greenhouse Gas Analysis of Catalytic Pyrolysis and Upgrading Fuel

9.3.1 Base Case Process Model (2012)

Greenhouse gas (GHG) emissions are estimated for the life cycle of fuel product from the catalytic fast pyrolysis process and compared to estimates from the GREET model[xvi]. This is a very high-level scoping analysis, the goal being to provide an initial estimate of GHG reductions associated with this pathway relative to petroleum-derived fuel and to help identify the major drivers affecting GHGs for the fuel production plant. The primary life cycle stages included in this analysis are feedstock production and harvest/collection, fuel production and fuel combustion in a vehicle (i.e., “field-to-wheels”), as illustrated in Figure 64. Feedstock production and harvesting are modeled for both a dedicated crop (hybrid poplar) and a waste woody product (forest residue). As shown, forest residue is considered to be a waste product, and as such, receives none of the burdens of cultivating a dedicated crop such as hybrid poplar. However, it is expected that forest residue will require longer average transportation distances than plantation poplar. Note that for this analysis, the composition of forest residue is assumed to be equal to that of hybrid poplar, and thus the potential effects of changes in feedstock composition on the conversion process are not considered here.

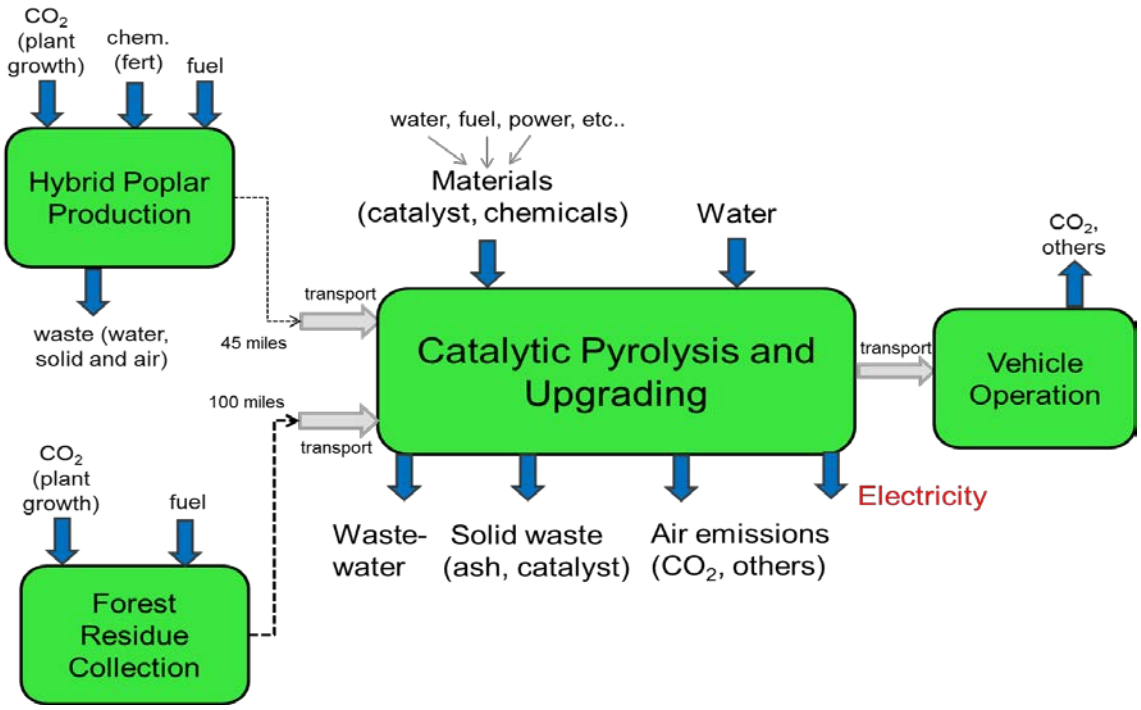

Figure 64. Life cycle of fuel made via catalytic pyrolysis and upgrading conversion of biomass feedstocks.

The life cycle of fuel from catalytic pyrolysis and upgrading is modeled in SimaPro using mass and energy balance data from the 2012 CHEMCAD process models for conversion, previous feedstock processes developed by NREL[xvii,xviii], and GREET data for vehicle operation emissions[xvi]. Transportation distances are assumed to be 100 miles for forest residue (adjusted from the NREL process) and 45 miles for hybrid poplar. Life cycle inventories for secondary materials and energy are taken from the Ecoinvent database[xix]. Calculation of greenhouse gases in CO_2-equivalents (CO_2-e) is based on the International Panel on Climate Change (IPCC) 100-year global warming potentials[xx], shown in Table 40. In order to compare the GHGs associated with this pathway to the conventional baseline fuel, the functional unit chosen for this study is one MJ of gasoline fuel combusted in an automobile. It is assumed that the upgraded oil can be easily separated into gasoline and diesel fractions using distillation and that the fossil energy use associated with this step is negligible. Energy and emission burdens are assigned to each of the fuels from the refinery using energy allocation (44% to gasoline, 56% to diesel). Direct and indirect land use change impacts resulting from conversion of land to plantation crops are not included in this analysis.

Table 40. IPCC 2007 global warming potentials of the primary greenhouse gases for fuel production.

Compound	Abbreviation	GWP, CO2-equivalents
Carbon dioxide	CO_2	1
Methane	CH_4	25
Nitrous oxide	N_2O	298

The GHG emissions results for bio-based gasoline from fast pyrolysis and upgrading are shown in Figure 65. Total emissions for fuel from short rotation hybrid poplar are 9.5 g CO_2-e/MJ gasoline, or a 90% reduction from the baseline for conventional petroleum gasoline[xvi]. Emissions for forest residue-based gasoline are 6.6 g CO_2-e/MJ gasoline, or a 93% reduction from the baseline. As shown, the conversion process has very little contribution to the total GHGs. The primary reason is that there are no direct fossil inputs to the process (e.g., hydrogen is entirely supplied by off-gas from the process) and the process is producing power. This power is assumed to be exported to the grid, effectively counting as an emissions credit (negative carbon emissions) due to the displacement of fossil-based power production from the average U.S. grid mix[xix]. The grid mix assumed is shown in Table 41. There is some criticism from within the LCA community for using the average U.S. grid mix to calculate a GHG emissions credit associated with biofuels processes that co-produce power. The argument is that co-produced power would likely displace renewable types of electricity, rather than conventionally generated power and thus it is unfair to assign a fossil GHG emissions credit to these fuels. As shown in Figure 65 when no electricity credit is assigned, carbon footprint increases to 18.0 g CO_2-e/MJ for poplar (81% reduction from the baseline), and 15.2 g CO_2-e/MJ for forest residue (84% reduction from the baseline).

Table 41. Average U.S. grid mix assumed for this analysis [15].

Power Source	% in Average US Mix
Coal	49.3
Nuclear	19.6
Natural Gas	17.3
Hydro	8.2
Oil	3.3
Other	2.3

As mentioned earlier, the feedstock production stage is more significant for the poplar-derived fuel, as it requires agricultural inputs for cultivation and harvesting that are not considered for the forest residue (which is simply collected at the landing after commercial logging). However, the feedstock transportation stage for residue is significantly larger because it is being transported over twice the distance as poplar. Feedstock preprocessing is also a significant contributor to GHGs and consists of power for the dryer fan and the hammermill. Note that the fuel use stage is nearly zero because biomass is considered a carbon-neutral feedstock. In other words, the CO_2 taken up during growth is nearly equal to that emitted from the combustion and reforming processes at the plant and during vehicle use (biogenic CO_2 uptake and emissions are not shown). The exception is a small amount of biogenic methane and N_2O emitted during vehicle operation, accounting for the small bar for fuel use in Figure 65..

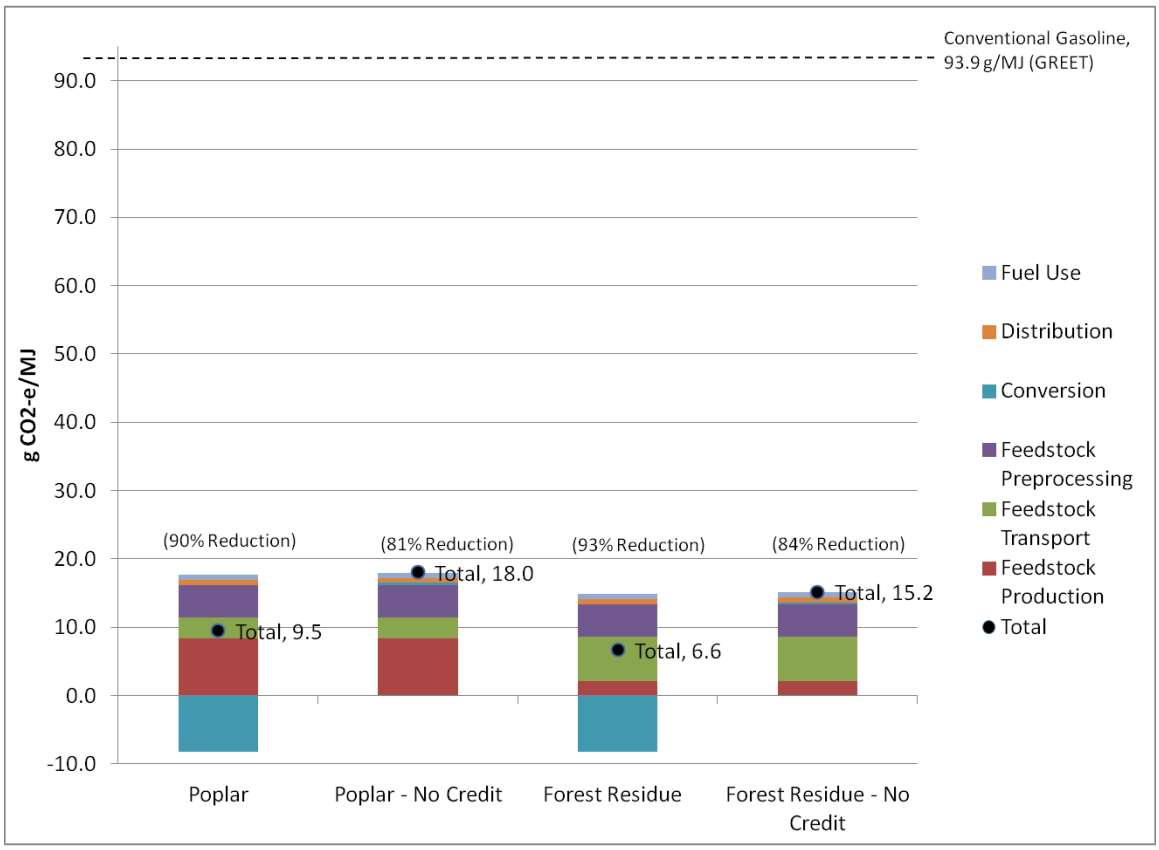

Figure 65. The life cycle GHG emissions for gasoline use from catalytic pyrolysis and upgrading.

It should be emphasized that these results are very preliminary and as such have a significant amount of associated uncertainty. Perhaps the greatest source of uncertainty is fuel yields from the process. As progress is made toward greater oil and fuel yields, less electricity will be produced, which will result in higher carbon footprint. In addition, as yield increases, oxygen content in the oil increases, resulting in a greater need for hydrogen. Supplemental natural gas may be required to supply this hydrogen at a given yield, resulting in greater GHG emissions for this fuel pathway. Striking the optimum balance between carbon-to-fuel yield (and cost) and fossil GHG emissions will continue to be a critical task when producing biofuels via hydrocarbon-based intermediates that require deoxygenation. As more laboratory data on both the catalytic pyrolysis and the upgrading processes become available, the SimaPro model for this pathway willn be updated and more exact GHG analyses can be performed.

9.3.2 Interim Process Model (2013)

Mass and energy balances from the updated 2013 process models were integrated into the SimaPro models to provide an updated estimate of GHG emissions for gasoline fuel from the catalytic pyrolysis and upgrading process. Results for the updated model are shown in Figure 66. Table 42 compares the results for the two cases, broken out by life cycle stage. Total GHG emissions for the updated model are higher than with the previous model, primarily due to higher hydrogen consumption in the hydrotreating section and lower fuel product mass yields from upgrading (see Table 34). Higher hydrogen consumption in the updated model results in less off-gas available for electricity generation at the plant, and therefore a lower GHG credit (for average U.S. grid mix) associated with exported power (the blue bars in Figure 66) compared to the 2012 model. The result is higher conversion stage GHGs for the 2013 model, as shown in Table 42. Lower fuel product yields result in higher amounts of feedstock required per MJ of fuel produced, and therefore GHGs associated with feedstock production, transportation, and grinding are

slightly higher in the 2013 model compared to the 2012 model, as shown in Table 42. Reductions in GHGs compared to the fossil baseline are still within the range of biofuel definitions under the Renewable Fuel Standard (50% reduction for advanced biofuel and 60% reduction for cellulosic biofuel).

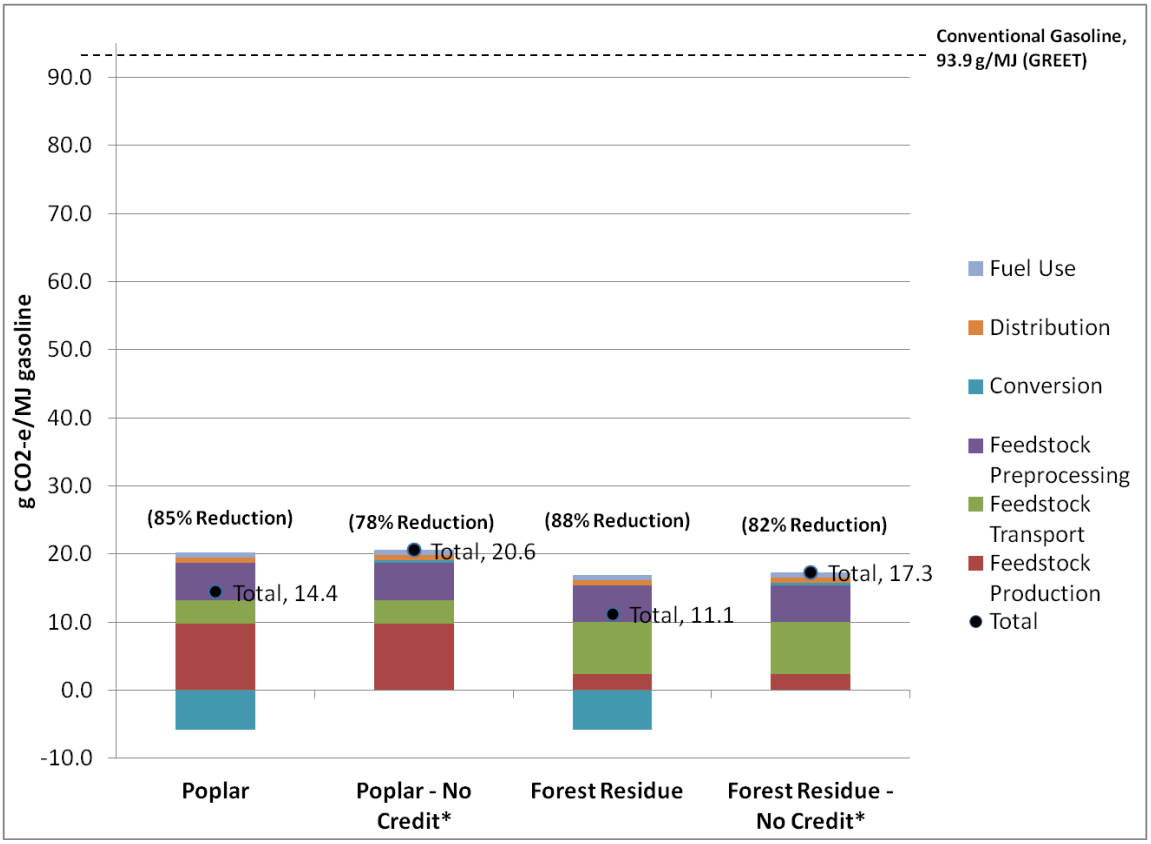

* No GHG electricity credit illustrates the case of a conversion plant in a region using renewable electricity.

Figure 66. Updated GHGs for fast pyrolysis and upgrading of poplar and forest residue feedstocks.

Table 42. Comparison of lifecycle GHG emissions for 2012 model and 2013 model.

	GHGs (g CO2-e/MJ gasoline)						
	Feedstock Production	Feedstock Transport	Feedstock Preprocess	Conversion	Distribution	Fuel Use	Total
Poplar 2012 Model	8.4	3.0	4.7	-8.2	0.7	0.8	9.5
Poplar 2013 Model	9.7	3.5	5.5	-5.8	0.7	0.8	14.4
Residue 2012 Model	2.1	6.5	4.7	-8.2	0.7	0.8	6.6
Residue 2013 Model	2.4	7.5	5.5	-5.8	0.7	0.8	11.1

9.3.3 Final Process Model (2015)

The 2015 process models were compared to the 2013 and 2012 process models to provide an updated estimate of GHG emissions for gasoline fuel from the pyrolysis and upgrading process.

The feedstock production, transport, and preprocessing GHG emissions were adjusted in proportion to the overall yield. Higher fuel product yields result in lower amounts of feedstock required per MJ of fuel produced, and therefore GHGs associated with feedstock production, transportation, and grinding. The 2015 overall yield of 18 g fuel per 100 g dry biomass feedstock is midway between the 19 g fuel per 100 g dry biomass feedstock in 2012 and the 17 g fuel per 100 g dry biomass feedstock in 2013 as shown in Table 34. As such, the average of 2012 and 2013 GHG emissions was used for 2015 values of the three feedstock GHG emissions shown in Table 43.

The 2015 conversion GHG emissions were taken to be equivalent to the 2013 conversion GHG emissions in the 2013 model where no GHG credit (for average U.S. grid mix) was taken for exported power. In the 2015 model, we made the conservative assumption of no electricity export from the plant, and therefore used the corresponding 2013 model values.

No changes were required of the distribution and fuel use categories.

The 2015 GHG emission estimates, shown in Table 43, are slightly below the 2013 No Credit cases. Reductions in GHGs compared to the fossil baseline, as depicted in Figure 67, are still within the range of biofuel definitions under the Renewable Fuel Standard (50% reduction for advanced biofuel and 60% reduction for cellulosic biofuel).

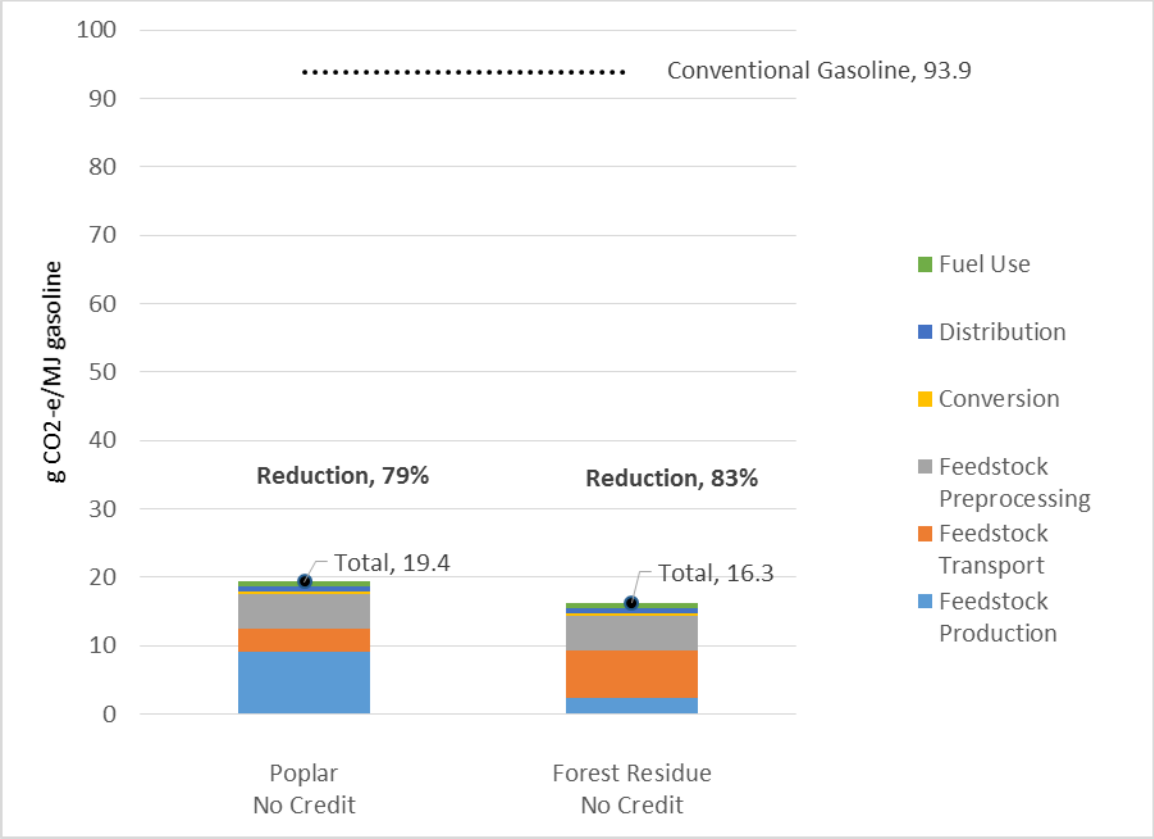

Figure 67. The life cycle GHG emissions for gasoline use from pyrolysis and upgrading (2015 model).

Table 43. Comparison of lifecycle GHG emissions for 2012, 2013, and 2015 models.

	GHGs (g CO2-e/MJ gasoline)						
	Feedstock Production	Feedstock Transport	Feedstock Preprocess	Conver-sion	Distribu-tion	Fuel Use	Total
Poplar 2012	8.4	3	4.7	-8.2	0.7	0.8	9.5
Poplar 2012 No Credit				0.3			18.0
Poplar 2013	9.7	3.5	5.5	-5.8	0.7	0.8	14.4
Poplar 2013 No Credit				0.4			20.6
Poplar 2015 No Credit	9.1	3.3	5.1	0.4	0.7	0.8	19.4
Residue 2012	2.1	6.5	4.7	-8.2	0.7	0.8	6.6
Residue 2012 No Credit				0.4			15.2
Residue 2013	2.4	7.5	5.5	-5.8	0.7	0.8	11.1
Residue 2013 No Credit				0.4			17.3
Residue 2015 No Credit	2.3	7	5.1	0.4	0.7	0.8	16.3

10.0 Products Developed Under the Award

10.1 Publications / Presentations

Battelle presented, Upgrading of Biomass Fast Pyrolysis Oil (Bio-oil), at the DOE Bioenergy Technologies Office (BETO) 2015 Project Peer Review on March 22, 2015.

10.2 Patents

Battelle filed a Provisional Patent Application: “Pre-processing Bio-oil Before Hydrotreatment” with the US Patent and Trademark Office (USPTO) on March 5, 2015. The USPTO has assigned Ser. No. 62/129,007 to this application.

REFERENCES

[i] A. Oasmaa, D. C. Elliot, and J. K. Korhonen. *Acidity of Biomass Fast Pyrolysis Bio-oils*. Energy and Fuels 24 (12): 6548-6554. 2010. doi:10.1021/ef100935r

[ii] C. M Schillmoller. *Selection and use of stainless steels and nickel-bearing alloys in organic acids*. Nickel Development Institute Technical Series No 10 063.

[iii] J. R. Keiser, M. Howell, S. A. Lewis, Sr, R. M. Connatser. *Corrosion Studies of Raw and Treated Biomass-Derived Pyrolysis Oils*. NACE Corrosion Conference and Expo 2012. C2012-0001645.

[iv] D. Elliott.2007. Historical Developments in Hydroprocessing Bio-oils, Energy & Fuels: 21

[v] A. Zacher, D. Santosa, D. Elliott, Mild Catalytic Fast Pyrolysis of Biomass and Catalytic Hydrotreating to Liquid Transportation Fuels. Plus Development of an Ebullated Bed Reactor, TC Biomass presentation. <media.godashboard.com/gti/tcbiomass2011-Upgrading-optimized.pdf>

[vi] S.B. Jones, et al. 2009. Production of Gasoline and Diesel from Biomass via Fast. Pyrolysis, Hydrotreating and Hydrocracking: A Design Case. PNNL-18284, Pacific Northwest National Laboratory, Richland, WA. <www.pnl.gov/main/publications/external/technical_reports/PNNL-18284rev1.pdf >

[vii] O.D. Mante and F.A. Agblevor. 2011. Catalytic conversion of biomass to bio-syncrude oil, Biomass Conversion and Biorefinery. 1 (4) : 203-215.

[viii] Aho et al. 2011. Catalytic Pyrolysis of Pine Biomass Over H-Beta Zeolite in a Dual-Fluidized Bed Reactor: Effect of Space Velocity on the Yield and Composition of Pyrolysis Products. To Catal. 54: 941-948.

[ix] Stefanidis et al. 2011. In-situ upgrading of biomass pyrolysis vapors: Catalyst screening on a fixed bed reactor. Bioresource Technology. 102: 8261–8267.

[x] Hong-yu et al. 2008. Online upgrading of organic vapors from the fast pyrolysis of biomass. J Fuel Chem Technol, 2008, 36(6), 666-671.

[xi] Mante et al. 2011. Fluid Catalytic Cracking of Biomass Pyrolysis Vapor. Biomass Conv. Bioref. 1: 189-201.

[xii] Mullen et al. 2011. Catalytic Fast Pyrolysis of White Oak Wood in a Bubbling Fluidized Bed. Energy&Fuels. 25: 5444-5451.

[xiii] Mante et al. 2012. The influence of recycling non-condensable gases in the fractional catalytic pyrolysis of biomass. Bioresources Technology, in-press.

[xiv] Agblevor et al. 2010. Fractional catalytic pyrolysis of hybrid poplar wood. Ind. Eng. Chem. Res. 49: 3533-3538.

[xv] H2A 2013. DOE EERE Fuel Cell and Hydrogen Program, “Current Forecourt Hydrogen Production from Natural Gas 1500 kg per day version 3.0” Accessed at http://www.hydrogen.energy.gov/h2a_prod_studies.html on March 26, 2015.

[xvi] GREET, The Greenhouse Gases, Regulated Emissions, and Energy Use in Transportation (GREET) Model, GREET 2011; Argonne National Laboratory: Argonne, IL, 2011.

[xvii] Hsu, D.D.; D. Inman, G. Heath, E.J. Wolfrum, M.K. Mann, and A. Aden (2010) “Life Cycle Environmental Impacts of Selected U.S. Ethanol Production and Use Pathways in 2022.” Environ. Sci. Technol., 44(13), 5289-5297. (see also Supporting Information).

[xviii] Hsu, D.D. (2011) “Life Cycle Assessment of Gasoline and Diesel Produced via Fast Pyrolysis and Hydroprocessing,” NREL/TP-6A20-49341, March 2011.

[xix] Ecoinvent. (2009) Duebendorf, Switzerland: Swiss Center for Life Cycle Inventories.

[xx] Solomon, S., D. Qin, M. Manning, R.B. Alley, T. Berntsen, N.L. Bindoff, Z. Chen, A. Chidthaisong, J.M. Gregory, G.C. Hegerl, M. Heimann, B. Hewitson, B.J. Hoskins, F. Joos, J. Jouzel, V. Kattsov, U. Lohmann, T. Matsuno, M. Molina, N. Nicholls, J. Overpeck, G. Raga, V. Ramaswamy, J. Ren, M. Rusticucci, R. Somerville, T.F. Stocker, P. Whetton, R.A. Wood and D. Wratt, 2007: Technical Summary. In: Climate Change 2007: The Physical Science Basis. Contribution of Working Group I to the Fourth Assessment Report of the Intergovernmental Panel on Climate Change [Solomon, S., D. Qin, M. Manning, Z. Chen, M. Marquis, K.B. Averyt, M. Tignor and H.L. Miller (eds.)]. Cambridge University Press, Cambridge, United Kingdom and New York, NY, USA.